Leaflet Material Selection for Aortic Valve Repair

Ovais Abessi

A thesis submitted to the Faculty of Graduate and Postdoctoral Studies
In partial fulfillment of the requirements for the degree of

MASTER OF APPLIED SCIENCE

in Mechanical Engineering

Ottawa-Carleton Institute for Mechanical and Aerospace Engineering
University of Ottawa
Ottawa, Canada

August 2013


به نام ایزد یکتا


uOttawa
L'Université canadienne
Canada's university

Abstract

Leaflet replacement in aortic valve repair (AVr) is associated with increased long-term repair failure. Hemodynamic performance and mechanical stress levels were investigated after porcine AVr with 5 types of clinically relevant replacement materials to ascertain which material(s) would be best suited for repair. Porcine aortic roots with intact aortic valves were placed in a left-heart simulator mounted with a high-speed camera for baseline valve assessment. Then, the non-coronary leaflet was excised and replaced with autologous porcine pericardium (APP), glutaraldehyde-fixed bovine pericardial patch (BPP; Synovis™), extracellular matrix scaffold (CorMatrix™), or collagen-impregnated Dacron (HEMASHIELD™). Hemodynamic parameters were measured over a range of cardiac outputs (2.5–6.5L/min) post-repair. Material properties of the above materials along with St. Jude Medical™ Pericardial Patch with EnCap™ Technology (SJM) were determined using pressurization experiments. Finite element models of the aortic valve and root complex were then constructed to verify the hemodynamic characteristics and determine leaflet stress levels.

This study demonstrates that APP and SJM have the closest profiles to normal aortic valves; therefore, use of either replacement material may be best suited. Increased stresses found in BPP, HEMASHIELD™, and CorMatrix™ groups may be associated with late repair failure.

Acknowledgements

I sincerely appreciate the guidance and support received from my supervisor, Dr. Michel Labrosse, to whom I owe a great deal of thanks. I would like to extend my gratitude to Drs. Munir Boodhwani and Hadi Toeg of the University of Ottawa Heart Institute for their active participation in the project, as well as the University of Ottawa Heart Institute and the Ottawa General Hospital for their equipment contributions.

I dedicate my thesis to my parents and Yaka, who have nurtured my potential with unconditional love and support throughout this experience, I am forever grateful.

Contents

Abstract iii

Acknowledgements iv

Summary of figures viii

Summary of tables xi

Acronyms xii

1 Introduction 1

1.1 Context of the study 1

1.2 Thesis objectives 2

1.3 Thesis contributions 3

1.4 Organization of the thesis 4

1.5 Statement of contribution 5

1.6 Additional information about this work 6

2 Background and literature review 8

2.1 Heart anatomy and physiology 8

2.2 Aortic valve anatomy and physiology 11

2.2.1 Aortic root 11

2.2.2 Aortic leaflets or cusps 12

2.3 Valvular diseases 18

2.3.1 Aortic valve stenosis 19

2.3.2 Aortic insufficiency 20

2.4 Surgical options 22

2.4.1 Aortic valve replacement 22

2.4.2 Valve-sparing procedures 23

2.4.3 Aortic valve repair 31
2.5 Computational modeling of the aortic valve 33
3 Experiments 40
3.1 Materials and Methods 41
3.1.1 Left-heart simulator 41
3.1.2 Control aortic roots 45
3.1.3 Valve repair with non-coronary cups replacement 46
3.1.4 Processing of data from the left-heart simulator and high-speed camera 49
3.1.5 Material testing of replacement materials 51
3.1.6 Theory underlying the processing of the pressurization testing data 55
3.2 Results 59
3.2.1 Valve repair with non-coronary cups replacement 59
3.2.2 Material pressurization testing 64
4 Finite element simulation of aortic valve with replacement material graft 71
4.1 Methods 71
4.1.1 Geometry 71
4.1.2 Material properties 76
4.1.3 Boundary conditions and loads 77
4.2 Results 79
5 Discussion 89
5.1 Experimental and computational results 92
5.2 Clinical relevance 94
5.3 Limitations of current study and recommendations for future work 95
6 Conclusions 97
References 98

Appendix A – MatLab code for GOA measurements 104

Appendix B – Measurements of hemodynamic performance 107

Appendix C – Boxplot comparison of valve sizes 110

Appendix D – MatLab / Excel interface for statistical analysis of data 111

Summary of figures

Figure 1: Section view of heart representing its valves and chambers. LA: left atrium, LV: left ventricle, RA: right atrium, RV: right ventricle, A: aortic valve, T: tricuspid valve, P: pulmonary valve, M: mitral valve, AO: aorta, and PA: pulmonary Artery. Arrows show the path of blood flow (Thubrikar, 1990). 9

Figure 2: Timing of events in the left heart during the cardiac cycle (Marieb & Hoehn, 2013).....10

Figure 3: Anatomy of aortic valve: the neutral aortic valve in physiological condition in body (a) and flat view of aortic valve (b) (Anderson, 2000). 11

Figure 4: Detailed anatomy of an aortic leaflet. 13

Figure 5: Flat view the aortic valve represent the leaflets (b) and interleaflets triangles (a) and leaflet commissures (c) (Underwood et al., 2000). 14

Figure 6: Aortic leaflet tissue showing the fibrosa, spongiosa and ventricularis. The fibrosa faces the aorta and the ventricularis faces the left ventricle of the heart (Robarts, 2007).....15

Figure 7: View of excised leaflet showing fiber bundles in the circumferential direction (Cox et al., 2006). 16

Figure 8: Leaflet layers arrangement (Vesely, 2005). 17

Figure 9: Leaflet layers arrangement (Peppas et al., 2007). 18

Figure 10: Calcified bicuspid aortic valve in two patients (Thubrikar, 1990). 19

Figure 11: The aortic valve with three thickened leaflets (Ho, 2009). 20

Figure 12: Normal aortic valve and aortic valve with aortic regurgitation illustrated in top and bottom of image respectively (Pai & Fort, 2011). 21

Figure 13: Doppler imaging of the regurgitant jet characteristic of aortic insufficiency (Čanádyová et al., 2011).....22

Figure 14: Ascending aorta replacement (Čanádyová et al., 2011). 25

Figure 15: Complete steps of Yacoub remodeling technique of the aortic valve (Yacoub & Takkenberg, 2005). 26

Figure 16: Diagram and pictures showing prosthesis preparation in reimplantation technique (Boodhwani et al., 2009). 27
Figure 17: A: dilated root, B: after resecting the diseased Valsalva sinuses and preparing the coronary artery buttons. C, D: reimplantation of the aortic valve into the prosthesis, E, F: distal anastomosis between the graft and the native ascending aorta (Čanádyová et al., 2011). 28
Figure 18: Complete remodeling (Underwood et al., 2000). 29
Figure 19: Technique of aortic annuloplasty (Underwood et al., 2000). 30
Figure 20: Free margin placation: determination of excess leaflet tissue (a) and extension of leaflet plication onto the leaflet body (Boodhwani et al., 2009). 32
Figure 21: Free margin resuspension on right coronary leaflet, whereas the left coronary and non-coronary leaflet appears to be normal (Boodhwani et al., 2009). 32
Figure 22: Pulse Duplicator and prototype photo-detection of Left –heart simulator (ViVitro systems). 41
Figure 23: Left –heart simulator (ViVitro systems) 43
Figure 24: An unrepaired aortic root was mounted in the jig. 44
Figure 25: Unrepaired aortic valves after removing fatty and muscle and blocking their right and left coronaries. 45
Figure 26: Transverse incision above the sinotubular junction. 46
Figure 27: Sizing the replacement material graft using the resected leaflet. 47
Figure 28: Repaired aortic valve after replacing the non-coronary leaflet with the replacement material graft. 47
Figure 29: Repaired aortic valve after closing the transverse incision. 48
Figure 30: Example of evolution of the geometric orifice area as a function of time in the valves studied. VO is the slope of the curve during the fast opening phase; VSC is the slope of the curve between fast opening and rapid closing; VC is the slope of the curve during the rapid closing phase. 50
Figure 31: Replacement material cylindrical tube capped and cannulated. 52
Figure 32: Sample mounted on the measure head and floating in 0.9% normal saline. 52

Figure 33: The replacement material was mounted as a tube in the pressurization testing equipment, including a syringe for pressure control (foreground), an ultrasound probe for measurement of radial dimensions (center), a webcam for measurement of longitudinal extension (right), and a manometer (almost completely outside of view, bottom right) 54

Figure 34: Cross-sectional view of ring after cutting from tube (a) and tissue strip after removing the suture (b). 55

Figure 35: Pressurization testing experiment.....65

Figure 36: The stress-strain properties of the original leaflets were derived from equibiaxial planar testing data (Martin and Sun, 2013). The stress-strain curves for the other replacement materials represent simulated equibiaxial planar testing using the properties determined from pressurization testing described herein.....70

Figure 37: Drawing of the aortic valve showing the side view of one leaflet. *H*: valve height, *Hs*: Sinus Height, *Xs*: Coaptation Height, *D b*: diameter of the base, *Dc*: diameter of the commissures, *Lf* : leaflet free-edge length, *Lh*: leaflet height (Labrosse et al., 2010). 72

Figure 38: (a) Line sketch of unpressurized aortic valve model, showing the left ventricular outflow tract, the aortic sinuses and the ascending aorta, including the 15 landmark points. (b) Line sketch of the aortic leaflets drawn in an assumed, unpressurized position (Labrosse et al., 2011).....74

Figure 39: Final finite element mesh of the aortic valve and root. Green: ascending aorta and aortic sinuses; blue: leaflets; red: base of the valve, including the left ventricular outflow tract (Labrosse et al., 2011). 76

Figure 40: Pressure curves applied in the finite element model, reproducing a physiologic cardiac cycle with a shorter diastole for $t \geq 0.4$ s (Labrosse et al., 2010).....78

Figure 41: Control model in dynamics, under physiologic longitudinal stretch ratio of 1.20. The model was studied over one cardiac cycle by application of the pressure pulses described in the upper left inset. The analysis started from the unpressurized geometry at Time 0. The pressure was ramped from 0 up to 80 mmHg at Time 1 before the cardiac cycle started in early systole. The valve was fully open at Time 2, was closing at Time 3 and was closed under maximum pressure at Time 4. Von Mises stresses are color coded in MPa. 80

Figure 42: Maximum values of Von Mises stress in the repaired valve with A: APP, B: HEMASHIELD, C: CorMatrix , D: BPP and E: SJM.....87

Summary of tables

Table 1: Functional classification of aortic regurgitation (Boodhwani et al., 2009)..24

Table 2: Repair-oriented functional classification of aortic insufficiency and repair technique used. FAA: functional aortic annulus; STJ: sinotubular junction; SCA: subcommissural annuloplasty (Boodhwani et al., 2009).....24

Table 3: Hemodynamic measurements for 6 repaired aortic valve with BPP. 60

Table 4: Hemodynamic performance in all replacement materials before and after repair.....62

Table 5: Experimental data from pressurization testing. 66

Table 6: Material constants of valve constituents and replacement materials. 69

Table 7: Unpressurized porcine aortic valve dimensions. 73

Table 8: FE simulation results for valve's opening, closing and GOA. 81

Table 9: Von Mises stress from FE simulation results in repaired valve with the different replacement materials. 82

Table B-1: Hemodynamic parameters as measured in valves.....107

Table B-2: Valve hemodynamic in un-repaired porcine valves at different cardiac outputs (CO). 109

Acronyms

AI: aortic insufficiency

APP: autologous porcine pericardium

AS: aortic stenosis

AV: aortic valve

AVR: aortic valve replacement

BPP: bovine pericardial patch

CT-A: computed tomography angiography

FE: finite element

GOA: geometric orifice area

LVOT: left-ventricular outflow tract

LVW: left ventricular work

MRI: magnetic resonance imaging

STJ: sino-tubular junction

SJM: St-Jude Medical

TAVR: transcatheter aortic valve replacement

TEE: transesophageal echography

VC: valve closing speed

VO: valve opening speed

VSC: valve slow closing speed

1 Introduction

1.1 Context of the study

The heart, as is well known, is a pump that circulates blood throughout the entire body. It consists of four chambers and four valves which allow blood to flow in only one direction. The aortic valve lies between the left ventricle and the aorta; it is the specific topic of this study.

Several diseases, such as aortic stenosis (i.e., the valve does not open properly) and aortic regurgitation (i.e., the valve leaks) can impair aortic valve performance. While aortic valve replacement is recommended for severe aortic stenosis, aortic insufficiency may possibly be treated by surgical procedures where some or most of the original valve is preserved (aortic valve repair). However, successful aortic valve repair requires the surgeon to addresses the specific anatomical defects with high surgical flexibility, knowledge, and adequate surgical tools. Among these tools are materials that can be used to replace a portion of or whole aortic valve components.

Attempts to replace aortic valve components with biological or man-made materials have been made since the 1960s with materials such as dura mater, facia lata, and bovine pericardium. Although the list of materials available to the surgeons has grown over the years, and despite existing experimental techniques, it is still unclear which of these materials provide the best valve performance and longevity. This is the central question of the present thesis.

On the other hand, recent research has shown that finite element modeling could help cardiac surgeons and scientists to improve aortic valve repair procedures, by providing information not available from experiments, such as mechanical stress levels. Therefore, the present study proposes to combine experiment and computational approaches.

1.2 Thesis objectives

The overall objective of this study is to investigate which replacement materials may be best suited for leaflet replacement in aortic valve repair. To properly address this question, a more specific description must be given of what is meant by "best suited". Firstly, a replacement material will be considered suitable if it can be used such that the hemodynamic performance of the repaired valve (e.g. opening and closing velocities, sealing quality) is close to that in normal valves. Therefore, comparison of hemodynamic performance between native normal valves and repaired ones is desirable. Secondly, a replacement material will be considered suitable if it induces acceptable levels of mechanical stress in the replaced and native valve components.

Given this interpretation, the main objective was broken down into the following specific objectives, based on porcine aortic valves models, chosen for their availability and good representativeness of the human aortic valves:

1. Compare the hemodynamic performance, as measured in a left-heart simulator, of native normal valves and repaired ones using different replacement materials;

2. Determine material properties of said replacement materials for use in computational finite element modeling;
3. Reproduce the cases studied in the left-heart simulator using finite element modeling to access mechanical stress information;
4. Combine all information to build a comprehensive assessment of the situation and draw informed conclusions.

1.3 Thesis contributions

The thesis contributions lie not just in the final proposed response to the question asked, but also in the procedural details of how the specific objectives above were achieved. Namely, 25 porcine aortic valves were considered and had one leaflet replaced with 4 different clinically relevant materials. The hemodynamic performance of each valve was measured, before and after leaflet replacement. In addition, the mechanical properties of 5 replacement materials were determined using pressurization testing. A finite element model of a representative native aortic valve was especially built and analyzed, and then modified and analyzed again to accommodate the substitution of one native leaflet by a leaflet made of replacement material, as done in the experiments. This was repeated for the 5 replacement materials as follows: Cor-Matrix patch, bovine pericardial patch, HEMASHIELD/Dacron patch, St. Jude Medical™ pericardial patch with EnCap Technology and an autologous porcine pericardium patch. The in-kind donations made by these manufacturers are gratefully acknowledged.

Ultimately, the autologous porcine pericardium and St. Jude Medical™ pericardial patches had the closest profiles to normal aortic valves in both experimental and computational models; therefore, they were ascertained as the best suited replacement materials for aortic valve repair.

1.4 Organization of the thesis

To engage the reader, the thesis begins with an extensive Background and literature review (Chapter 2) giving a detailed description of the heart and aortic valve anatomy and function. Valvular diseases are then introduced focusing on aortic valve stenosis and aortic insufficiency, and so are surgical aortic valve replacement, and aortic valve repair techniques to treat pathologies of the aortic valve. Relevant published research in computational modeling of the aortic valve is also discussed in the chapter. Chapter 3 presents the experimental aspects of the evaluation hemodynamic performance of the native and repaired aortic valves using a left-heart simulator as well as the details of the pressurization testing and data processing toward determination of the mechanical properties of the replacement materials. Results are also included in Chapter 3. Chapter 4 covers the geometric modeling of the aortic valve, the implementation of material properties, and the boundary conditions and loads applied in the finite element models, it also includes results. Chapter 5 discusses all the results obtained, as well as the clinical relevance and limitations of study, with recommendation toward future work. The final chapter briefly concludes the study.

1.5 Statement of contribution

The present study being multidisciplinary in nature, the following presents a breakdown of who did what:

- Ovais Abessi: a) experimental aspects of the evaluation hemodynamic performance of the native and repaired aortic valves using a left-heart simulator (ran the experiments, processed the data)

  b) pressurization testing and data processing toward determination of the mechanical properties of the replacement materials (ran the experiments, processed the data)

  c) finite element modeling (ran the analyses, analyzed the results)

  d) statistical analyses (ran the analyses)
- Dr. Hadi Toeg: a) experimental aspects of the evaluation hemodynamic performance of the native and repaired aortic valves using a left-heart simulator (surgically prepared the valves, participated in the design of the experiments and statistical analyses)

  b) publication of results (co-wrote abstracts as detailed in next section)
- Dr. Michel Labrosse: a) experimental aspects of the evaluation hemodynamic performance of the native and repaired aortic valves using a left-heart simulator (participated in the design of the experiments and statistical analyses, and wrote programs for data processing)

b) pressurization testing and data processing toward determination of the mechanical properties of the replacement materials (designed the experiments, and wrote programs for data processing)

c) finite element modeling (wrote programs, and analyzed the results)

d) publication of results (co-wrote abstracts as detailed in next section)

1.6 Additional information about this work

The work done in this study has been or will be presented on various occasions and in different formats, as listed below:

- 250-word abstract, oral presentation by Dr. Hadi Toeg at the University of Ottawa Heart Institute Collins Day on April 4, 2013; awarded the W.E. Collins Day prize for best overall paper.
- 400-word abstract, poster presentation by Dr. Hadi Toeg at the University of Ottawa Heart Institute 26th annual Research Day on May 14, 2013.
- 400-word abstract, highlighted poster/mini-oral presentation to be given by Dr. Hadi Toeg at the Canadian Cardiovascular Congress in Montreal, October 17-20, 2013.
- 300-word abstract, oral presentation to be given by Dr. Hadi Toeg at the American Heart Association Scientific Sessions in Dallas, TX, November 16-

20, 2013. The abstract is one of 4 finalists selected for the Vivian Thomas Young Investigator Award.

Dr. Hadi Toeg also received the 2013 Physician Services Incorporation (PSI) Resident Research Award prize from the Postgraduate Medical Education program of the Faculty of Medicine at the University of Ottawa for his contribution to the study.

2 Background and literature review

For better understanding of the present study, the following section begins with a brief review of cardiac anatomy and pathology with special attention to the aortic valve anatomy and pathology.

2.1 Heart anatomy and physiology

The heart is a vital part of the cardiovascular system and provides continuous blood circulation to the body. The heart has two receiving chambers, the right and left atria that receive returning blood, and two main pumping chambers, the right and left ventricles that have thick muscular walls that cyclically contract and relax to create pressure gradients to pump blood around the body (Figure 1). Deoxygenated blood is collected from the body into the right atrium and is pumped to the lungs by the right ventricle. Then oxygenated blood collected in the left atrium moves into the left ventricle, and is finally ejected into the aorta from where it irrigates the whole body (Marieb & Hoehn, 2013).

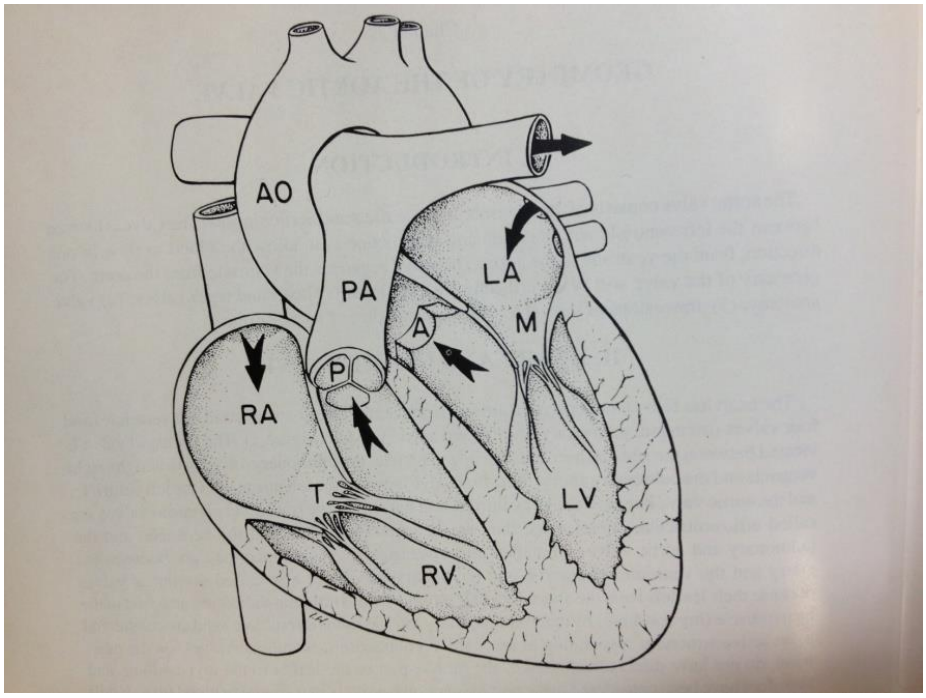

Figure 1: Section view of heart representing its valves and chambers. LA: left atrium, LV: left ventricle, RA: right atrium, RV: right ventricle, A: aortic valve, T: tricuspid valve, P: pulmonary valve, M: mitral valve, AO: aorta, and PA: pulmonary Artery. Arrows show the path of blood flow (Thubrikar, 1990).

Four valves enforce the one-directional flow of blood in the heart (Figure 1) by passive pressure-driven closing and opening during the cardiac cycle. The tricuspid valve, with three flexible leaflets (or cusps), allows one-way blood flow between the right atrium and the right ventricle. The mitral valve, a two-leaflet structure resembling a miter, allows one-way blood flow between the left atrium and the left ventricle. The pulmonary valve allows one-way blood flow between the right ventricle and the pulmonary vein leading into the lungs. The aortic valve allows one-way blood flow between the left ventricle and the aorta.

The cardiac cycle consists of five major stages. In the first stage, late diastole, the whole heart muscle is relaxed and the mitral and tricuspid valves are open while the aortic and pulmonary valves are closed. In the second stage, early systole, blood flows from the left

atrium to the left ventricle and from the right atrium to the right ventricle, respectively, after atrial contraction to fill the ventricles, in the third stage, the mitral and tricuspid valves close and the ventricles begin to contract without any volumetric changes, which causes blood pressure to increase. When the pressure is high enough, blood gets ejected from the heart (systole). Lastly, the heart muscle starts relaxing, the mitral and tricuspid valves open while the aortic and pulmonary valves close before a new cycle starts (Figure 2).

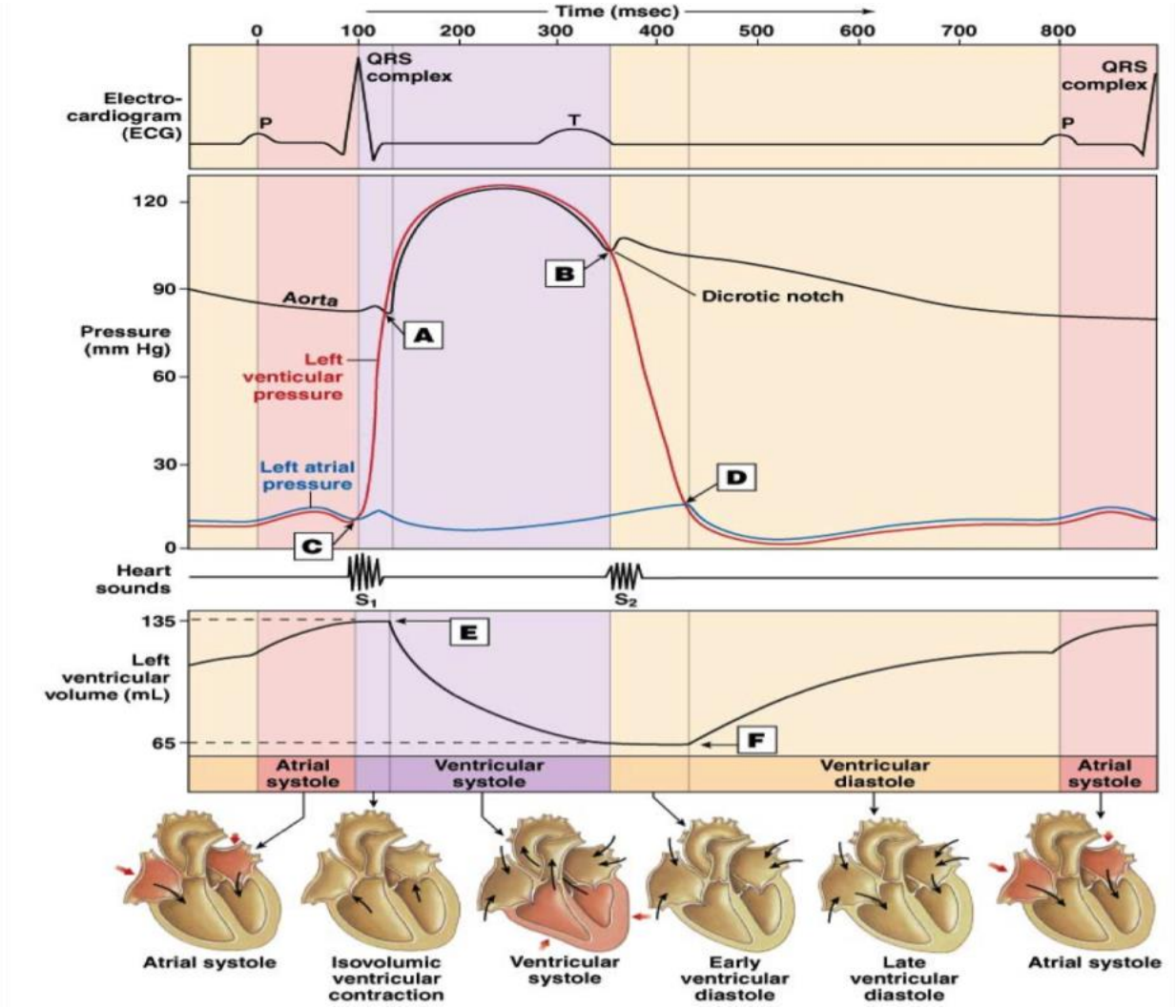

Figure 2: Timing of events in the left heart during the cardiac cycle (Marieb & Hoehn, 2013).

For the average human, the heart will beat approximately 80 million times a year without any stopping to rest except for a fraction of a second between beats.

2.2 Aortic valve anatomy and physiology

2.2.1 Aortic root

The aortic valve consists of the sinotubular junction, three aortic sinuses and three aortic leaflets (Figure 3).

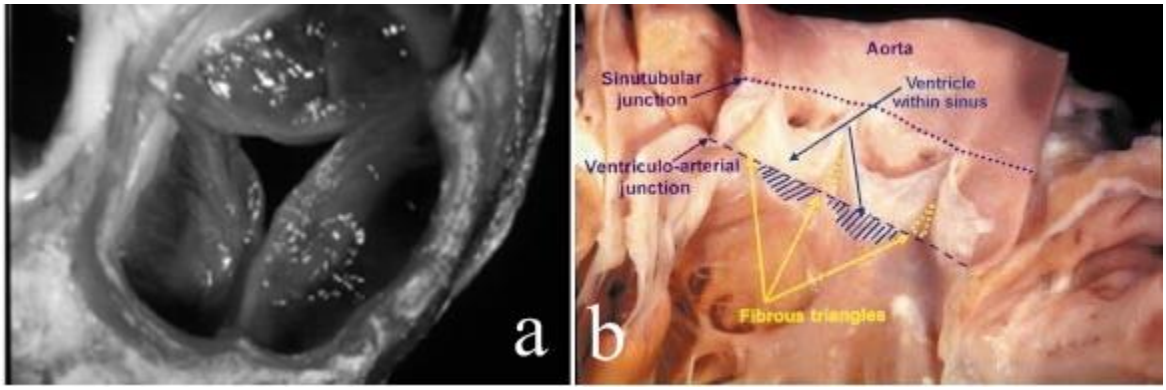

Figure 3: Anatomy of aortic valve: the neutral aortic valve in physiological condition in body (a) and flat view of aortic valve (b) (Anderson, 2000).

The sinotubular junction (STJ) is the region of the ascending aorta between the aortic sinuses and the superior aspect of the aortic root; it has a circular shape and supports the peripheral attachment of the aortic leaflets.

The expanded portions of the aortic root around the leaflet attachments compose the three aortic sinuses. The aortic sinuses are named according to their arising arteries as right-coronary sinus, left-coronary sinus and non-coronary sinus. The curved shapes of the sinuses

are thought to create sufficient gap between the aortic leaflets and the coronary arteries so that the aortic leaflets do not occlude the coronary inlets during systole (Underwood et al., 2000). This space is also supposed to improve the turbulent current behind the leaflets. According to this view, the aortic leaflets will be caught and closed by the blood flow at the end of systole. Finally, this specific shape for the sinuses can minimize the mechanical stress concentration between the aortic sinuses and the leaflets (Thubrikar & Robicsek, 2001).

Gundiah et al. (Gundiah et al., 2008) and Azadani et al. (Azadani et al., 2012) demonstrated that the aortic sinuses and the ascending aorta have different material properties. Gundiah's study showed that the aortic sinus is significantly stiffer than the ascending aorta, while both demonstrated anisotropic behaviors with the circumferential direction being stiffer than the longitudinal direction.

2.2.2 Aortic leaflets or cusps

The aortic valve comprises of three leaflets: the right-coronary leaflet, left-coronary leaflets and non-coronary leaflets. The aortic leaflets are different in size and are approximately cylindrical in shape when closed (Thubrikar, 1990; Clark et al., 1974).

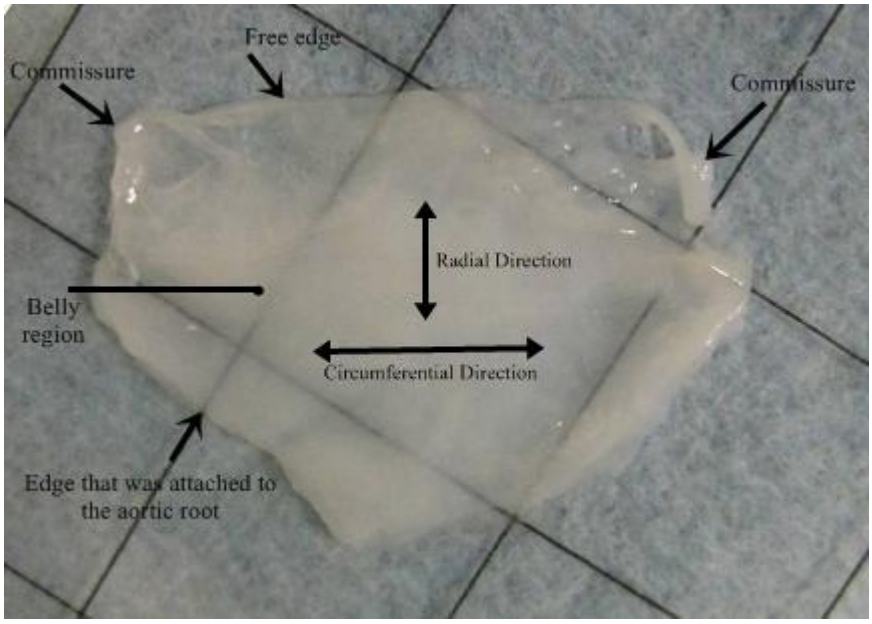

Figure 4: Detailed anatomy of an aortic leaflet.

The leaflets are connected to the aortic wall by the semilunar attachment line and the commissures (Figure 5) which are formed by two portions of attachment lines of adjacent leaflets running side by side (Figure 5).

During valve loading, adjacent leaflets come in contact with each other over the coaptation area and create a seal against backflow from the aorta into the left ventricle (Ho, 2009; Grande et al., 1998; Silver & William, 1965).

Measurements by Silver & William revealed that sinuses volume, sinotubular junction area and leaflets area increase with age and heart weight (Silver & William, 1965).

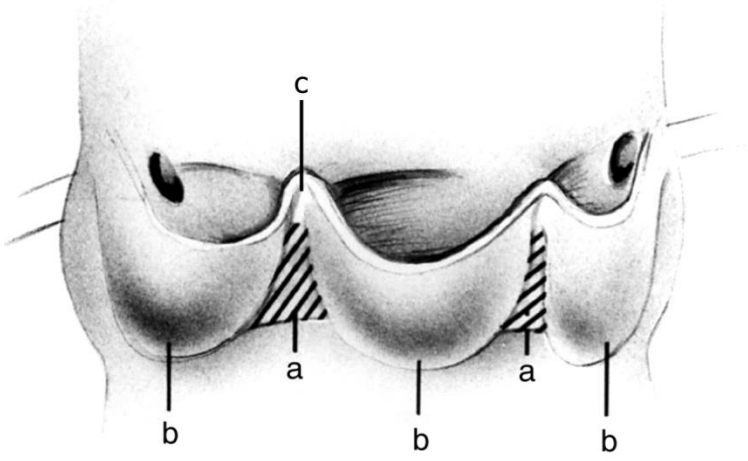

Figure 5: Flat view the aortic valve represent the leaflets (b) and interleaflets triangles (a) and leaflet commissures (c) (Underwood et al., 2000).

The aortic leaflets are pliable and thin in young people and become stiffer and thicker with age (Ho, 2009). The leaflets are also known to be thinner in the leaflet belly and the coaptation area, and thicker at the leaflets attachment and free margin (Grande et al., 1998).

The aortic leaflets are mostly (90%) water and connective tissue with unique mechanical properties. The main structural component of connective tissue consists of proteins collagen types I and III, elastin, GAG's (glycosaminoglycans - long chain sugars) and other small amount of cells. The internal collagen of leaflets forms a framework with three distinct layers: the fibrosa, spongiosa and ventricularis (Figure 6) (Robarts, 2007).

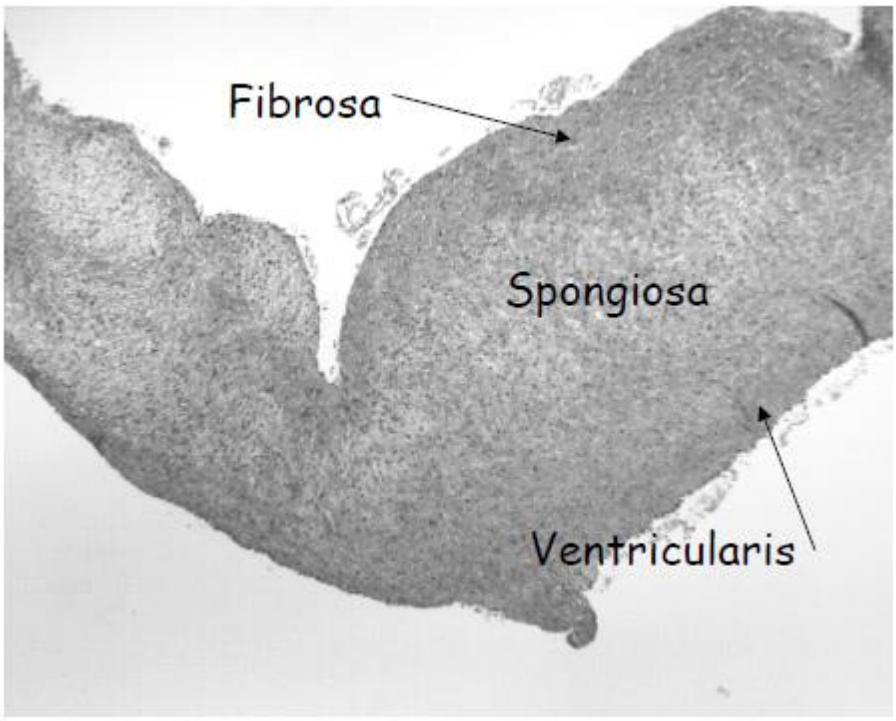

Figure 6: Aortic leaflet tissue showing the fibrosa, spongiosa and ventricularis. The fibrosa faces the aorta and the ventricularis faces the left ventricle of the heart (Robarts, 2007).

The layer facing the aorta is the fibrosa which is arranged as a series of parallel bundles of collagen fibers into a stretch-resisting sheet of tissue. Fiber bundles are oriented in a circumferential direction (Figure 7), starting at one commissure, then spreading out into an isotropic mesh near the belly and finally combining again at the opposite commissure to provide the essential strength of the leaflets. Radial expansion of the leaflets allows them to mate together and seal off the aortic orifice (Billiar & Sacks, 2000).

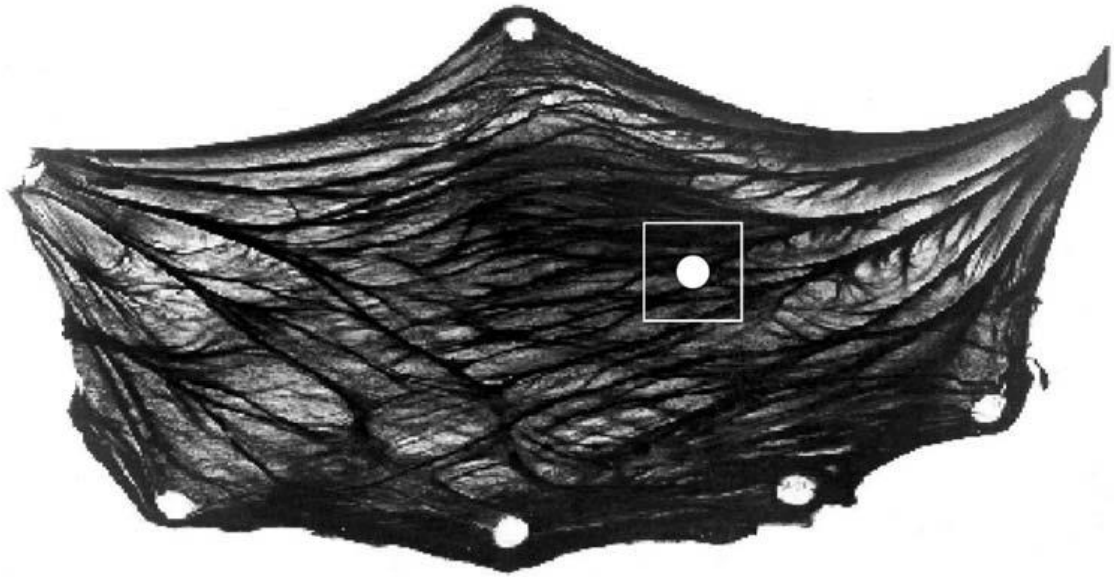

Figure 7: View of excised leaflet showing fiber bundles in the circumferential direction (Cox et al., 2006).

The ventricularis facing the left ventricle consists of elastin sheets and collagen. This layer has more extensible properties than the fibrosa due to its higher concentration in elastin. The spongiosa fills the space between the fibrosa and ventricularis and is composed of collagen, elastin, proteoglycans and mucopolysaccharides (Figure 8).

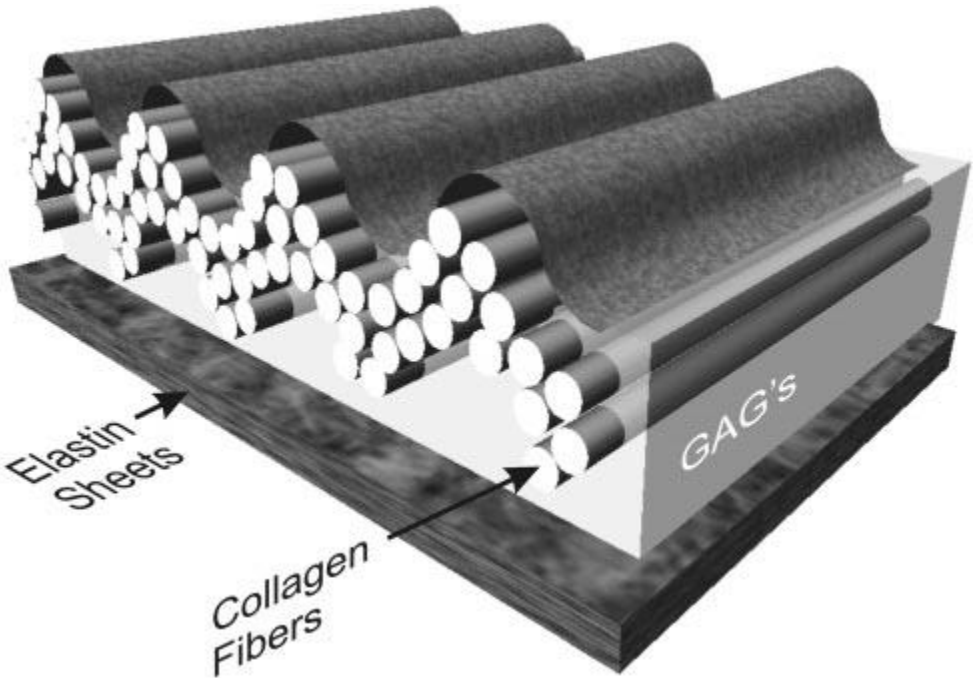

Figure 8: Leaflet layers arrangement (Vesely, 2005).

The spongiosa has a gelatinous, watery consistency due to its long, multi-chain proteins. The specific function of the spongiosa is not well understood; however it is believed that it is facilitates the localized movement and shearing between the fibrosa and the ventricularis during loading and unloading and thereby minimizes mechanical interaction between the two fibrous layers (Figure 9) (Stella, 2007; Robarts, 2007).

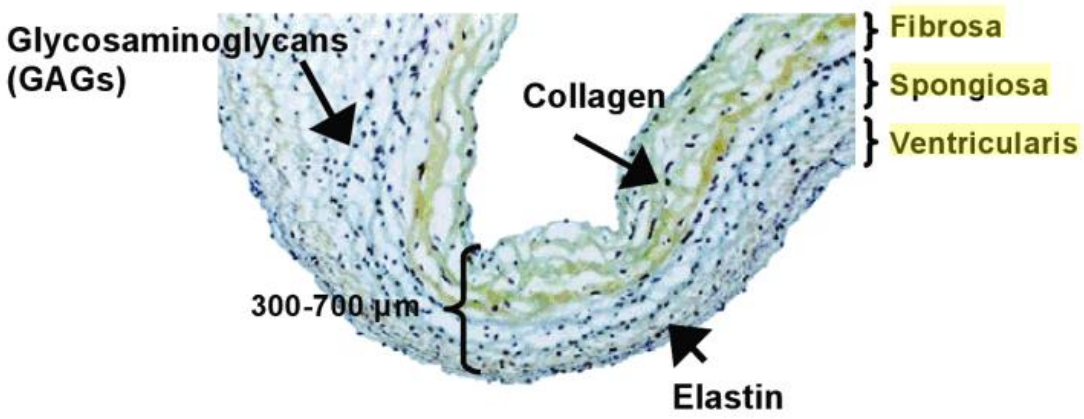

Figure 9: Leaflet layers arrangement (Peppas et al., 2007).

2.3 Valvular diseases

Diseases of the aortic valve are related to abnormalities and malfunction of the aortic valve (Thubrikar, 1990). The normal function of the aortic valve is to ensure that blood flows at the proper time, in the right direction and with adequate pressure. A valvular disease can be present at birth (congenital) or can be acquired as time passes, such as aortic valve stenosis (AS) and aortic insufficiency (AI) also known as aortic valve regurgitation. Congenital valve disease relates to abnormalities in the valve structure, such as bicuspid, unicuspid and quadricuspid valves. Bicuspid aortic valve disease is the most frequent congenital valve disease and bicuspid valves tend to become diseased more often than normal tricuspid valves (Thubrikar, 1990).

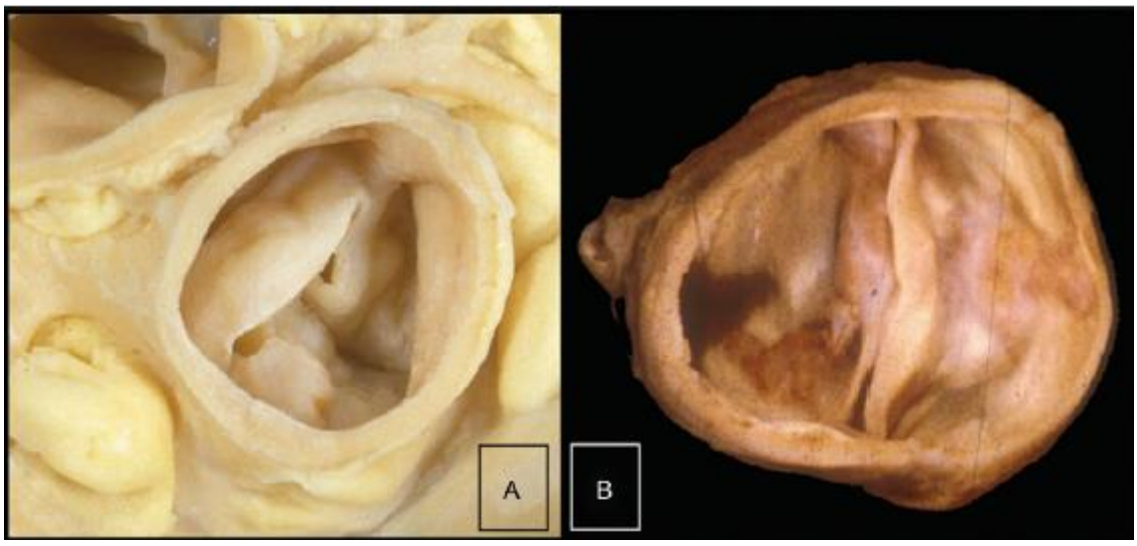

Figure 10: Calcified bicuspid aortic valve in two patients (Thubrikar, 1990).

2.3.1 Aortic valve stenosis

Aortic stenosis (AS) is the narrowing of the aortic valve orifice and obstruction of the left ventricular outflow tract. AS can develop later in life by calcium deposition on the aortic side of the leaflets or can be congenital by abnormality of the valve. When the opening of the aortic valve becomes narrowed, the left ventricle work load is significantly increased to maintain an adequate flow rate. The muscle in the left ventricle walls become thicker and dilate to support this extra load. Common causes of AS include leaflets degeneration and congenital valve malformations and inflammation, e.g. rheumatic fever (Figure 11).

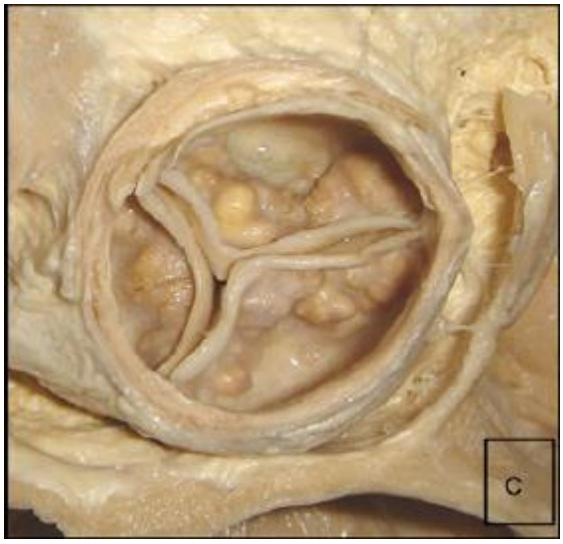

Figure 11: The aortic valve with three thickened leaflets (Ho, 2009).

In general, surgery is the primary treatment when narrowing becomes severe and symptoms develop, but in mild to moderate aortic valve stenosis without any symptoms, doctors will start medication and echocardiography to control the stenosis progression and the patient may never need surgery. Surgical treatment includes aortic valve replacement, balloon valvuloplasty (valvotomy), transcatheter aortic valve replacement (TAVR) and surgical valvuloplasty (Aksoy et al., 2013).

2.3.2 Aortic insufficiency

Aortic insufficiency (AI) is a disease where the aortic valve leaks. AI occurs when the aortic valve fails to close tightly and blood flows in the reverse direction during diastole, from aorta to left ventricle. AI can be due to abnormalities of the aortic valve and/or aortic root dilatation. Studies have shown that more than 50% of AI cases are due to aortic dilatation, 15% are due to congenital abnormalities such as bicuspid aortic valves, and the rest of the

cases are due to endocarditis in rheumatic fever and various collagen vascular diseases (Agabegi, 2008; Thubrikar & Robicsek, 2001). Consequently to AI, the left ventricle has to pump more blood to compensate the physiological blood flow rate. In this case, the muscle in the left ventricle enlarges, thickens (dilate) and loses its initial elasticity and efficiency. AI can be caused by age-related degeneration of the leaflets, endocarditis, rheumatic fever, congenital defects, and aortic enlargement associated with chronic hypertension. Patients with AI are at increased risk of developing heart valve infection (Figure 12).

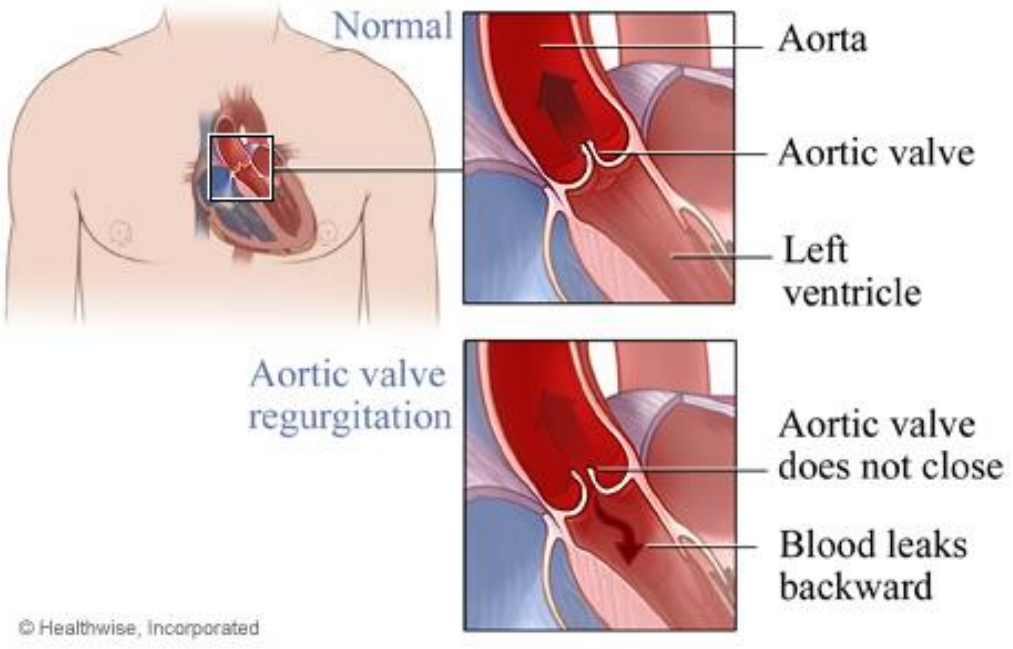

Figure 12: Normal aortic valve and aortic valve with aortic regurgitation illustrated in top and bottom of image respectively (Pai & Fort, 2011).

AI can be treated either medically or surgically, depending on the symptoms and severity associated with the disease process. As details below, the most popular surgical treatment is aortic valve replacement, an open-heart procedure in which the patient's aortic

valve is replaced with an alternate healthy valve (e.g. mechanical or bioprosthetic heart valve). Another option is aortic valve repair.

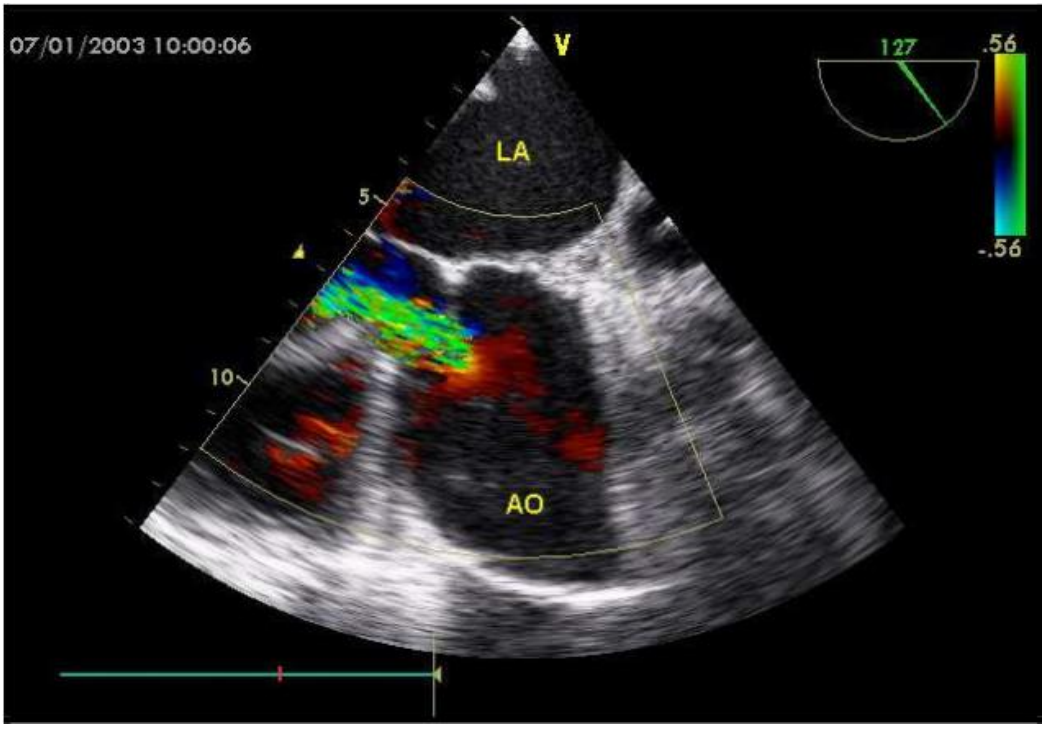

Figure 13: Doppler imaging of the regurgitant jet characteristic of aortic insufficiency (Čanádyová et al., 2011).

2.4 Surgical options

2.4.1 Aortic valve replacement

Aortic valve replacement (AVR) is the most frequent and standard surgery to treat pathologies of the aortic valve, including AS and AI. The first valve replacement was done in the 1950's and the number of AVRs has increased considerably in the past decades. Recent studies show that AVR numbers will continue to increase worldwide, from approximately 290,000 in 2003 to over 850,000 by 2050 (Yacoub & Takkenberg, 2005).

In typical AVR, the diseased aortic valve is replaced with a prosthetic heart valve. The common prosthetic valves can be classified in two major types: mechanical or bioprosthetic valves. Mechanical valves are fabricated from non-biological materials (e.g. pyrolytic carbon), while the bioprosthetic valves are made from biological tissue (e.g. treated porcine or bovine tissues) (Thubrikar, 1990). The main disadvantages of mechanical valves are thromboembolic complications (e.g. formation of blood clots) and the need for chronic anticoagulation therapy. However, this type of prosthetic valve is durable and lasts at least for 10 to 15 years. In contrast, bioprosthetic valves generally do not require anticoagulation, but they fail by tissue degeneration and are less durable than mechanical valves. The lifetime risk of reoperation or serious complications for patients undergoing AVR depends on the health and age of the patient as well as on the surgeon's skills. Bloomfield found that biological valves have a higher failure rate due to structural deterioration in younger patients. Their study showed that only a third of young patients who undergo AVR may are free of structural valve deterioration as compared to more than 90% of patients over 70 at the time of implantation (Bloomfield, 2002).

2.4.2 Valve-sparing procedures

While AVR is probably the best strategy in case of severe AS, AI is amenable to a wider array of surgical procedures where the original aortic valve of the patient may be left in place, hence the generic name of valve-sparing procedures. The large number of possible procedures has led to different attempts at rationalizing the decision process based on the pathophysiological mechanism of AI. For instance, Boodhwani and colleagues have developed a functional classification of AI as shown in Table 1.

Table 1: Functional classification of aortic regurgitation (Boodhwani et al., 2009).

Type I	**Normal leaflets motion with functional aortic annulus dilatation or leaflet perforation**
Ia	Ascending aorta dilatation and sinotubular junction enlargement
Ib	Valsalva sinuses and sinotubular junction dilatation
Ic	Dilatation of aortic annulus
Id	Leaflet perforation without a primary functional aortic annular lesion
Type II	Leaflet prolapsed
Type III	Leaflets retraction and thickening

Similarly, Table 2 lists different mechanisms of AI and recommended repair techniques (Boodhwani et al., 2009).

Table 2: Repair-oriented functional classification of aortic insufficiency and repair technique used. FAA: functional aortic annulus; STJ: sinotubular junction; SCA: subcommissural annuloplasty (Boodhwani et al., 2009).

AI Class	Type I Normal cusp motion with FAA dilatation or cusp perforation				Type II Cusp Prolapse	Type III Cusp Restriction
	Ia	Ib	Ic	Id		
Mechanism		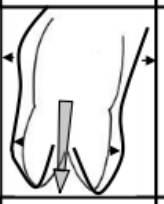	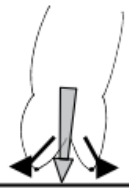			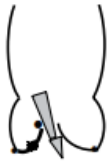
Repair Techniques (Primary)	STJ remodeling *Ascending aortic graft*	Aortic Valve sparing: *Reimplantation or Remodeling with SCA*	SCA	Patch Repair *Autologous or bovine pericardium*	Prolapse Repair *Plication* *Triangular resection* *Free margin Resuspension* *Patch*	Leaflet Repair *Shaving* *Decalcificatio* *Patch*
(Secondary)	SCA		STJ Annuloplasty	SCA	SCA	SCA

As illustrated in Table 2 (case Ia), supracommisural ascending aorta replacement may be sufficient in patients with isolated dilatation of the sinotubular junction (STJ) and ascending aorta. A Dacron tube prosthesis with a diameter larger by 10% (2 or 3 mm) than the native aortic annulus is used to replace the dilated portion of the aorta (Figure 14). Restoration of a normal diameter of STJ is important and adequate to correct the aortic incompetence. Harringer et al. demonstrated that ascending aorta replacement may achieve perfect coaptation of the valve leaflets with no or only trace AI. This technique is associated with good durability and low mortality, lack of anticoagulation, and acceptable hemodynamics (Harringer et al., 1999).

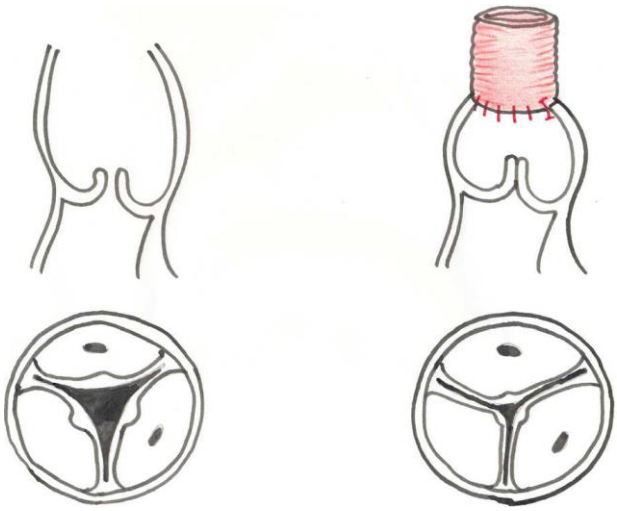

Figure 14: Ascending aorta replacement (Čanádyová et al., 2011).

Yacoub and colleagues believe that valve-sparing procedures are suitable for the aortic valve complex and dynamic geometry to preserve their hemodynamic functions. In Yacoub's remodeling technique (Table 2, case Ib), the prosthesis is sized 10% larger than the native annulus diameter or equal to the STJ diameter. Then, a Dacron tube graft is trimmed to produce three separate tongue-shaped portions to replace the sinuses. After this step, the

Dacron tube graft is sutured to the aortic annulus and top of the commissures and the coronary arteries are finally attached to the Dacron tube (Figure 15).

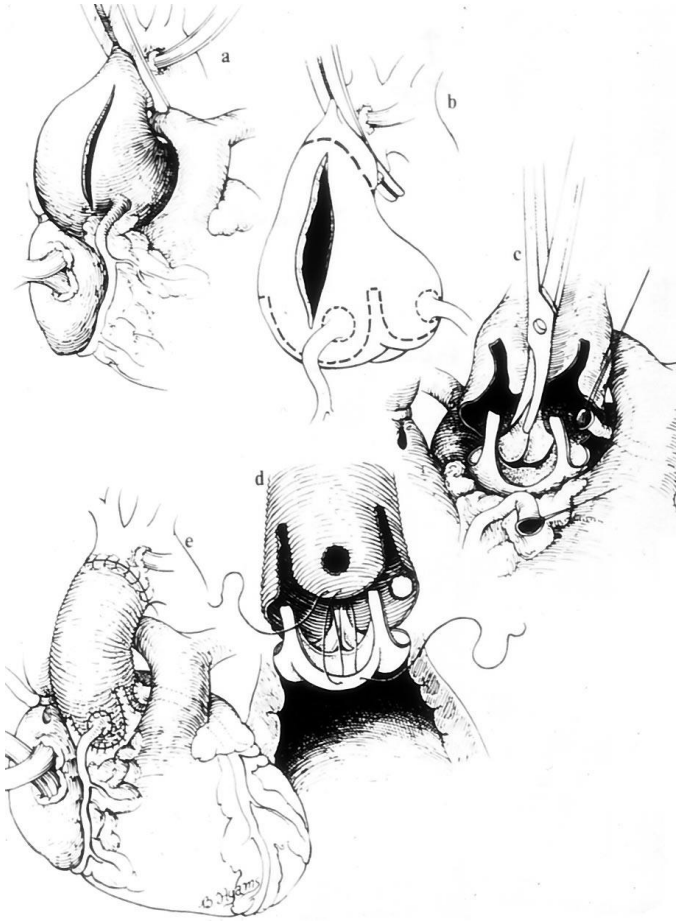

Figure 15: Complete steps of Yacoub remodeling technique of the aortic valve (Yacoub & Takkenberg, 2005).

The remodeling technique has been shown to maintain the dynamic behavior of the valve and can be implemented in large groups of patients with aneurysm or dissection of the aortic root. Early and long-term results are encouraging, especially in patients with early signs of disease (Yacoub et al., 1998).

In another variant of the valve-sparing technique introduced by David and Feindel and called reimplantation, the aorta is cut above the STJ and the diseased sinuses of Valsalva are resected leaving approximately 3-5 mm of aortic wall attached. Dacron tube graft prosthesis is selected with diameters 50% smaller than the average length of the free margins of the aortic leaflets. After this step, the graft height is matched to that of the unrestricted LC/NC commissure (Figure 16).

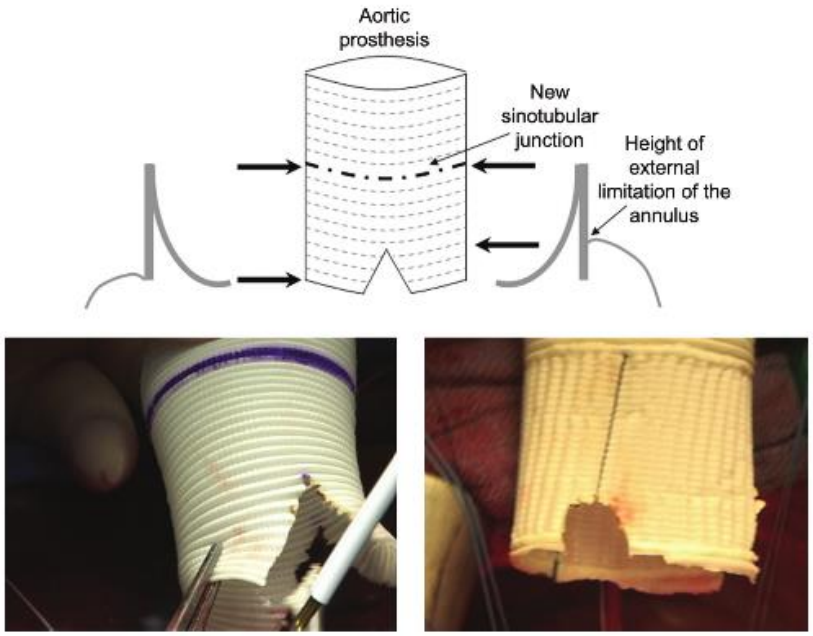

Figure 16: Diagram and pictures showing prosthesis preparation in reimplantation technique (Boodhwani et al., 2009).

The prosthesis is implanted between the native ascending aorta and the remaining sinuses and finally the coronary arteries are attached to the prosthesis (Figure 17). Boodhwani et al. noted that systematic AV reimplantation can result in consistent and excellent long-term outcomes (Boodhwani et al., 2009; Čanádyová et al., 2011).

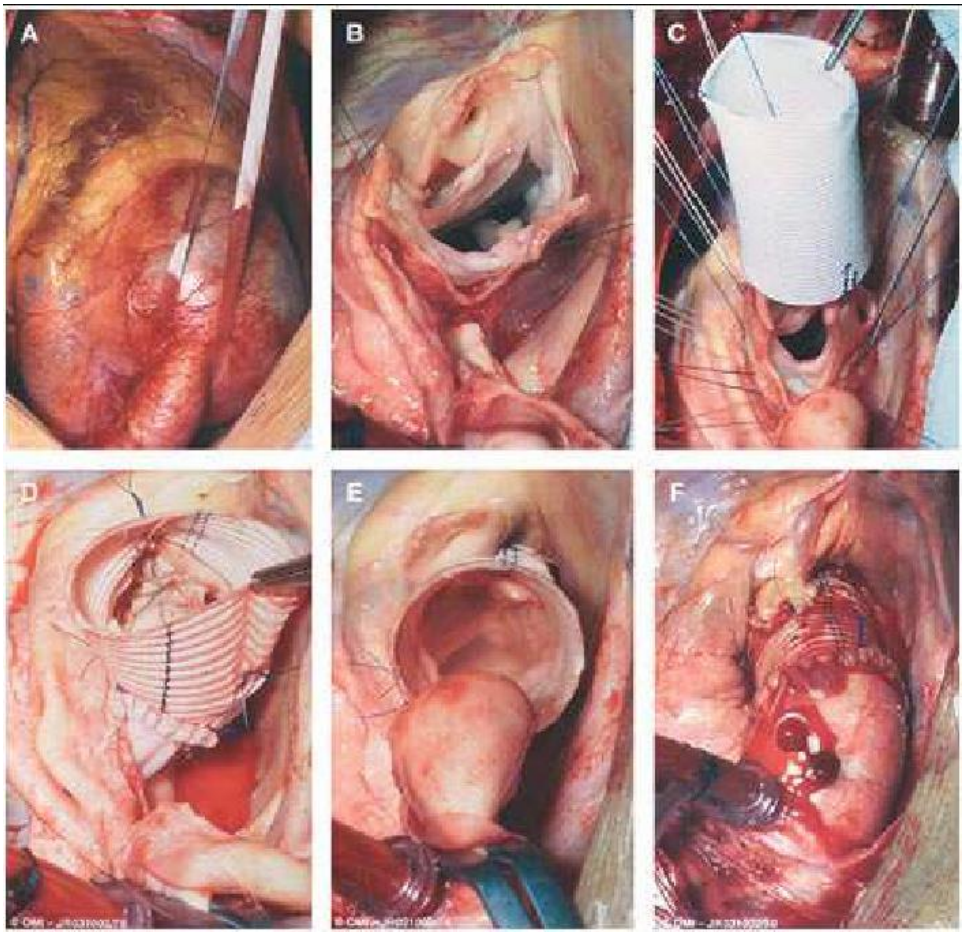

Figure 17: A: dilated root, B: after resecting the diseased Valsalva sinuses and preparing the coronary artery buttons. C, D: reimplantation of the aortic valve into the prosthesis, E, F: distal anastomosis between the graft and the native ascending aorta (Čanádyová et al., 2011).

Lansac et al.'s experimental study combined the remodeling and reimplantation techniques. They replaced the aortic root by a Dacron tube graft and then used the root reconstruction technique which was standardized by scalloping a bulged graft (Gelweave Valsalva) in three symmetric neo-sinuses. This study revealed that the remodeling procedure improved the reproducibility of subvalvular external aortic annuloplasty and short-term results (Lansac et al., 2006).

Underwood and colleagues developed surgical reconstruction instead of valve and ascending aorta replacement. They used transesophageal echocardiography (TEE) to assess the valve dimensions and disease severity to plan for the surgical procedure. In diseased ascending aorta with a normal annulus, a Dacron tube graft was chosen 10% smaller than the annulus diameter; the graft was then trimmed to shape crescent-like incisions. The graft was finally sutured to the supravalvular region to create sinuses (Figure 18).

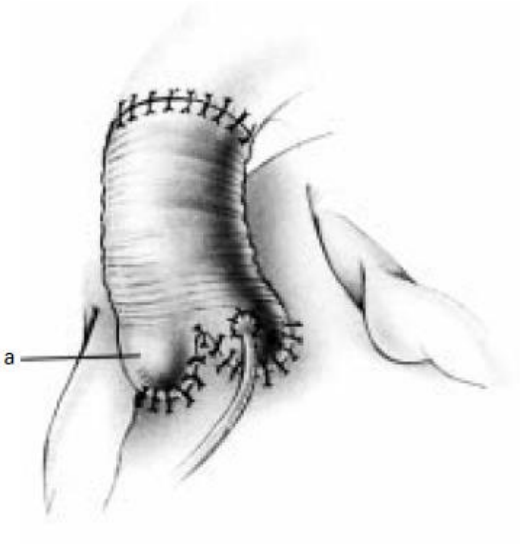

Figure 18: Complete remodeling (Underwood et al., 2000).

In cases with dilated ascending aorta and/or annulus, annuloplasty can be added to the procedure (Figure 19). This is meant to control the annulus dilation by placing a Teflon belt on the outside of the aortic root in the horizontal plane below the leaflets level (Table 2, case Ic). The preoperative and postoperative follow up confirmed that this technique is successful in restoring valve competence without any significant mortality change compared to root replacement (Underwood et al., 2000).

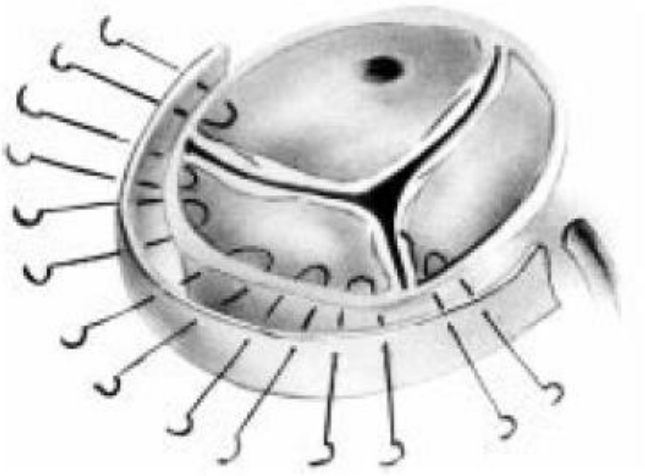

Figure 19: Technique of aortic annuloplasty (Underwood et al., 2000).

Matalanis et al. observed that patients with aortic root dilatation and leaflet prolapse (leaflet prolapse arises when coaptation between neighboring leaflets occurs below the physiologic plane of coaptation) develop early failure when they underwent aortic valve-spring surgery with only root geometry correction. They showed that patients with root geometry and leaflets prolapse correction have equivalent durability to patients with non-prolapsing leaflets (Matalanis et al., 2010). Leaflet prolapse correction is achieved by another level of surgical refinement, one where, in addition to replacing/resizing the aortic root, the leaflets may individually be resized to achieve valve competence. This is the full aortic valve repair, as detailed next.

2.4.3 Aortic valve repair

Patients with aortic valve and annulus dilatation regularly have leaflet pathology that requires treatment. Repair techniques for AI and particularly for leaflet diseases are implemented often and heterogeneously (Boodhwani et al., 2009; Boodhwani et al., 2009). Better hemodynamic function and freedom from anticoagulation treatment are the major benefits of repair compared with replacement with a prosthetic valve, while the disadvantages are the lack of a common framework, early failure risks of reconstructed valve that develop AI again and need early reoperation (Boodhwani et al., 2009; Boodhwani et al., 2009; Miller, 2007). Successful repair can be achieved if the surgeon addresses the specific anatomical defects with high surgical flexibility, knowledge, and adequate surgical tools in his armamentarium (Langer et al., 2004; Boodhwani et al., 2009).

Leaflet prolapse is a pathologic mechanism of AI which is exhibited by up to 50% of patients undergoing aortic valve repair surgery (Boodhwani et al. 2009). For instance, leaflet prolapse is a frequent disease in bicuspid aortic valves which is caused by distension of the free margin of a leaflet. The free margin plication and free margin resuspension techniques are available to correct leaflet prolapse. As illustrated in Figure 20, the free margin plication technique decreases the leaflet belly distension by performing a suture in the center of the free margin and then extending it perpendicular to the free margin to preserve the natural leaflets shape (Boodhwani et al., 2009; De Kerchove et al., 2009).

Figure 20: Free margin placation: determination of excess leaflet tissue (a) and extension of leaflet plication onto the leaflet body (Boodhwani et al., 2009).

The resuspension technique shown in Figure 21 is performed by passing the suture twice at the top of the commissure and over the length of the free margin in a running fashion. This technique controllably reduces the length of free margin until it becomes the same as that of the adjacent reference leaflet (Boodhwani et al., 2009; De Kerchove et al., 2009).

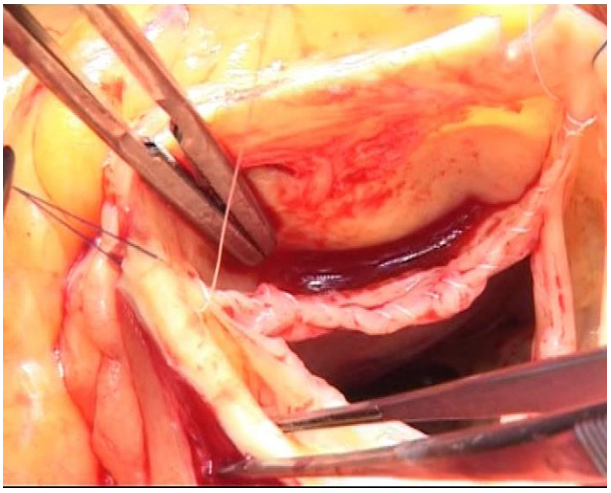

Figure 21: Free margin resuspension on right coronary leaflet, whereas the left coronary and non-coronary leaflet appears to be normal (Boodhwani et al., 2009).

Boodhwani et al. confirmed that free margin plication and free margin resuspension are effective and durable techniques to correct the leaflet prolapse with or without aortic root pathology. Furthermore, these two techniques can be used alone or in combination without any difference in midterm outcome. However, free margin plication, due to its ease of use and lower risk is the first choice in leaflet prolapse, although free margin resuspension is recommended in specific situations (Boodhwani et al., 2009; De Kerchove et al., 2009).

Le Polain de Waroux et al. showed that intraoperative TEE can be used for patients who undergo AI valve repair to assess the risk of AI developing; they also showed that the patients with a coaptation height of more than 4 mm have less risk of AI (le Polain de Waroux et al., 2009).

2.5 Computational modeling of the aortic valve

Although many studies have been carried out about heart valves, understanding of their unique material properties and complex function still needs improvement. Various methods have been used to study the aortic valve, namely in vivo studies using cardiac imaging, in vitro experimental tests, and numerical simulations. Computational models of the aortic valve have been utilized to study both normal and diseased valves and to better understand the aortic valve behavior. The advantage of computational modeling over other methods of investigation is that varied range of inputs can help researchers to analyze and explore their models as different replacement materials or tissues and various assumptions can be made; in turn, the models may be used to predict the durability and long-term durability of repair method, as they provide information about mechanical stress which is otherwise not measurable experimentally.

In complement to substantial progress made recently in terms of the geometrical description and of the material properties of the aortic valve, computational studies using finite element (FE) models have revealed important information about stress-strain patterns in the aortic valve and may be used to assess potential valve failure mechanisms. Briefly, the first step in finite element modeling consists in creating the geometry of interior, meshing it with adequate elements, assigning material properties to these elements and then setting appropriate loads and boundary conditions. Next, the FE program solves the equilibrium equation simultaneously for each element. Ultimately, structural results such as stress, strain and displacements for the whole model are obtained.

A number of computational challenges have always been present in modeling the aortic valve, such as its complex geometry, unique relation between components, large range of motions and dynamics. Dealing with all of these issues simultaneously is quite difficult and also increases the complexity of the analysis.

In 1990, Huang et al. proposed a two dimensional FE model based on their experimental behavior of bovine pericardial tissue (Sheffield bicuspid valve). They considered two models based on radial and circumferential cross sections using an updated Lagrangian method in order to capture the dynamical behavior. The model was used to compute the stress distribution in the deformable leaflets based on the assumption of hyperelastic material (Huang et al., 1989).

Black et al. established a three-dimensional (3-D) Sheffield bioprosthetic geometry based on real valve measurements and applied a nonlinear elastic material. They proved that accurate results were not achieved by 4-node shell elements (Black et al., 1991).

Grande et al. developed an FE model of the aortic valve based on a realistic geometric from the MRI images incorporating the valve's inherent asymmetry using ANSYS software. They assigned anisotropic material with higher order elastic shell element in their FE analysis. The results showed peak strain in the root sinus walls and the leaflets, and higher stress in the belly near the coaptation surface and the free margin. Furthermore, they found that the different stress distribution in the sinuses and leaflets are due to their asymmetry. This study also revealed that increasing the root dimensions and stiffness will increase leaflets stress and strain and will affect the leaflet coaptation area (Grande-Allen et al., 2001; Grande et al., 1998).

To understand the behavior of a normal valve, Labrosse et al. described a range of dimensions in normal aortic valves and then established geometric guidelines to allow for proper functioning of the leaflets (Labrosse et al., 2006). They measured silicone rubber casts of human aortic valves in closed position and developed the analytical equations to explore a fully 3-D geometric model.

Recognizing that the material definition of aortic valve leaflets has considerable effects on the valve mechanical behavior and failure mechanisms, Li et al. developed a static finite element model of a porcine aortic valve using a nonlinear anisotropic material with non-uniform thickness based on 8-node super-parameter nonlinear shells. They demonstrated that nonlinear anisotropic behavior can notably affect the stress distribution is the valve leaflets. Furthermore, it was inferred that maximum stress location and longitudinal stress distribution may be changed with the valve nonlinearity (Li et al., 2001).

Recent work investigated the variations in material properties between the different valve components (Gundiah et al., 2008; Azadani et al., 2012).

Arcidiacono et al. studied the effect of orthotropic properties of bovine pericardium on the mechanical behavior of tricuspid bioprosthetic aortic valves. The result showed that small variations in the material's principal axes can change the displacement and stress distribution in the leaflets. The authors claimed that manufacturing processes can optimize bovine pericardium properties to be similar to those of natural human heart valves in order to increase the durability of pericardial bioprosthetic valves (Arcidiacono et al., 2005).

Labrosse et al. developed a FE model based on experimental measurements using anisotropic hyperelastic material properties. The model was run with LS-Dyna software with brick elements under time varying pressures. The analysis illustrated that the leaflets attachment near the commissures experience the highest stresses in the model. Furthermore they confirmed that a dry model (wherein the fluid flow is not included and time-varying pressures are used instead) can be appropriate for dynamic structural analyses of the aortic valve (Labrosse et al., 2010).

Ranga et al. developed a numerical model of the aortic valve to investigate the effect of reimplantation and remodeling procedures. This model could help to evaluate the dynamic and hemodynamic functions of the valve. The control model was validated using MRI imaging data; then, remodeling with a shaped graft and reimplantation with a straight conduit were modeled. The results revealed that reimplantation increased the peak velocities and that small vortices may cause rapid valve closing. In addition, high stress was seen in the leaflet belly that may induce long-term issues with reimplantation; on the other hand, remodeling was closer to the normal aortic valve and provided better dynamic and flow pattern as compared to the normal state. They used linear material properties for the aortic tissues,

which is not adequate and may have significant effect on the hemodynamic function as well (Ranga et al., 2006).

Soncini et al. developed a FE model to analyze the David and Yacoub surgical techniques during a cardiac cycle. They created the model in commercial FE analysis software and assumed identical leaflets sizes with linear elastic and isotropic material properties for all the components. The results demonstrated that mechanical stress was increased in all leaflets, particularly in the commissural region, in the pathological models as compared to the normal valve and that Yacoub's technique is more adequate in term of coaptation area and valve opening, although surgeons are more interested in David's technique for its durability and ease (Soncini et al., 2009).

Conti et al. started from MRI images to create a realistic FE model of the physiological aortic valve and examined the geometric differences between leaflets and sinuses with non-linear and anisotropic material properties. The results again showed that anatomical differences cause variations in stress and strain patterns. The FE model was validated against experimental data in terms of real aortic valve function, leaflets coaptation and stretch, and timing of aortic valve leaflets opening and (Conti et al., 2010).

Auricchio et al. simulated a tissue valve based on CT-A imaging to provide better understanding of valve physiology. The FE simulation indicated that valve size and anatomical differences affect the stress distribution in the leaflets, the expected durability and the performance of the prosthesis, and the leaflet coaptation area. Furthermore, this study showed that choosing appropriate prosthesis size is more important than the actual position of the valve and the suturing sites (Conti et al., 2011).

Koch et al. presented a computational model of the aortic valve using hyperelastic, anisotropic material properties for the leaflets to explore the effect of leaflets non-linearity on the valve mechanics. The material parameters were obtained from curve fits to results of orthogonal uniaxial tensile tests on porcine aortic valve leaflets. The computational static analysis indicated similar circumferential maximum stresses in the leaflets models. In contrast, nonlinear elastic leaflets also showed identical stress and strain distribution that is relevant to its long term scaffold stability and cell mechanics furthermore not sufficient coaptation surface which proved significant impact of transverse isotropy and hyperelastic effects on leaflet mechanics (Koch et al., 2010).

Labrosse et al. presented a FE model to simulate the dynamic function of normal and repaired valves. They implemented the resuspension and central or commissural placation techniques in a normal valve to determine the surgical technique with the best performance. The geometry was discretized with a hexahedral brick mesh and hyperelastic, anisotropic material properties in commercial finite element software LS-Dyna. The results revealed the one-row leaflets resuspension technique as the best technique compared to the other techniques in terms of mechanical stress, valve orifice area and coaptation area. In particular, leaflets stress did not change significantly with the resuspension technique while it increased notably with the central and commissural techniques. Furthermore, the leaflet coaptation area was larger with resuspension than the other techniques, thereby promoting better sealing performance (Labrosse et al., 2011).

Aortic valve reconstruction with autologous pericardium is an effective surgical treatment. Hammer et al. investigated the height and widths of graft to achieve effective sealing with the native leaflets element an FE model. They described the native and

pericardium as anisotropic, hyperelastic materials. They showed that the graft must be significantly larger in both height and width to achieve normal coaptation area and proper valve closure. They validated their results against experimental data in porcine valves (Hammer et al., 2012).

In conclusion, the careful review of experimental and structural modeling studies reveals that various candidates for leaflets graft material have not been fully investigated before, although this topic deserves attention. This is what motivated the experiments described next.

3 Experiments

As discussed earlier, aortic valve repair has evolved into an alternative strategy for the correction of AI (Fattouch et al., 2012; Carr & Savage, 2004). Attempts to replace leaflet tissue with biological material have been made since the 1960s with materials such as dura mater, facia lata, and bovine pericardium (Hearn et al., 1973; Puig et al., 1972; Al-Halees et al., 1998). Glutaraldehyde-treated bovine pericardial patch and either treated or non-treated autologous human pericardial tissue are common replacement materials used in both cardiac and vascular surgery (Boodhwani et al., 2010; Lausberg et al., 2006). Pericardial patch repair may be used for 2 distinct cases. The first entails leaflet restoration due to either leaflet perforation or after resection of a restrictive, calcified raphe in the bicuspid aortic valve. The second scenario includes pericardial leaflet extension whereby pericardial tissue is added to the free margin in efforts to augment the coaptation surface (Boodhwani et al., 2010).

While no significant recurrence of AI was determined at mid-term follow-up when autologous pericardium was used for Aortic valve repair (Doss et al., 2008), long-term recurrent AI was demonstrated in a predominately porcine pericardial patch technique used for leaflet restoration (Boodhwani et al., 2010). Thus, while the perfect replacement material remains elusive, we intended to ascertain which material(s) would be best suited in the setting of leaflet restoration. The pericardial patch repair for complex aortic regurgitation lesions with augmentation or partial replacement is typically placed in fixation solution like 0.2 % glutaraldehyde before correcting the leaflet defect.

As detailed below, multiple healthy (control) aortic valves and valves repaired with four types of graft replacement material were analyzed in the left-heart simulator.

3.1 Materials and Methods

3.1.1 Left-heart simulator

The Vivitro left-heart simulator (Vivitro Lab Inc., Victoria, BC, Canada) was used as a pulse duplicator to produce physiological flow, pressure, and generate a range of cardiac outputs (Figure 22).

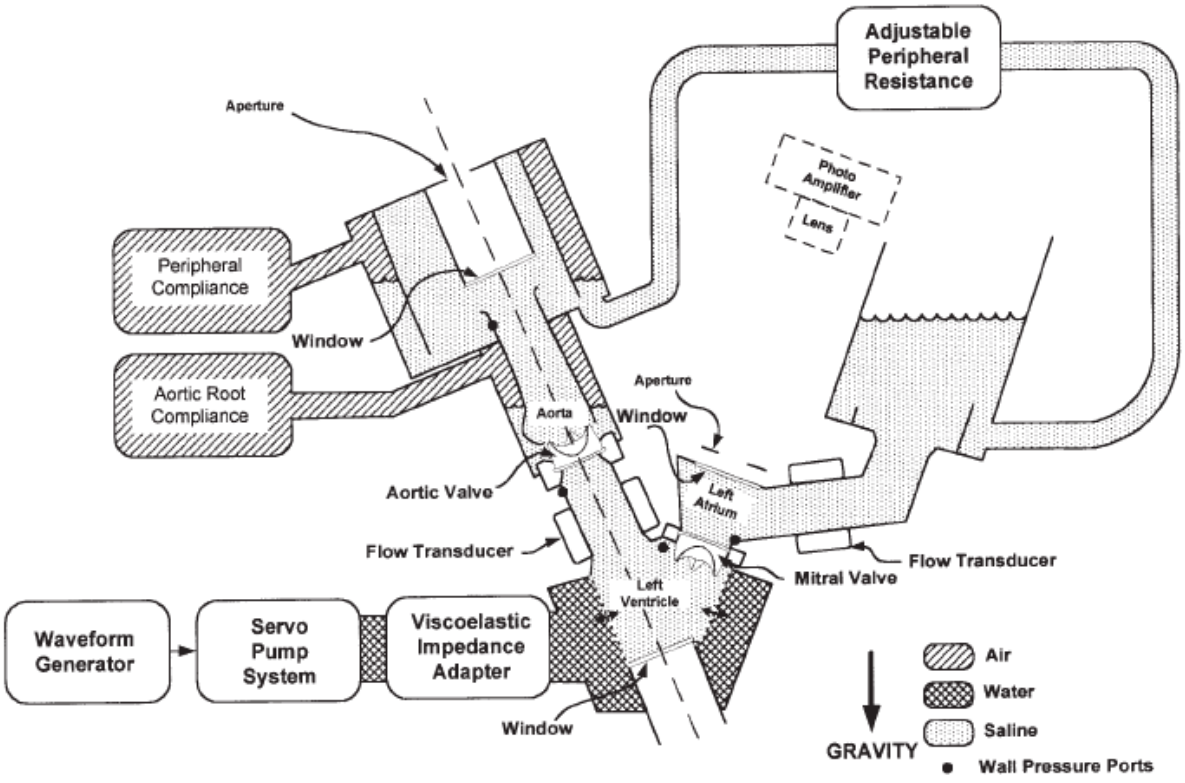

Figure 22: Schematic of ViVitro left-heart simulator (ViVitro systems).

The system consists of several components including a piston pump system driven by a wave form generator, a left ventricular membrane, a visco-elastic impedance adaptor for afterload generation, flow and pressure monitoring systems and a data acquisition system (Figure 22).

The linear actuator (pump) driven by a waveform generator converts the rotary motion of the electric motor into linear displacement of a piston using a ball-screw system. The piston drives a volume of water in a confined transparent hydraulic chamber limited on one side by a flexible membrane representing the left ventricle. The membrane is made of silicone rubber with a density of 1,200 kg/m^3, a thickness of 0.584 mm, a tensile strength of 9 MPa, and a quiescent volume of 133 ml. The visco-elastic impedance adaptor is used to adjust the pressure and flow waveforms created by the piston motion via a combination of resistive and compliance elements. Pressure sensors are located at selected points in the chamber to monitor pressure in the aorta, mitral valve, aortic valve and left ventricle. The flow measuring system records the cardiac output using an electromagnetic flow probe. The flow probe requires a conductive fluid such as saline to function. Acquisition of the pressure and flow data is run by the VIVITEST software sold with the ViVitro system (Figure 23).

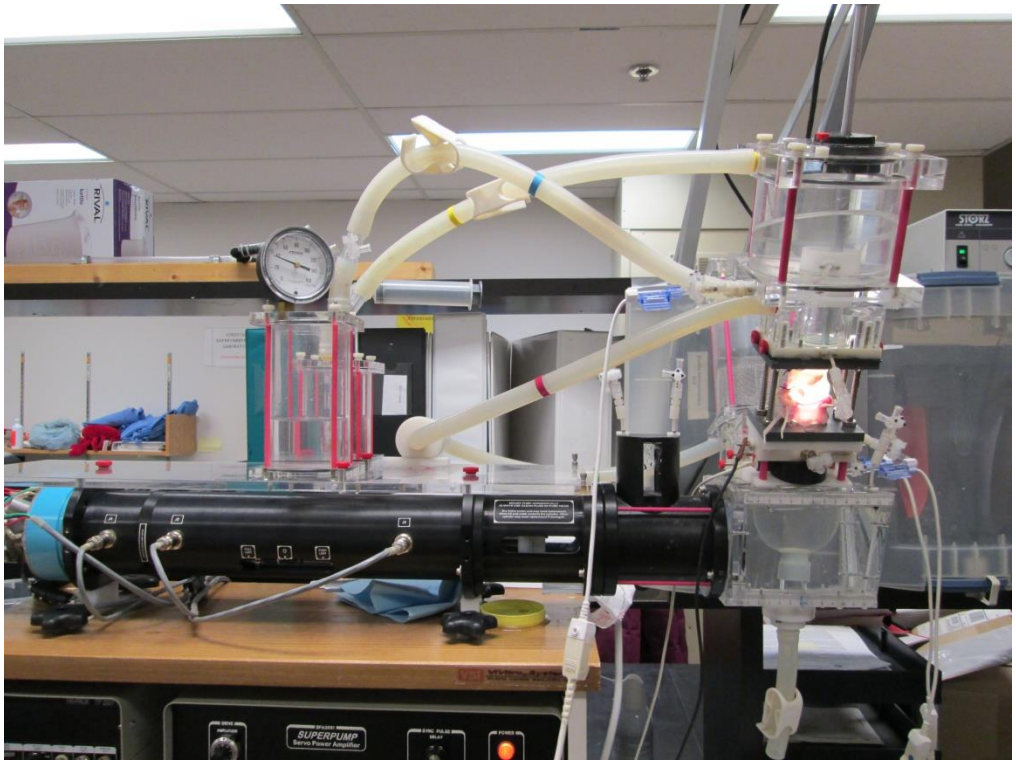

Figure 23: Left –heart simulator (ViVitro systems)

The left-heart simulator is typically designed for testing prosthetic valves, so natural valves cannot easily be fixed to the simulator. Toward this goal, an adjustable jig was used to attach the unrepaired and repaired aortic roots to the left-heart simulator. The jig was composed of two horizontal plates with top and bottom cannulas for appropriate connections. The two plates can be adjusted to appropriate lengths using four screws at the corners of the plate (Figure 24). For this experiment, a longitudinal stretch ratio of 1.2 was applied (Fung & Han, 1995).

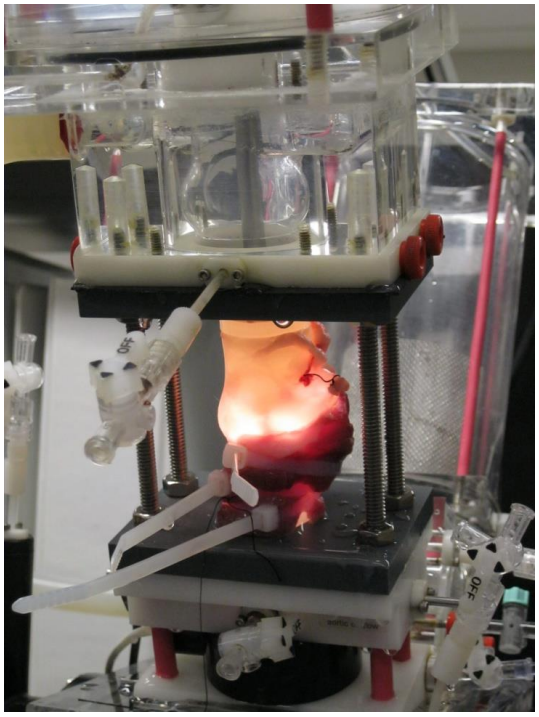

Figure 24: An unrepaired aortic root was mounted in the jig.

In addition, a high-speed camera (Phantom V4.2, Vision Research, Wayne, NJ, USA) was used to investigate the valve kinetics during the cardiac cycle. This camera can capture up to 2,000 frames per seconds. The camera connects to an endoscope and light source to acquire good views of the aortic root.

The system, containing 0.9% normal saline (density of 0.9 g/ml and a viscosity of 1 mPa.s) as the fluid medium, was pressurized to a systolic pressure of 120 mmHg and diastolic pressure of 80 mmHg. The heart rate was set at 70 bpm for all the experiments, while the cardiac output was set at 2.5, 5.0, or 6.5 L/min.

3.1.2 Control aortic roots

Twenty five (*N*=25) porcine aortic valves along with 6 cm of ascending aorta were obtained from a local abattoir. The valves were carefully dissected out from the cardiac muscle and any excess fatty tissues were removed around the aortic valve. After separating the valve, the coronary ostia were blocked using 0-silk sutures (Ethicon, Johnson & Johnson Inc., Montreal, Canada). All surgical procedures were performed by a trained cardiac surgery resident (Dr. Hadi Toeg with the University of Ottawa Heart Institute). Throughout the experiments, the aortic valves were soaked in saline solution containing 0.9% normal saline to preserve the freshness of the samples (Figure 25).

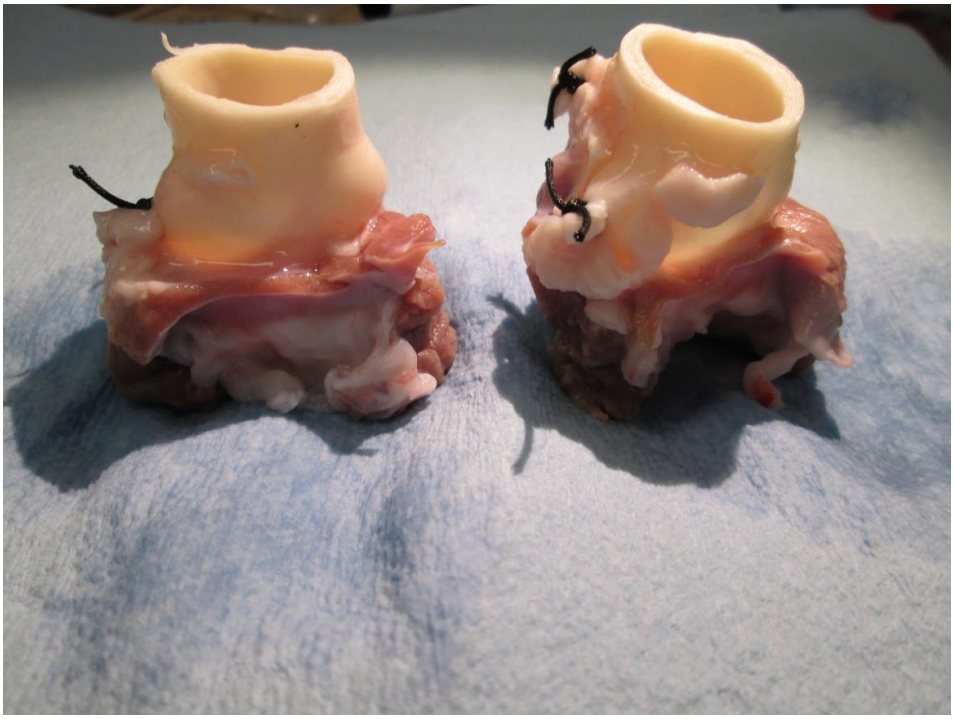

Figure 25: Unrepaired aortic valves after removing fatty and muscle and blocking their right and left coronaries.

3.1.3 Valve repair with non-coronary cups replacement

After the baseline recordings in the control valves, a transverse aortotomy was created 1 cm above the sinotubular junction (Figure 26).

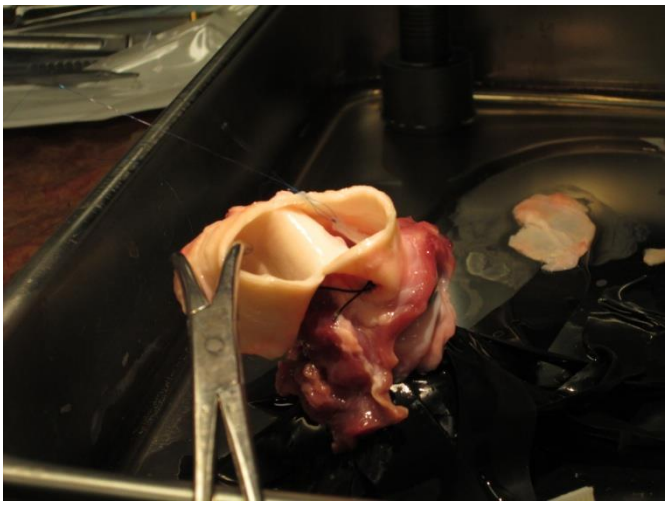

Figure 26: Transverse incision above the sinotubular junction.

The non-coronary leaflet was resected leaving only a small 3 mm cuff of tissue remaining attached to the aortic wall. An outline of the excised leaflet was used to cut out similar sized leaflet tissue from various replacement materials (Figure 27) as will be explained shortly.

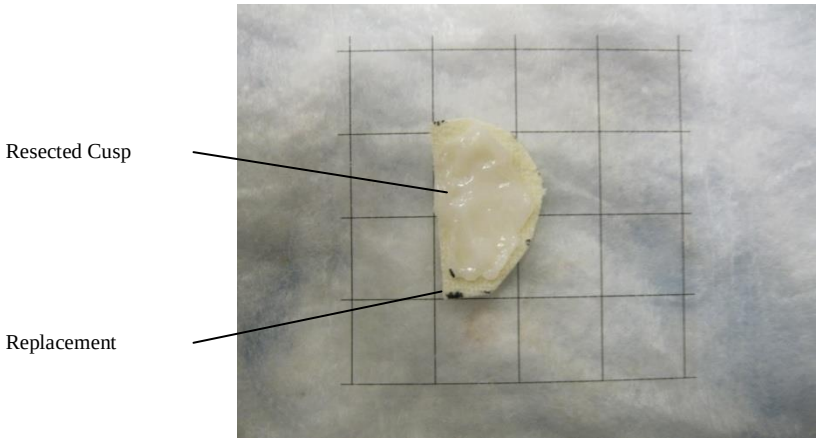

Figure 27: Sizing the replacement material graft using the resected leaflet.

The replacement material was then connected, at both lateral edges, with two 6-0 prolene sutures (Ethicon) to both commissures. Suturing was done in a continuous fashion from one commissural margin to the next (Figure 28).

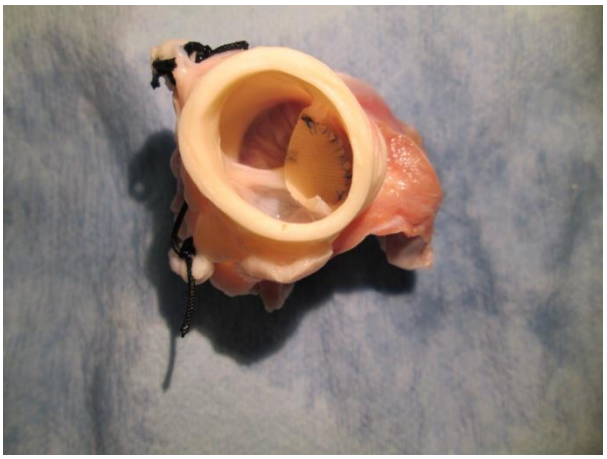

Figure 28: Repaired aortic valve after replacing the non-coronary leaflet with the replacement material graft.

The transverse aortotomy was closed in double layers with 5-0 prolene (Ethicon). Subsequently, post-aortic valve repair measurements were made (Figure 29).

Figure 29: Repaired aortic valve after closing the transverse incision.

Four clinically relevant replacement materials were used in this study, all of which were donated in-kind by their respective companies. The first material was derived from fresh porcine pericardial tissue kept in 0.9% normal saline. This replacement material will be referred to as autologous porcine pericardium (APP) (N=7). Next, a collagen impregnated double woven Dacron HEMASHIELD patch™ was used (N=7). This material is commonly used in both cardiac and vascular surgery (Vermeulen et al., 2001; AbuRahma et al., 2001). Another material utilized was CorMatrix™ (CorMatrix™, Roswell, GA, USA) (N=5). This material is derived from porcine small intestinal submucosa and has been used previously for ventricular septum defect closure, aortic root enlargement, and pericardial reconstruction (Quarti et al., 2012; Scholl et al., 2010). Finally, with over 30 years of cardiovascular implantation experience, the PERI-GUARD bovine pericardial patch (BPP) was used (Synovis Surgical Innovations, Deerfield, IL, USA) (N=6).

All the materials above were tested in the left-heart simulator model. In the finite element model developed next, we considered in addition another bovine pericardial patch

donated by St. Jude Medical™ (SJM™,St. Jude Medical Inc., St. Paul, MN, USA). The SJM™ Pericardial Patch with EnCap™AC Technology (SJM™) is a thinner, flexible bovine pericardial patch with a different anti-calcification treatment compared to BPP (Hoffman et al., 1992; Hopkins et al., 2004).

3.1.4 Processing of data from the left-heart simulator and high-speed camera

While the left-heart simulator made sure that pressure pulses and fluid flow rates were controlled for, the high-speed camera provided information about the opening and closing characteristics of the valve. Normal valves have a distinctive behavior whereby they open fast during early systole, stay open during systole, and close fast during early diastole (Figure 2) (Handke et al., 2003). Therefore, the following parameters were determined to characterize the hemodynamic performance of the valves: valve opening velocity (VO) (cm^2/s), valve slow closing velocity (VSC) (cm^2/s), valve closing velocity (VC) (cm^2/s), and maximum geometric orifice area (GOA) (cm^2). A MatLab code (Appendix A) was specially developed to process the data recorded with the left-heart simulator and calculate these parameters. In the clinical context, parameters describing hemodynamic performance would also possibly include the pressure gradient through the aortic valve if it were stenotic. Since valves with AI do not exhibit flow restriction, the pressure gradient through them is expected to be insignificant, and was not investigated.

Specifically, the high-speed video recordings were trimmed to show only one cardiac cycle, and aligned to start when the valve is still closed, and end before another cycle begins. For each dataset, a small number of still snapshots (say 10) are automatically selected by the program from the whole record, to show the progression of the valve dynamics. The user is

then asked to identify snapshots where the valve is fully open and starting to close. In addition, the user is asked to select a snapshot to trace the inner contour of the bottom cannula of the valve. Since the actual inner diameter of the cannula is known (20.5 mm), this provides for calibration of the GOA measurements to follow. Then, the user is asked to trace the contour left open by the leaflets at multiple times between early systole and late systole, so that the geometric orifice area can be known as a function of time, VO, VSC, VC and GOA can be determined (Figure 30). Note that the GOA is a direct two-dimensional description of the cross-sectional area of the open valve, as opposed to the valve effective orifice area (EOA) calculated by clinicians from Doppler echography data, based on the laws of fluid mechanics.

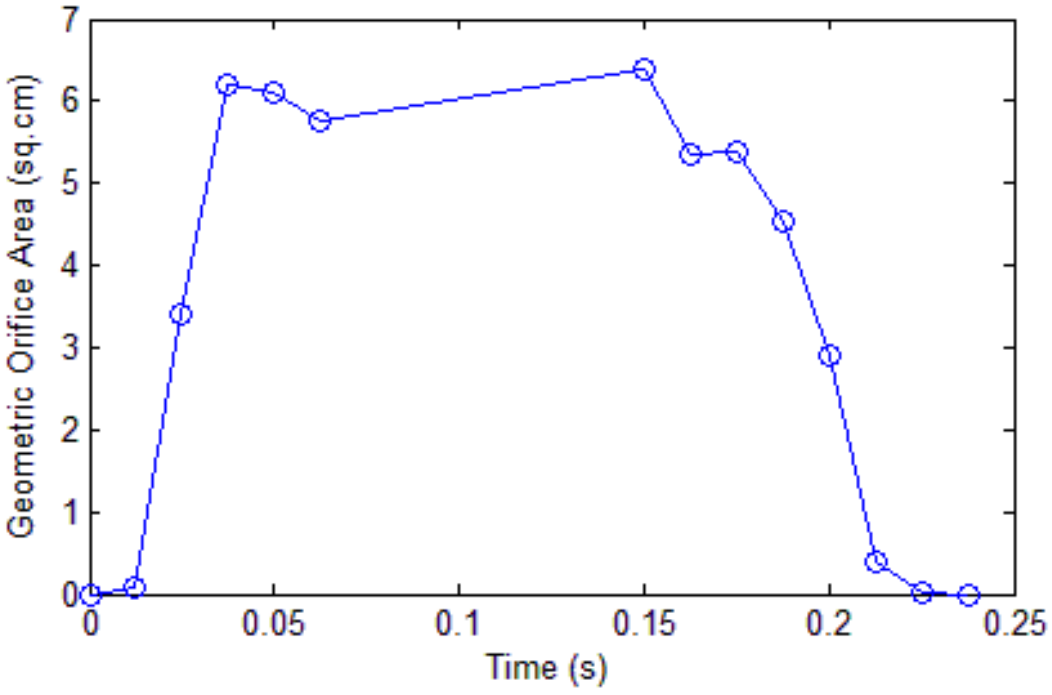

Figure 30: Example of evolution of the geometric orifice area as a function of time in the valves studied. VO is the slope of the curve during the fast opening phase; VSC is the slope of the curve between fast opening and rapid closing; VC is the slope of the curve during the rapid closing phase.

In addition, the left ventricular work (LVW) (mJ) was calculated using processing software provided by the manufacturer of the left-heart simulator to assess any changes between native and repaired valves.

3.1.5 Material testing of replacement materials

Toward finite element modeling of the repaired valves, we measured the material properties of the five replacement materials described in the previous section, using pressurization testing. Although a planar biaxial machine would have been the preferred choice for material characterization of anisotropic tissues, in its absence, we used closed-end, free extension pressurization testing which our laboratory has plenty of experience with to determine the mechanical properties of fresh human aorta (Labrosse et al., 2009).

The replacement materials presented themselves as flat sheets. First, the replacement material was rolled up into a cylinder and sutured. Due to the different sizes of available replacement materials, it was not possible to roll them into cylinders of the same diameter. The cylindrical tube was capped at one end with a plastic cap and cannulated at the other end. The connections were secured with plastic ties (Figure 31). The sample was finally placed in room-temperature saline.

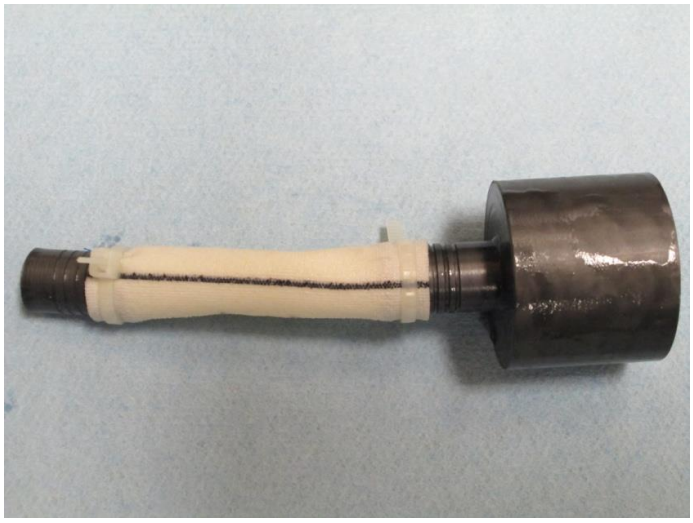

Figure 31: Replacement material cylindrical tube capped and cannulated.

The cannulated end was held horizontally and connected to 0.9% saline solution pressure head (Figure 32).

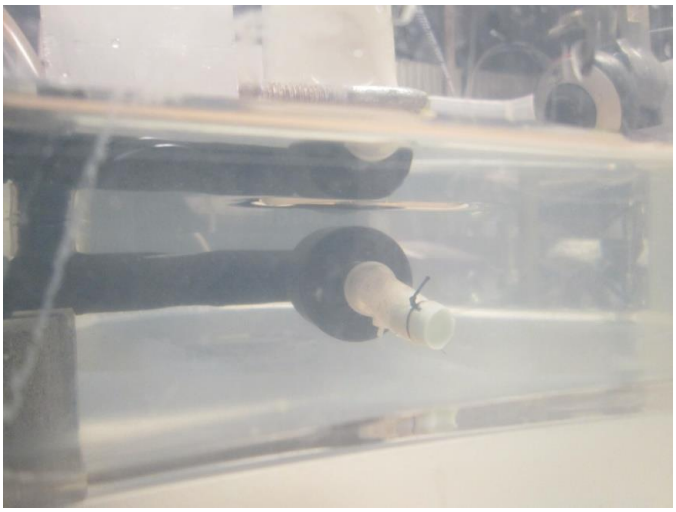

Figure 32: Sample mounted on the measure head and floating in 0.9% normal saline.

The inlet pressure was measured by a digital manometer (33500-082, VWR International, Mississauga, ON, Canada). The sample was preconditioned by three one-

minute pressurizations from 0 to 160 mmHg to 0 up and down (100 mmHg = 13.3 kPa). Furthermore, the elongation of the sample was monitored using a web camera (QuickCam, Logitech, Newark, CA, USA) and two markers affixed to it. For the measurement run, pressure was slowly stepped up from 0 to 160 mmHg in increments of 20 mmHg. In order to measure the tissue circumferential stretch, an ultrasonic external probe (Terason SMARTProbe, 5-8 MHz 4-cm linear array "T" probe, Teratech Corporation, Burlington, MA, USA) was used to record cross-sectional views of the sample. The ultrasound signal was generated and processed by PC-based TelaVet 1000 system (Classic Medical, Tequesta, FL, USA). All the recording steps were synchronized with the pressure increment steps (Figure 33). Processing of the recorded images was done using MatLab programs created for previous similar studies (The MathWorks, Natick, MA, USA) (Labrosse et al., 2013).

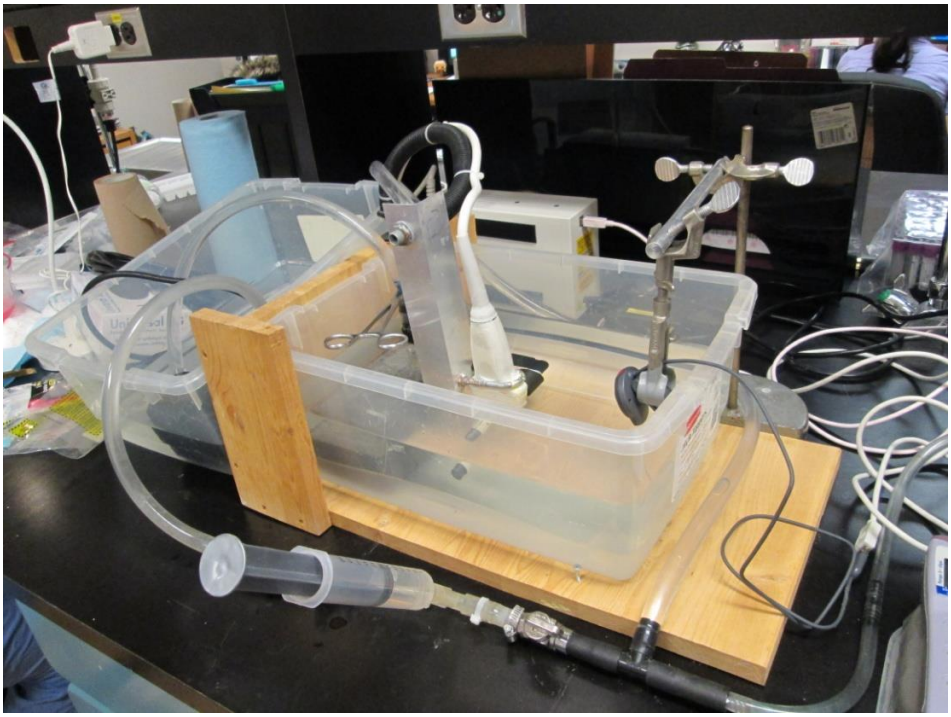

Figure 33: The replacement material was mounted as a tube in the pressurization testing equipment, including a syringe for pressure control (foreground), an ultrasound probe for measurement of radial dimensions (center), a webcam for measurement of longitudinal extension (right), and a manometer (almost completely outside of view, bottom right)

For measurement of the original radial dimensions, the sample tube was sliced circumferentially and the material was cut at the suture, leaving a strip whose length could be measured as the circumference of the original sample. To this end, photographs were taken of the strip with a calibration grid in the field of view for ulterior digital processing of the images.

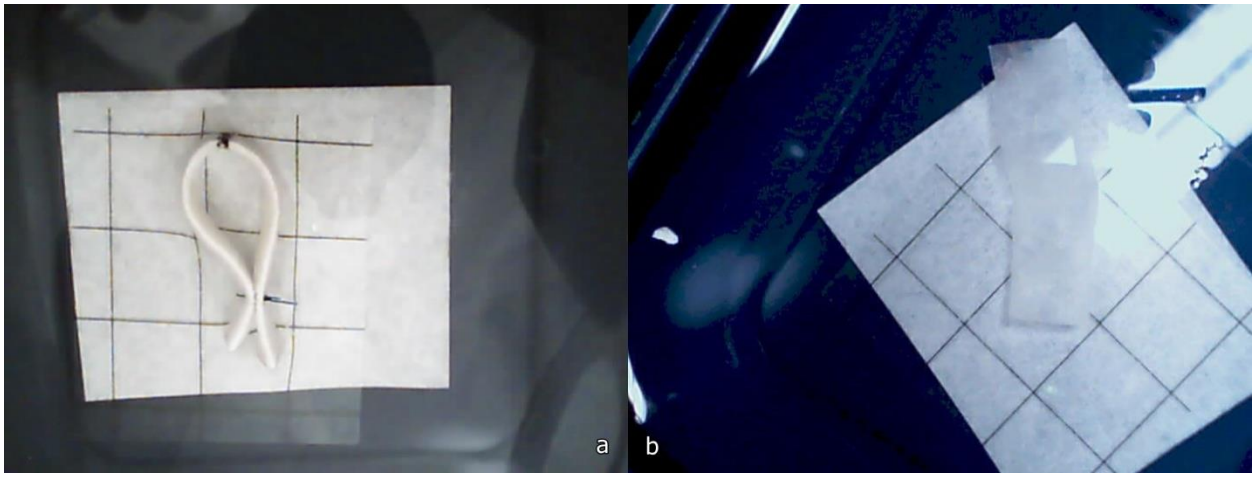

Figure 34: Cross-sectional view of ring after cutting from tube (a) and tissue strip after removing the suture (b).

The tissue thickness was measured using a micro meter (N-293-340, Mitutoyo, Japan). The average of three measurements at three different locations was taken for each sample.

3.1.6 Theory underlying the processing of the pressurization testing data

As the replacement materials tested were susceptible to exhibit large deformations according to hyperelastic, anisotropic behavior, we were able to use well established equations originally derived for straight segments of aorta subjected to internal pressure (Humphrey, 2002). Classically, the aortic segment is treated as a thick walled cylinder with hyperelastic elastic material properties described by strain energy function *W*.

In a cylindrical coordinate system, and assuming orthotropicity in the principal directions of the cylinder, aortic tissue behavior is different in the radial, circumferential and longitudinal directions. A material particle located at (r, θ, z) in the deformed arterial section will be mapped to (R, Θ, Z) in the undeformed section such that:

$$r = r(R), \theta = \Theta, z = z(Z)$$

In this notation, $R_i < R < R_o$, where R_i and R_o are the inner and outer radii in the undeformed geometry, respectively. Also, $r_i < r < r_o$, where r_i and r_o are respectively the inner and outer radii in the deformed arterial section under an internal pressure p and an applied axial force F_z . F_z represents the required force to keep the pressurized sample at the constant length. When the closed end of the sample is free to move longitudinally, then $F_z \equiv 0$, even thought internal axial forces compensate for the pressure acting on the cap and the external force is assumed to be zero.

Briefly, a basic definition for deformation in the present case is given by the deformation gradient tensor $\bar{\bar{F}}$ whose matrix representative is as follows:

$$[\bar{\bar{\boldsymbol{F}}}] = \begin{bmatrix} \boldsymbol{\partial r/\partial R} & \mathbf{0} & \mathbf{0} \\ \mathbf{0} & \boldsymbol{r/R} & \mathbf{0} \\ \mathbf{0} & \mathbf{0} & \boldsymbol{\partial z/\partial Z} \end{bmatrix}$$

where the components of this tensor are the radial, circumferential and longitudinal stretch ratio ratios, respectively:

$$\boldsymbol{\lambda_r = \frac{\partial r}{\partial R}, \lambda_\theta = \frac{r}{R}, \lambda_z = \frac{\partial z}{\partial Z}}$$

These equations are used in describing the Cauchy-Green strain tensor defined as $\bar{\bar{C}} = \bar{\bar{F}}^T . \bar{\bar{F}}$:

$$[\bar{\bar{C}}] = \begin{bmatrix} \lambda_r^2 & 0 & 0 \\ 0 & \lambda_\theta^2 & 0 \\ 0 & 0 & \lambda_z^2 \end{bmatrix}$$

The Green-Lagrange strain tensor is also used to describe the material deformation; it is defined as $\bar{\bar{E}} = \frac{1}{2}(\bar{\bar{C}} - 1)$ and gives $\bar{\bar{E}}$ as:

$$[\bar{\bar{E}}] = \begin{bmatrix} E_r = \frac{1}{2}(\lambda_r^2 - 1) & 0 & 0 \\ 0 & E_\theta = \frac{1}{2}(\lambda_\theta^2 - 1) & 0 \\ 0 & 0 & E_z = \frac{1}{2}(\lambda_z^2 - 1) \end{bmatrix}$$

The Cauchy stress tensor is defined as $\bar{\bar{t}} = \frac{1}{\det \bar{\bar{F}}} \, \bar{\bar{F}} . \frac{\partial W}{\partial \bar{\bar{E}}} . \bar{\bar{F}}^{\boldsymbol{T}}$. From equilibrium equations, it can be shown (Humphrey, 2002) that the internal pressure *p* can be expressed as:

$$p = \int_{r_i}^{r_o} \frac{1}{r} \lambda_\theta^2 \frac{\partial W}{\partial E_\theta} dr$$

and that the applied axial load and pressure on the end of the arterial section are balanced by the longitudinal stresses in the arterial wall such that

$$\boldsymbol{F_z = \pi \int_{r_i}^{r_o} \left(2 \lambda_z^2 \frac{\partial w}{\partial E_z} - \lambda_\theta^2 \frac{\partial w}{\partial E_\theta} \right) r dr}$$

In brief, the equations for F_z and *p* completely describe the equilibrium of a closed-end segment of replacement material under pressure.

A strain energy function *W* must now be chosen such that the theoretical method and the experimental data closely match. Many strain energy functions have been developed over the years for different types of biological tissues. One of the main models is the exponential one developed by Fung et al. (Fung et al., 1979) for soft tissue biomechanics:

$$W = \frac{1}{2} c_1 [exp(c_2 E_\theta^2 + c_3 E_z^2 + 2 c_4 E_\theta E_z) - 1]$$

where $c_1, c_2, c_3, \ c_4$ are the material constants and $E_\theta, \ E_z$ are the Green strains defined previously.

In Guccione's model (Guccione, et al., 1991), Fung's model is modified by assuming transverse isotropy.

$$W = \frac{C_1}{2}\left[\exp\left(c_2E_\theta^2 + c_3(E_z^2 + E_r^2 + E_{rz}^2 + E_{zr}^2) + c_4\left(E_{\theta z}^2 + E_{\theta r}^2 + E_{r\theta}^2 + E_{z\theta}^2\right)\right) - 1\right]$$

In both model c_1 is a material parameter with the dimension of stress and c_2, c_3 and c_4 are non-dimensional material parameters. The radial component of the strain can be determined from the incomparability assumption such that:

$$E_r = \frac{1}{2}\left[\frac{1}{(2E_\theta + 1)(2E_z + 1)} - 1\right]$$

Labrosse et al. proved that Guccione's model is a good candidate for modeling different cardiovascular tissues and also presents the unique advantage of having already been implemented and tested in commercial finite element software (Labrosse et al., 2009).

Characterization of the material constants is performed using data collected during experiments. Suppose *m* data points are available. Regardless of type of data as: force, pressure and stress, the difference between each experimental and theoretical quantity at each data point k must be minimized to obtain accurate material constants. A possible error function can be defined as:

$$e = \sum_{k=1}^{m}\left(\left(\frac{p_{theo} - p_{exp}}{p_{exp}}\right)_k^2 + \left(\frac{F_{z\,theo} - F_{z\,exp}}{F_{z\,exp}}\right)_k^2\right),$$

where 'theo' refers to theoretical and 'exp' refers to experimental. p_{theo} and F_{theo} are computed using the equations shown above for p and F_z, respectively. The error function e being a function of the material constants, characterization of the material properties is classically done by optimizing these constants using the Levenberg-Marquardt nonlinear multivariate optimization scheme (Humphrey, 2002).

The material constants for the replacement material grafts were calculated using the experimental inputs as pressure, force (set to zero), longitudinal stretch and inner radius at each pressure increment. Again, processing of the data was done using MatLab programs created for previous similar studies (Labrosse et al., 2013).

3.2 Results

3.2.1 Valve repair with non-coronary cups replacement

In total, 25 samples of fresh porcine aortic roots underwent hemodynamic measurements. Aortic valves subsequently underwent randomized allocation to non-coronary leaflet excision and leaflet replacement with APP (*N*=7), HEMASHIELD (*N*=7), CorMatrix (*N*=5), or BPP (*N*=6). Each unrepaired and repaired aortic valve underwent a minimum of 3 runs at 70 bpm heart beating for all experiments, while the cardiac output was set at 2.5, 5.0, or 6.5 L/min.

As an example, Table 3 presents the hemodynamic parameters for porcine aortic valves before and after they were repaired with glutaraldehyde-fixed bovine pericardial patch (BPP Synovis™). The hemodynamic results for these and other cases are provided in full in Appendix B, Table B-1.

Table 3: Hemodynamic measurements for 6 repaired aortic valve with BPP.

			Before repair					After repair				
STJ Diameter (mm)	Case	CO (L/min)	Velocities (sq.cm/s)			Max GOA (sq.cm)	LV Work (mJ)	Velocities (sq.cm/s)			Max GOA (sq.cm)	LV Work (mJ)
			VO	VSC	VC			VO	VSC	VC		
24	B1	2.5	153	5.8	48	5.76	736	126	7.6	57	4.73	714
		5.0	142	3.9	46	5.32	1083	203	7.8	55	5.16	1023
		6.5	135	2.2	63	5.29	1242	190	7.4	62	5.00	1287
22	B2	2.5	78	1.7	46	4.90	684	108	4	40	4.09	700
		5.0	197	2.9	91	4.99	1045	121	4.1	53	4.54	1075
		6.5	212	4.7	62	5.31	1287	156	4.4	61	4.48	1253
29	B3	2.5	169	8.5	83	6.36	709	186	3.3	74	6.96	1029
		5.0	177	9.3	86	6.64	983	262	0.4	75	6.62	1391
		6.5	265	5.5	94	6.67	1190	201	7.3	87	7.52	1611
22	B4	2.5	144	11.2	64	5.39	703	111	1.4	46	4.16	730
		5.0	246	13.8	60	6.23	1053	176	3.6	65	4.56	986
		6.5	213	11.3	78	5.58	1280	156	3.3	80	4.49	1199
22	B5	2.5	173	19.6	54	6.50	661	195	4	88	4.93	694
		5.0	240	11.5	69	6.06	1033	158	3.4	113	6.08	1062
		6.5	255	13.5	89	6.49	1222	207	-0.2	142	5.30	1205
26	B6	2.5	177	7.3	74	4.62	686	127	11.2	77	6.37	717
		5.0	153	6.2	67	4.18	1018	178	10	71	6.70	1057
		6.5	180	7.2	58	4.54	1250	171	11.8	79	6.59	1256

For appropriate comparisons, each treatment sample was compared to its original valve measurements. In Table 4, data are expressed as median values with interquartile ranges in parentheses. Wilcoxon-rank sum tests were used to determine significance between two sample sets while Kruskal-Wallis rank test was used for more than two sample sets. Significance was set at $P < 0.05$. The statistical calculations were run in SPSS Statistics, IBM, NY, USA.

The dynamics of the valves were assessed by measuring the opening velocity (VO) (cm^2/s), slow closing velocity (VSC) and closing velocity (VC) (cm^2/s). As can be seen from Table 4, valve opening velocity of repaired valve with APP and CorMatrix indicated slower

values in comparison to the native valves, but did not significantly change in repaired valve with BPP and HEMASHIELD. Slow closing velocity results show no statistically significant difference between any groups. Therefore, slow closing velocity was not considered in further analysis. Valve closing velocity (VC), on the other hand, indicates more changes. VC results reveal statistically significant decreases with the native valves for all groups except BPP. Overall, the valves repaired with APP, HEMASHIELD and CorMatrix opened and closed more slowly than the original valves by 30% ($P<0.05$).

Post-repair geometric orifice areas (GOA) were 10 ± 2% smaller in all groups compared to the native valves, and this decrease was statistically significant ($P<0.05$) (Table 4). Left ventricular work (LVW) was not significantly different for any type of replacement materials. At a cardiac output 2.5 L/min, the LVW was increased after repairs; however, no difference was revealed at 5.0 and 6.5 L/min. The LVW only increased with the cardiac output, as expected.

Table 4: Hemodynamic performance in all replacement materials before and after repair.

Table 4 (A)

Autologous porcine pericardium (APP) *N* = 7			
Measure	**Baseline**	**APP**	***P* value**
VO (cm^2/s)	157 (140-213)	113 (67-163)	0.03
VSC (cm^2/s)	6.3 (4.5-8)	5.35 (2.6-6.9)	0.2
VC (cm^2/s)	68 (53-76)	48 (44-55)	0.02
GOA (cm^2)	5.74 (5.29-6.87)	5.25 (4.16-5.99)	0.08
LVW (mJ)	1002 (703-1238)	1016 (932-1229)	0.6

Table 4 (B)

Collagen-impregnated Dacron (HEMASHIELD™) *N* = 7			
Measure	**Baseline**	**HEMASHIELD**	***P* value**
VO (cm^2/s)	136 (109-167)	120 (100-164)	0.3
VSC (cm^2/s)	3.3 (0.3-7.5)	4.4 (2.4-6.7)	0.4
VC (cm^2/s)	63 (59-71)	48 (35-61)	0.01
GOA (cm^2)	5.91 (5.58-6.43)	5.06 (4.24-5.73)	0.05
LVW (mJ)	1018 (689-1234)	1106 (763-1249)	0.3

Table 4 (C)

Extracellular matrix scaffold (CorMatrix™) *N* = 5			
Measure	**Baseline**	**CorMatrix**	***P* value**
VO (cm^2/s)	219 (188-241)	111 (76-150)	0.0001
VSC (cm^2/s)	6.2 (5.2-13.1)	4.3 (1.5-6)	0.01
VC (cm^2/s)	81 (69-86)	52 (44-63)	0.0001
GOA (cm^2)	6.08 (5.82-6.83)	5.27 (4.57-5.56)	0.0001
LVW (mJ)	1033 (694-1221)	1086 (727-1241)	0.4

Table 4 (D)

Glutaraldehyde-fixed bovine pericardial patch (BPP;Synovis™) *N* = 6			
Measure	**Baseline**	**BPP**	***P* value**
VO (cm^2/s)	177 (153-213)	173.5 (127-195)	0.4
VSC (cm^2/s)	7.25 (4.7-11.3)	4.05 (3.3-7.6)	0.08
VC (cm^2/s)	65.5 (58-83)	72.5 (57-80)	0.8
GOA (cm^2)	5.45 (4.99-6.36)	5.08 (4.54-6.59)	0.5
LVW (mJ)	1039 (709-1222)	1059 (730-1253)	0.4

In addition, as expected, when native porcine valve hemodynamic at CO settings of 2.5, 5.0, and 6.5 L/min were compared, significantly increased LVW and VO with increasing CO settings were observed (P = 0.001, P = 0.002, respectively). All other parameters, including GOA were not significantly different (P > 0.05, see Appendix B, Table B-2).

3.2.2 Material pressurization testing

Figure 35 illustrates cross-sectional images captured by the ultrasonic probe (for determination of radial dimensions) synchronized with digital camera recordings of the sample being pressurized (for determination of longitudinal extensions) for glutaraldehyde-fixed bovine pericardial patch (BPP). The procedure was repeated for all replacement material samples listed in Table 4. In addition, we considered another bovine pericardial patch donated by St. Jude Medical™ (St. Jude Medical Inc., St. Paul, MN, USA). The SJM™ Pericardial Patch with EnCap™AC Technology (SJM™) is a thinner, flexible bovine pericardial patch with a different anti-calcification treatment compared to BPP.

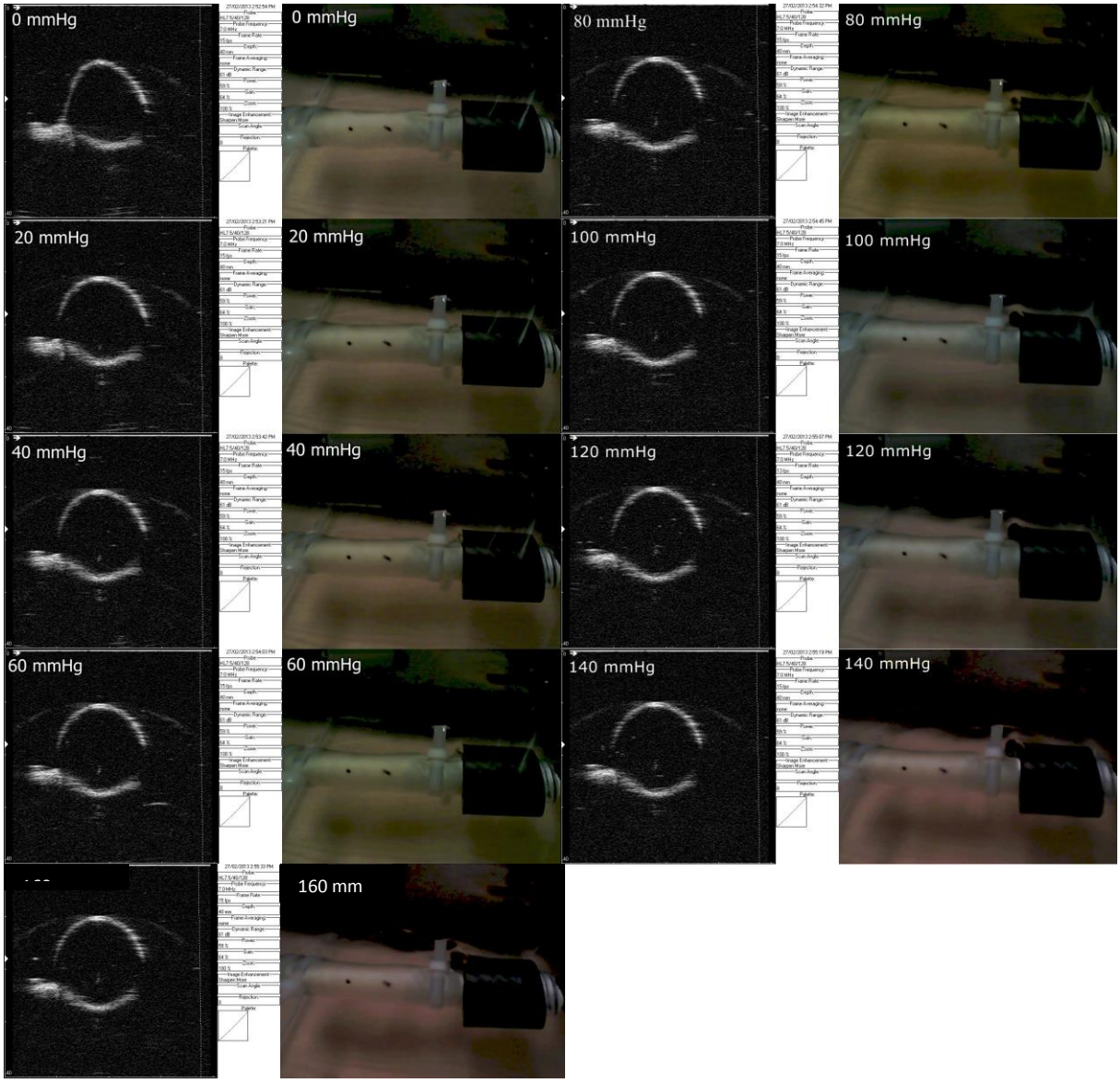

Figure 35: Pressurization testing experiment.

Table 5 lists the circumferential and longitudinal stretch ratios for all replacement materials according to the pressure increment and their unpressurized inner radius and thickness.

Table 5: Experimental data from pressurization testing. *IR*: unpressurized inner radius (mm); *t*: unpressurized thickness (mm)

Table 5 (A)

Autologous porcine pericardium (APP) ***IR* = 4.75; *t* = 0.12**		
Pressure (mmHg)	λ_θ	λ_z
0	1.0000	1.0000
20	1.0005	1.0000
40	1.0010	1.0033
60	1.0015	1.0033
80	1.0020	1.0067
100	1.0025	1.0200
120	1.0030	1.0200
140	1.0035	1.0200
160	1.0040	1.0200

Table 5 (B)

Collagen-impregnated Dacron (HEMASHIELD™) ***IR* = 6.13; *t* = 0.74**		
Pressure (mmHg)	λ_θ	λ_z
0	1.0000	1.0000
20	1.0033	1.0000
40	1.0067	1.0000
60	1.0067	1.0000
80	1.0067	1.0033
100	1.0100	1.0033
120	1.0133	1.0033
140	1.0133	1.0033
160	1.0133	1.0067

Table 5 (C)

Extracellular matrix scaffold (CorMatrix™) ***IR* = 4.63; *t* = 0.19**		
Pressure (mmHg)	λ_θ	λ_z
0	1.0000	1.0000
20	1.0050	1.0000
40	1.0010	1.0000
60	1.0015	1.0200
80	1.0020	1.0300
100	1.0025	1.0300
120	1.0030	1.0400
140	1.0035	1.0400

Table 5 (D)

Glutaraldehyde-fixed bovine pericardial patch (BPP;Synovis™) ***IR* = 8.12; *t* = 0.48**		
Pressure (mmHg)	λ_θ	λ_z
0	1.0000	1.0000
20	1.0050	1.0000
40	1.0010	1.0000
60	1.0015	1.0100
80	1.0020	1.0200
100	1.0025	1.0267
120	1.0030	1.0300
140	1.0035	1.0300
160	1.0040	1.0300

Table 5 (E)

Pericardial Patch with EnCap AC Technology (SJM) ***IR* = 4.39; *t* = 0.21**

Pressure (mmHg)	λ_θ	λ_z
0	1.0000	1.0000
20	1.0010	1.0000
40	1.0020	1.0100
60	1.0030	1.0267
80	1.0040	1.0267
100	1.0050	1.0267
120	1.0060	1.0267
140	1.0070	1.0267
160	1.0080	1.0300

The material constants for Guccione's material model detailed previously were determined for all native and replacement materials as listed in Table 6. The material constants for the original porcine aorta and leaflets were derived from published experimental data (Martin and Sun, 2012) as c_1 = 6.35 kPa and 2.01 kPa, c_2 = 2.62 kPa and 221 kPa, c_3 = 3.72 kP and 48.2 kPa, respectively.

Table 6: Material constants of valve constituents and replacement materials.

Material	c_1 (kPa)	c_2 (-)	c_3 (-)	Thickness (mm)
Porcine aorta	6.35	2.62	3.72	1.9
Porcine leaflet	2.01	221	48.2	0.53
APP	3.00	11,200	375	0.53 (0.12)*
HEMASHIELD	2.26	2,130	1,060	0.74
CorMatrix	3.00	15,700	111	0.53 (0.19)*
BPP	2.59	15,300	376	0.48
SJM	3.00	4,180	186	0.53 (0.21)*

***: The measured values in parenthesis were corrected to 0.53 mm for stability of the finite element simulation. The material constants were obtained based on the corrected thicknesses.**

Since the material constants in Table 6 do not have a direct physical meaning, Figure 36 illustrates the different properties of the materials under equibiaxial planar testing driven in tension.

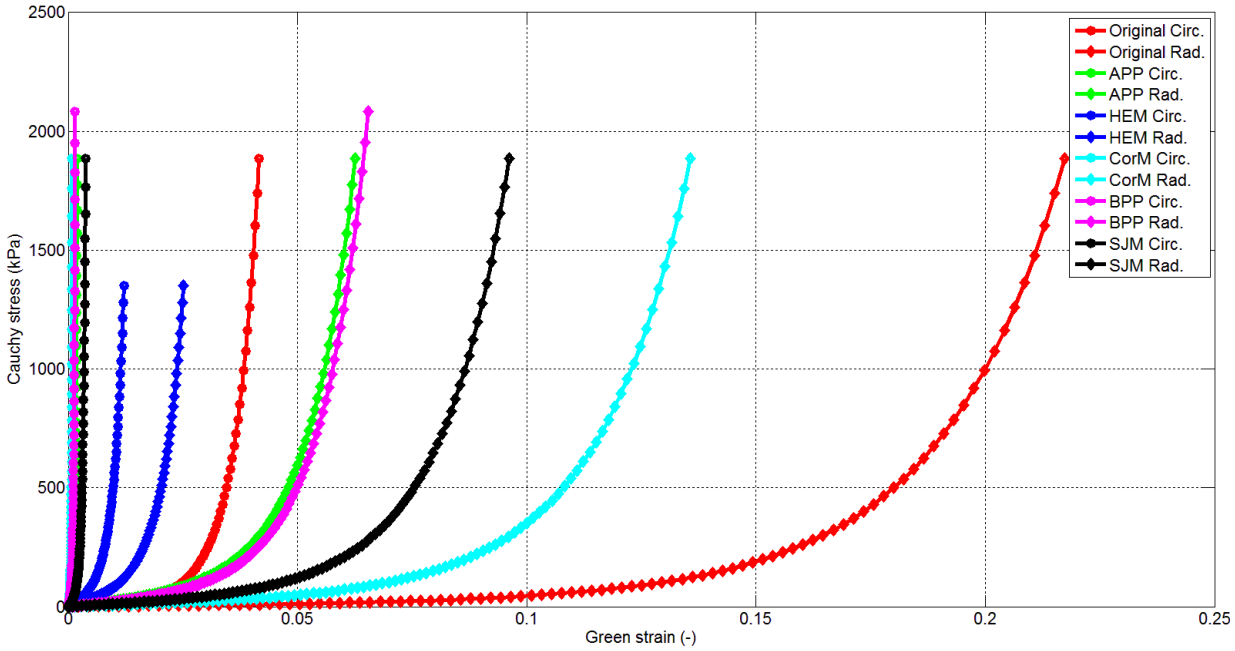

Figure 36: The stress-strain properties of the original leaflets were derived from equibiaxial planar testing data (Martin and Sun, 2013). The stress-strain curves for the other replacement materials represent simulated equibiaxial planar testing using the properties determined from pressurization testing described herein.

4 Finite element simulation of aortic valve with replacement material graft

In spite of the wealth of information about hemodynamic function of the native and repaired valves provided by testing in the left-heart simulator, crucial pieces of information are missing. In particular, the mechanical stress levels in the different replacement materials used to repair the valves are still unknown. Stress information is necessary for two reasons: 1) the stress level is limited by the material strength, i.e., if the stress is too high, immediate tearing may occur; 2) in case of high stress, even if the replacement materials were not to fail, the sutures used to hold them in place may well fail, also bringing about catastrophic failure of the repair. Therefore, quantitative assessment of the stresses present in the repaired valves is necessary, as permitted by finite element modeling. In this chapter, geometric modeling of the aortic valve, implementation of material properties, boundary conditions and applied loads will be presented. Finally, results for all replacement materials grafts obtained from the numerical simulation of the entire cardiac cycle, starting from the unpressurized geometry, will be presented.

4.1 Methods

4.1.1 Geometry

It is well known that the three aortic leaflets and sinuses are different in size. However for simplicity, the model developed herein assumed an idealized, symmetrical geometry. An average of the physical dimensions was taken and the sinuses were assumed to be 120 degrees from each other in the circumferential direction.

The model developed assumed sinuses without coronaries ostia (origins of the coronary arteries). The height of each sinus was averaged from the three sinuses of a single valve.

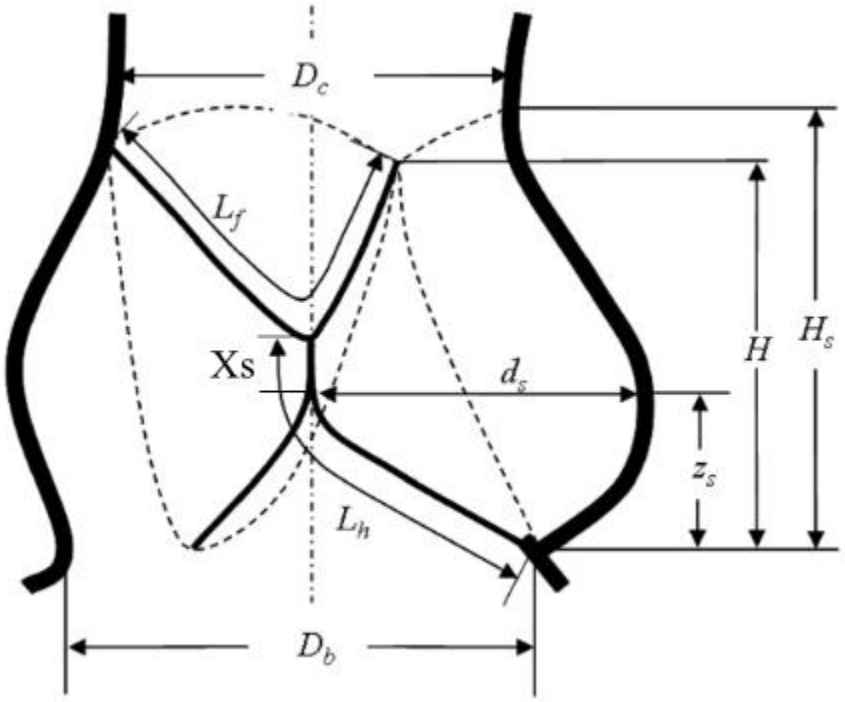

Figure 37: Drawing of the aortic valve showing the side view of one leaflet. *H*: valve height, H_s: Sinus Height, X_s: Coaptation Height, D_b: diameter of the base, D_c: diameter of the commissures, L_f: leaflet free-edge length, L_h: leaflet height (Labrosse et al., 2010).

Table 7: Unpressurized porcine aortic valve dimensions.

Parameters	Value
Diameter of left-ventricular outflow tract, D_b (mm)	24
Diameter of sinotubular junction, D_c (mm)	22
Valve height, H (mm)	17.8
Maximum radius of aortic sinuses, *rsm* (mm)	15
Leaflet height, L_h (mm)	17
Leaflet free-edge length, L_f (mm)	34
Sinus height, h_s (mm)	19
Height of commissures, H_s (mm)	9.6

Following an approached established and documented in (Labrosse et al., 2011), construction of the unpressurized aortic valve was started from the 8 parameters in Table 7 and three dimensional coordinates of 15 landmark points as shown in Figure 38 (a) (Labrosse et al., 2011). Assuming that the unpressurized geometry is stress and strain free, using it as the reference configuration makes it possible to compute the total stress and strain state when the model is pressurized to physiological conditions. This is a necessary requirement dictated by continuum mechanics under finite deformations (Humphrey, 2002).

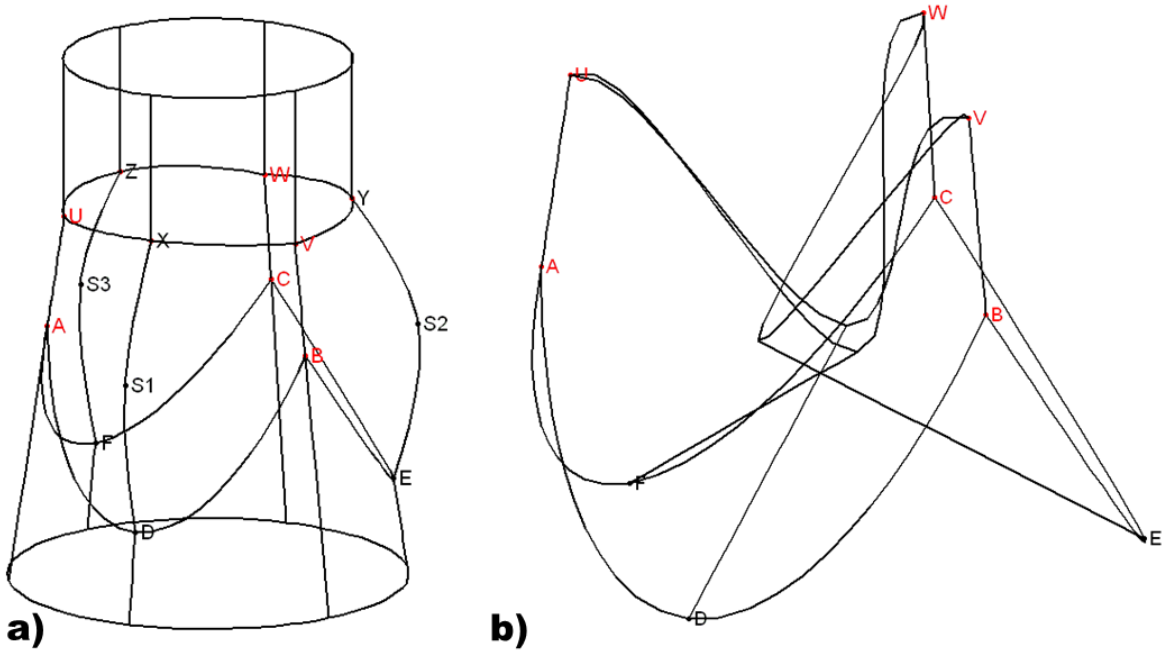

Figure 38: (a) Line sketch of unpressurized aortic valve model, showing the left ventricular outflow tract, the aortic sinuses and the ascending aorta, including the 15 landmark points. (b) Line sketch of the aortic leaflets drawn in an assumed, unpressurized position (Labrosse et al., 2011).

In Figure 38 (a), landmarks *A, B* and *C* represent the lowest point of commissural attachments and landmarks *D, E* and *F* are the nadirs of leaflet attachment lines. Based on experimental study (Clark et al., 1974), landmarks *A, B, D* landmarks *B, E, C* and landmarks *C, F, A* are each assumed to lie in different plans. Landmarks *U, V* and *W* are the highest points of the commissural attachments, and landmarks *X, Y* and *Z* correspond to the sinuses' highest points. Finally, landmarks *S1, S2* and *S3* are the outermost locations of the three aortic sinuses. The left ventricular outflow tract (LVOT, D_b) was built by extending the bottom of the valve defined by landmarks *D, E* and *F*. Similarly, the ascending aorta was built by extending the top of the valve defined by landmarks *U, V* and *W*.

In Table 7, D_b (resp. D_c) is the diameter of the circle circumscribing landmarks *D, E* and *F* at the base of the valve (resp. landmarks *U, V* and *W* at the top of the commissural attachments) in Figure 38 (a). Similarly, *rsm* is the radius of the circle circumscribing landmarks *S1, S2* and *S3* at the maximum protrusion of the sinuses. Valve height *H* is the distance between planes *D, E, F* and *U, V, W*. Sinus height h_s is the distance between planes *D, E, F* and *X, Y, Z*. Commissural height H_s is the length of the commissural attachments (segments *AU, BV* and *CW*) (Labrosse et al., 2011). From these points, lines and curves were drawn using MatLab to sketch the aortic root. Then, the leaflet contours were created in partially closed position using a straight line for the leaflet height, and a sine curve of known length for the leaflet free margin as illustrated in Figure 38 (b).

All the curves created formed the edges of linear and bicubic Coons surfaces (Salomon, 2006), each of which was discretized using structured meshing. The process was repeated to produce 4 (resp. 3) surfaces at a small distance from each other to allow for the creation of 3 (resp. 2) finite elements through the aortic (resp. leaflet) thickness, as a structured hexahedral FE mesh of the whole valve was generated by connecting the nodes from adjacent surfaces (Figure 39). The final mesh consisted of approximately 11,800 nodes and 8,600 elements.

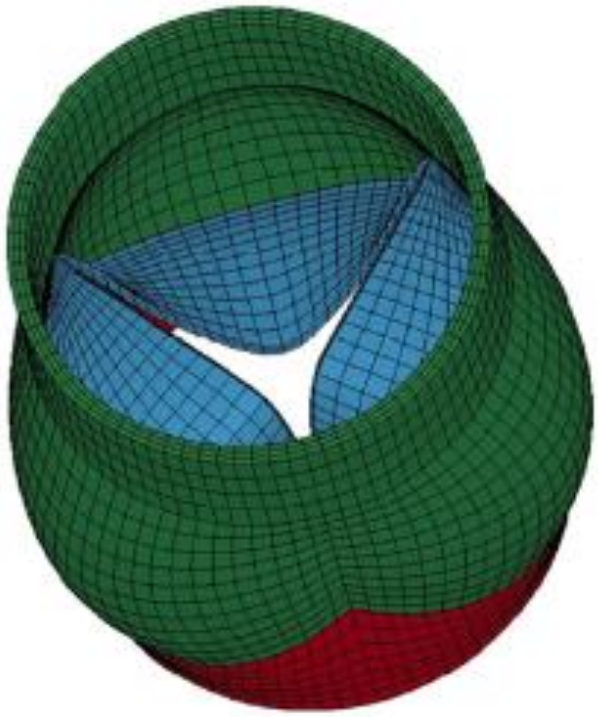

Figure 39: Final finite element mesh of the aortic valve and root. Green: ascending aorta and aortic sinuses; blue: leaflets; red: base of the valve, including the left ventricular outflow tract (Labrosse et al., 2011).

4.1.2 Material properties

Table 6 presents the material properties for all the materials used in this study. Their mass density was set at 1,000 kg/m^3 like water, because biological tissues have a water content above 70%, and because the tested man-made materials were approximately neutrally buoyant. As can be seen, all materials were modeled using the same hyperelastic, transversely isotropic material model, with different constants.

4.1.3 Boundary conditions and loads

The base of the valve in vivo is normally unconstrained as it expands and moves along with the left ventricular contractions. However, no quantified data were available for implementation, therefore simplified fixed end conditions were preferred, all the more so as they also represent what happens in the left-heart simulator.

For loads, nodes at the top of the ascending aorta were moved longitudinally. A longitudinal displacement was prescribed to reproduce the experimental stretch of 20 percent of initial length (Fung & Han, 1995).

Since the valve model was created in the unpressurized configuration, an arbitrary pressurization ramp was applied, bringing all the valvular components from 0 to 80 mmHg pressure between time 0 and 0.04 s (Figure 40). The longitudinal stretch ratio described above was applied in the meantime, and then held throughout the simulation. Thereafter, the model entered a physiologic cardiac cycle, with the ventricular pressure raising to 120 mmHg and returning to zero while the aortic pressure dropped to 80 mmHg (Figure 40).

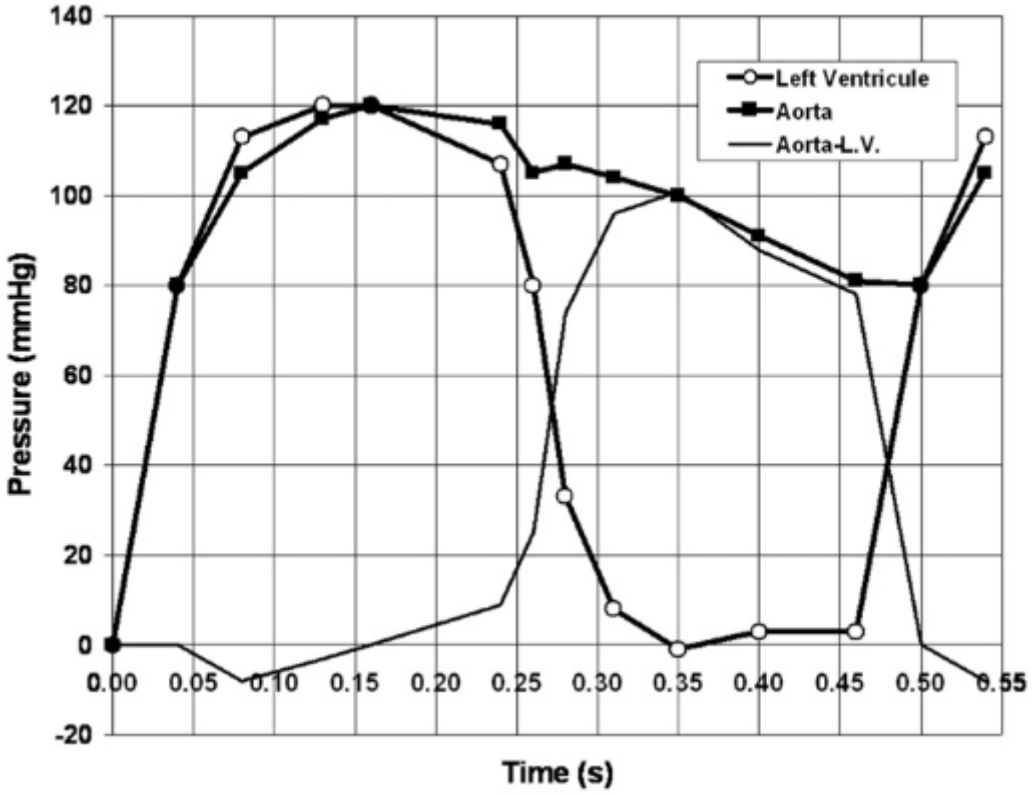

Figure 40: Pressure curves applied in the finite element model, reproducing a physiologic cardiac cycle with a shorter diastole for t ≥0.4 s (Labrosse et al., 2010).

The applied pressure on the leaflets was obtained from the difference between the aortic and ventricular pressures. This pressure difference was applied to the ventricular side of the leaflets. The pressure was applied only to one side of the leaflets instead of applying pressure to both aortic and ventricular respective leaflets sides, because this caused the leaflets element to thin out and experience numerical problems. In addition, the diastolic phase was shortened in the simulation because extended period of high pressure caused the element in simulation to become numerically unstable, leading to undesirable jagging shapes that did not recover upon pressure decrease.

In the dynamic simulations, the time step was automatically determined by the size of the smallest element. In order to save time and speed up the computation, time was scaled to 1/10 of the real time for the whole cardiac cycle. Differences in stress and strain and overall dynamic function from the simulation with the short and full diastolic phases were previously found to be negligible and therefore the short diastolic period was used in the simulations (Labrosse et al., 2010).

All numerical analyses were carried out with commercial FE software LS-Dyna 971 (LSTC, Livermore, CA, USA) on a workstation with two Intel Xeon E5640 2.67 GHz 4-core processors and 6 GB of RAM.

4.2 Results

All FE valve models for the original aortic and repaired valves under longitudinal stretch ratio of 1.20 opened and closed properly. The valve opening and closing characteristics were evaluated by measuring the GOA of the valve as a function of time from the calculated leaflet motions throughout one cardiac cycle. This was done by using the post-processor of LS-Dyna to take top view snapshots of the valve at regular time intervals during the cardiac cycle and by measuring the projected area created by the open leaflets (Figure 41).

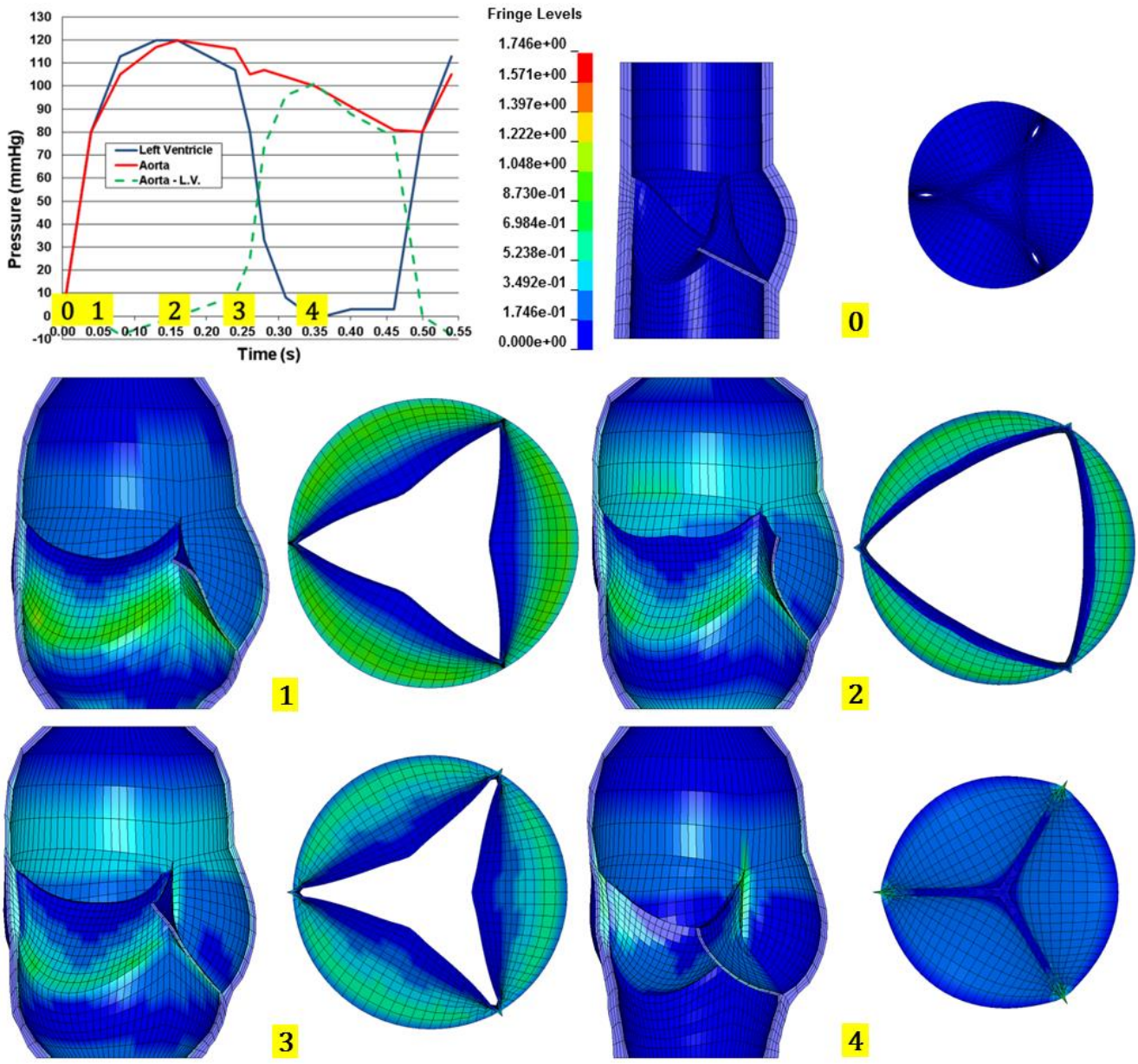

Figure 41: Control model in dynamics, under physiologic longitudinal stretch ratio of 1.20. The model was studied over one cardiac cycle by application of the pressure pulses described in the upper left inset. The analysis started from the unpressurized geometry at Time 0. The pressure was ramped from 0 up to 80 mmHg at Time 1 before the cardiac cycle started in early systole. The valve was fully open at Time 2, was closing at Time 3 and was closed under maximum pressure at Time 4. Von Mises stresses are color coded in MPa.

The dynamics (VO, VC) of the repaired valves were practically not distinguishable from those of the original valve (

Table 8). The repaired valves opened and closed more slowly than the original valve, by at most 9%. The geometric orifice areas of the repaired aortic valves were also insignificantly smaller than that of the original valve.

Table 8: FE simulation results for valve's opening, closing and GOA.

Measure	Original	APP		HEMASHIELD		CorMatrix		BPP		SJM	
VO (cm^2/s)	70	65	-7%	64	-9%	66	-6%	65	-7%	66	-6%
VC (cm^2/s)	55	53	-4%	52	-5%	53	-4%	55	0%	53	-4%
GOA (cm^2)	5.6	5.2	-7%	5.1	-9%	5.3	-6%	5.2	-7%	5.3	-6%

On the other hand, the aortic valve is subjected to relatively large amounts of mechanical stress. The distribution of stress in the valve varies with time in different locations. In particular, stress in the leaflets needs to be scrutinized throughout the evolution of the load cycle.

In all the FE simulation cases, the maximum values of mechanical Von Mises stress in the leaflet were determined, along with their location and timing (Figure 41). Von Mises stress, although more suited for describing stresses in isotropic materials, conveniently summarizes in one number the stresses present in different directions of the material at one specific location.

Table 9 presents the finite element results in the non-coronary, left and right leaflets repaired valve with the different replacement materials.

Table 9: Von Mises stress from FE simulation results in repaired valve with the different replacement materials. N: Von Mises stress in the non-coronary leaflet and R, L: Von Mises stress in the right and left coronary leaflets, respectively.

Measure	Original	APP		HEMASHIELD		CorMatrix		BPP		SJM	
N (kPa)	1,746	1,841	+5%	2,263	+30%	1,973	+13%	1,946	+11%	1,809	+4%
R,L (kPa)	1,746	2,206	+26%	1,895	+9%	2,309	+32%	2,212	+27%	2,159	+24%

In the repaired valves, different materials produced different stresses in the leaflets. The repaired leaflets with the smallest stresses were made of St. Jude Medical™ Pericardial Patch (SJM) (Figure 42-E) and Autologous porcine pericardium (APP) (Figure 42-A) (1,809 kPa and 1,841 kPa in the non-coronary leaflet, respectively). These stresses were about 5% higher than the stresses in the native leaflets.

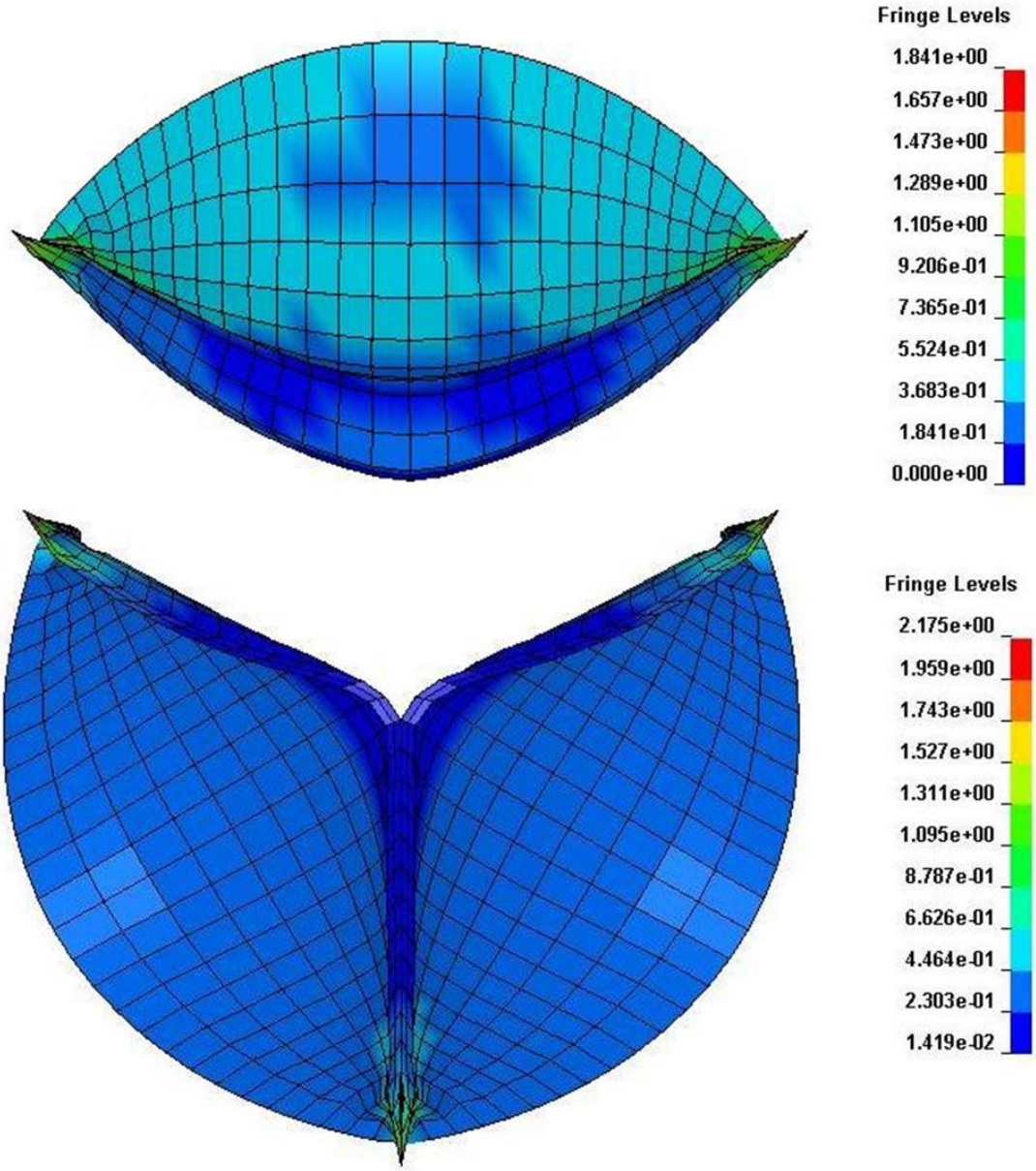
Fringe Levels
1.841e+00
1.657e+00
1.473e+00
1.289e+00
1.105e+00
9.206e-01
7.365e-01
5.524e-01
3.683e-01
1.841e-01
0.000e+00
Fringe Levels
2.175e+00
1.959e+00
1.743e+00
1.527e+00
1.311e+00
1.095e+00
8.787e-01
6.626e-01
4.464e-01
2.303e-01
1.419e-02

Figure 42 (A)

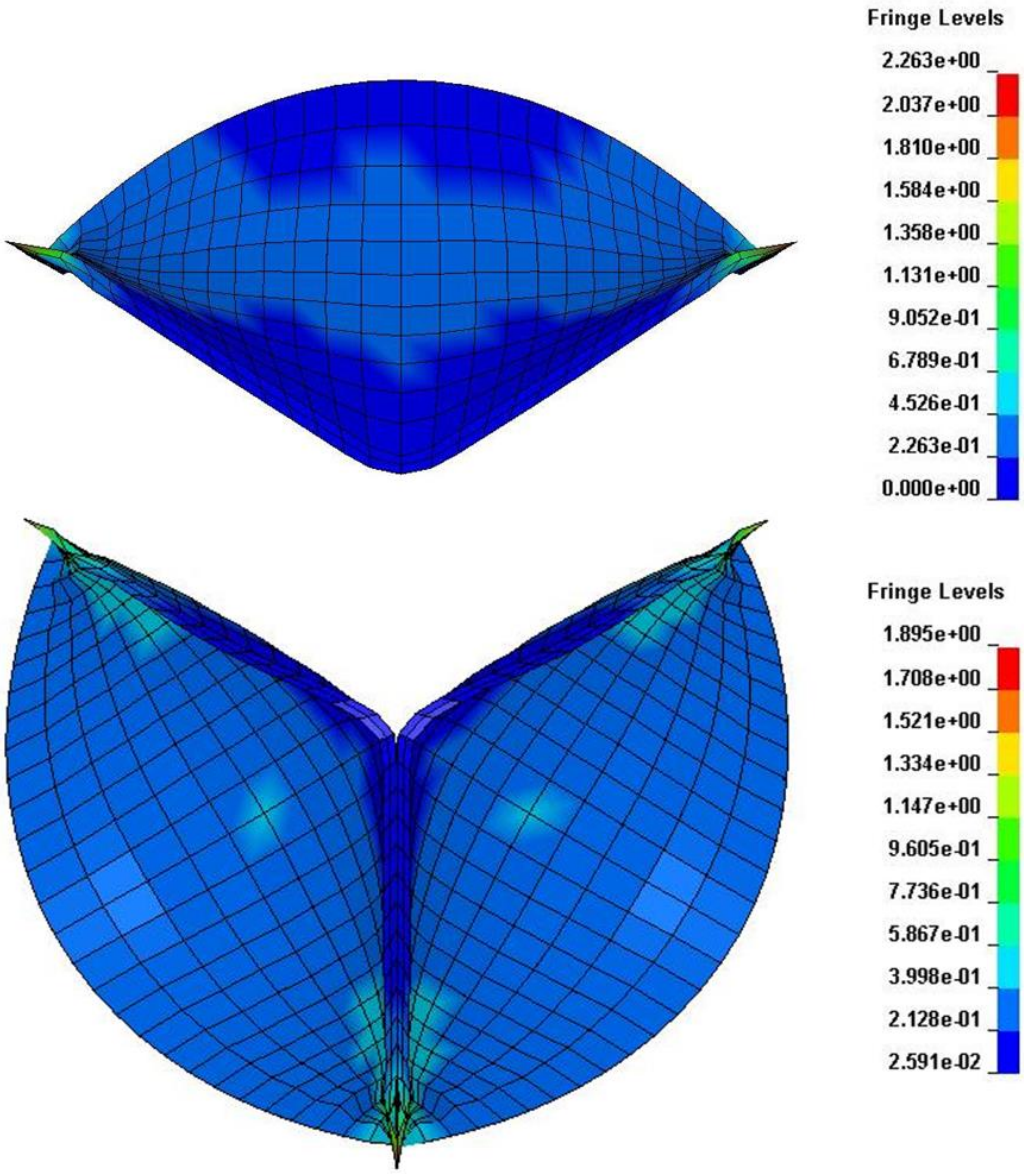
Fringe Levels
2.263e+00
2.037e+00
1.810e+00
1.584e+00
1.358e+00
1.131e+00
9.052e-01
6.789e-01
4.526e-01
2.263e-01
0.000e+00
Fringe Levels
1.895e+00
1.708e+00
1.521e+00
1.334e+00
1.147e+00
9.605e-01
7.736e-01
5.867e-01
3.998e-01
2.128e-01
2.591e-02

Figure 42(B)

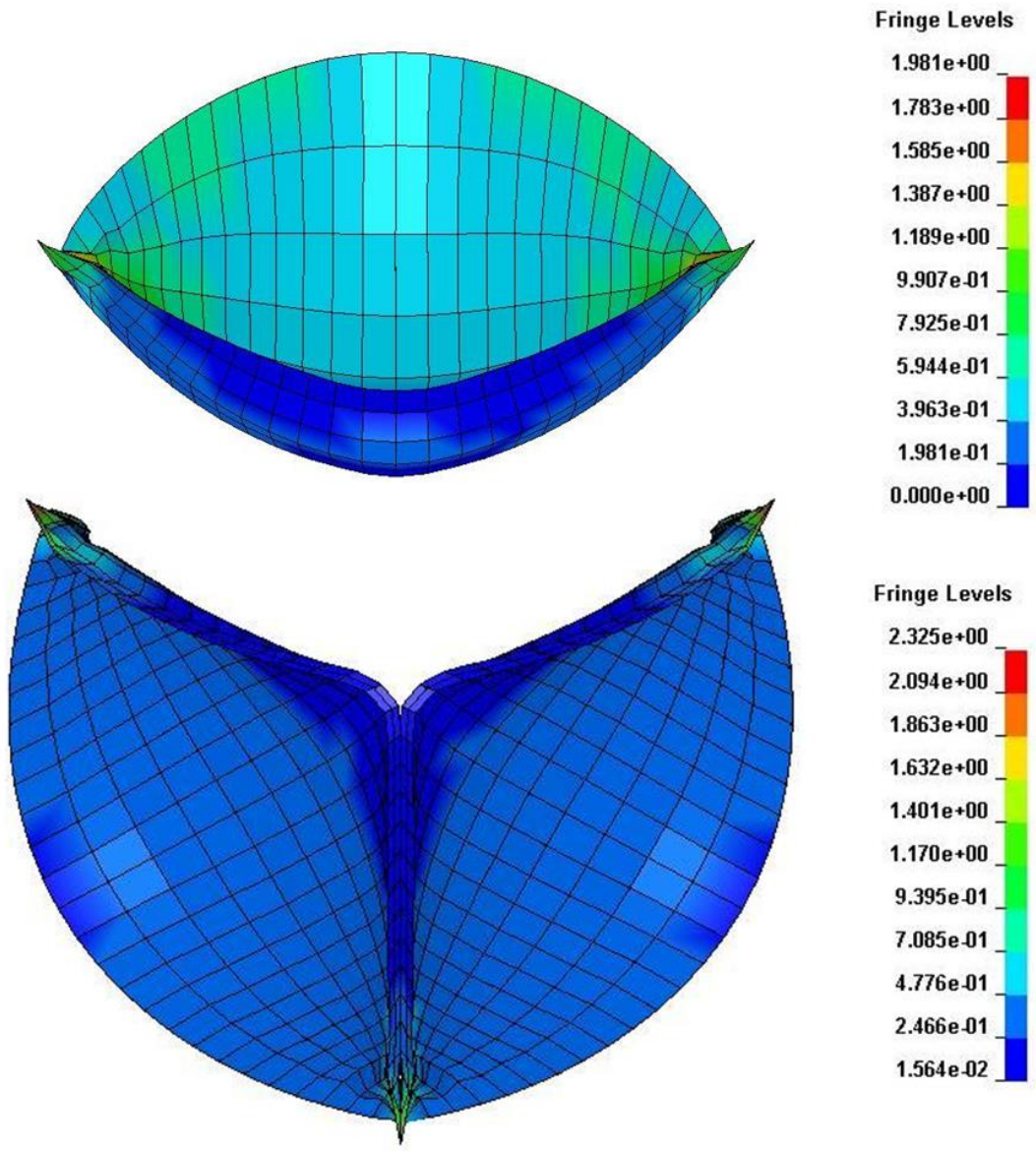
Fringe Levels
1.981e+00
1.783e+00
1.585e+00
1.387e+00
1.189e+00
9.907e-01
7.925e-01
5.944e-01
3.963e-01
1.981e-01
0.000e+00
Fringe Levels
2.325e+00
2.094e+00
1.863e+00
1.632e+00
1.401e+00
1.170e+00
9.395e-01
7.085e-01
4.776e-01
2.466e-01
1.564e-02

Figure 42(C)

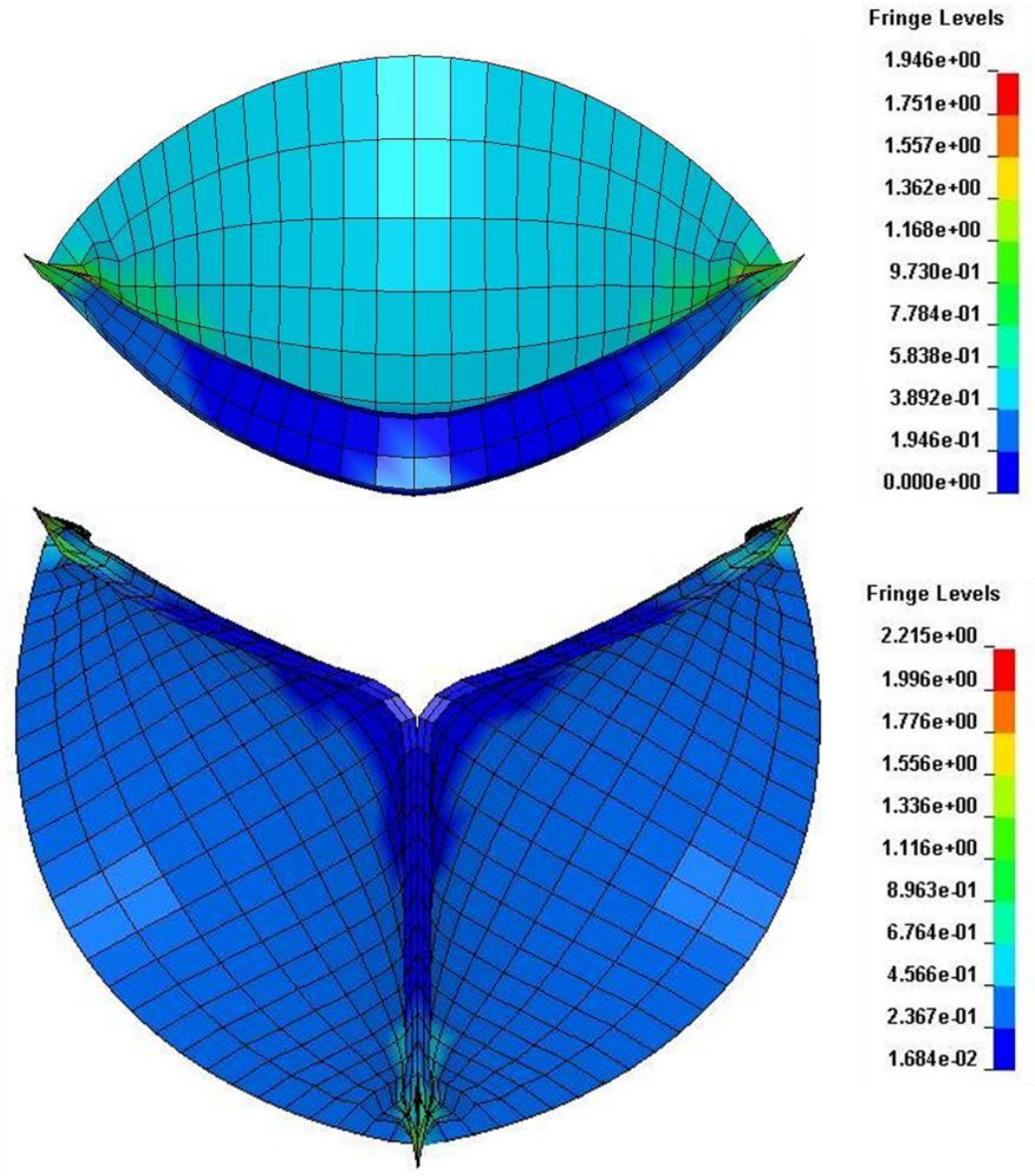
Fringe Levels
1.946e+00
1.751e+00
1.557e+00
1.362e+00
1.168e+00
9.730e-01
7.784e-01
5.838e-01
3.892e-01
1.946e-01
0.000e+00
Fringe Levels
2.215e+00
1.996e+00
1.776e+00
1.556e+00
1.336e+00
1.116e+00
8.963e-01
6.764e-01
4.566e-01
2.367e-01
1.684e-02

Figure 42(D)

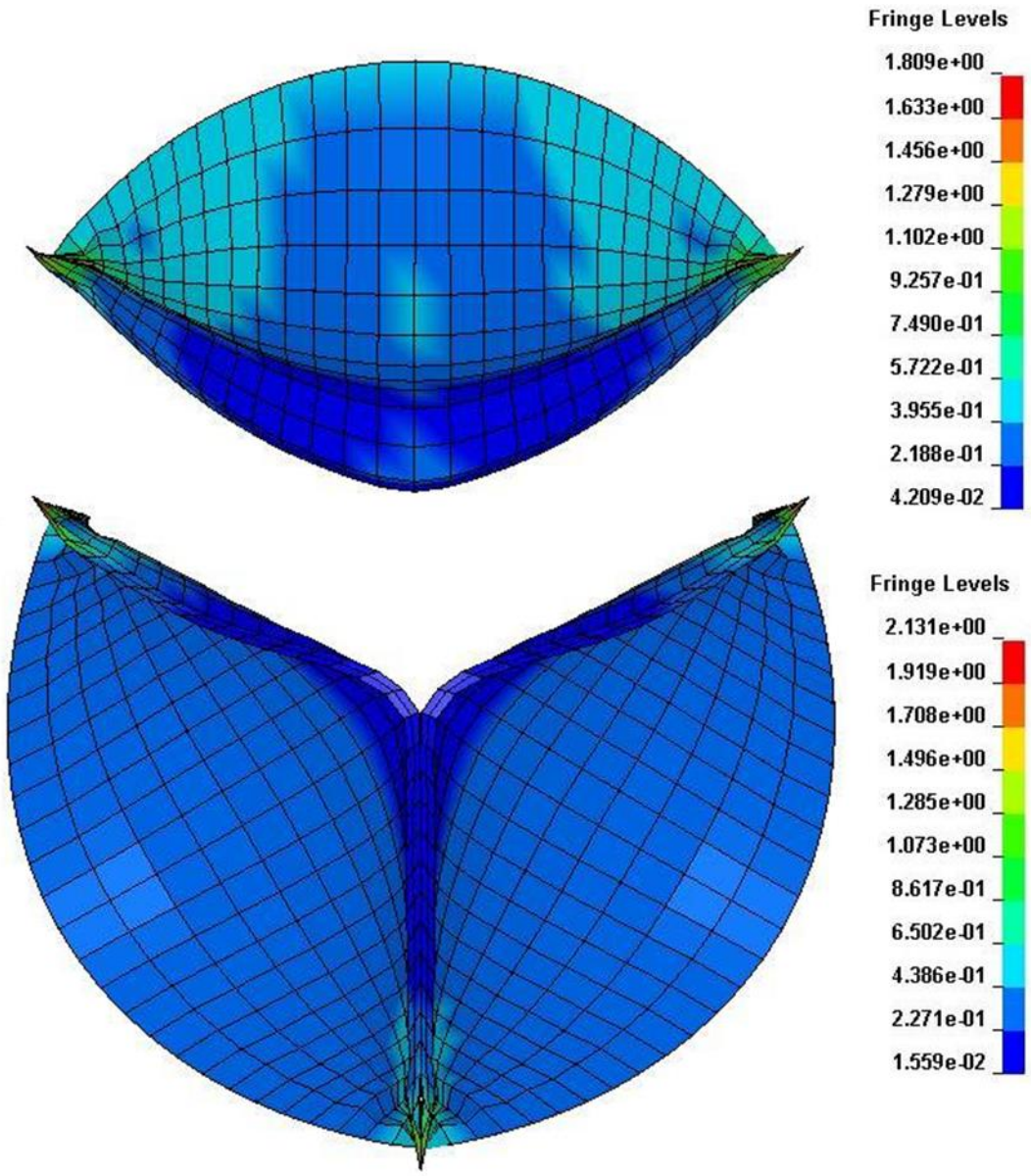

Figure 42(E)

Figure 42: Maximum values of Von Mises stress in the repaired valve with A: APP, B: HEMASHIELD, C: CorMatrix , D: BPP and E: SJM.

Conversely, the repaired leaflets that experienced the highest stresses were made of collagen-impregnated Dacron (HEMASHIELD) (Figure 42-B), extracellular matrix scaffold (CorMatrix) (Figure 42-C), and glutaraldehyde-fixed bovine pericardial patch (BPP) (Figure 42-D) (2,263 kPa, 1,973 kPa and 1,946 kPa, respectively). These stresses were about 30%, 13% and 11% higher in the HEMASHIELD, CorMatrix and BPP materials, respectively, than the stresses in the native leaflets.

Interestingly, due to the way the three aortic leaflets lean on each another, the stresses in the native leaflets were also affected by the material chosen for the replaced leaflet. The smallest increases in stress experienced by the native leaflets were 9% when HEMASHIELD was used for the replaced leaflet, 24% with St. Jude Pericardial Patch, and 26% with autologous pericardium. The highest increases in stress were 32% with CorMatrix, and 27% with bovine pericardium.

5 Discussion

The aim of this study was to determine which material(s) would be best suited in the aortic valve repair setting, when partial or complete replacement of one leaflet is required. As revealed by a survey of the literature, no such work had been undertaken before, and therefore, this work represents a step forward in the state-of-the-art. Thus, it is important to first discuss the appropriateness of the methods used in this study.

The combination of experimental and computational investigations is valuable in that it allows for comparisons of results when both methods can provide the same type of information, and in that each approach yields unique additional pieces of information. For instance, the experimental model provided values for the cardiac output, whereas the finite element model did not, but yielded stress information that was not available from the experiments.

The porcine valve model was chosen for its close similarity with the human anatomy, as well as for its availability. The only anatomical difference between the human and the porcine aortic heart valve is the presence of a muscular shelf on the right coronary leaflet. The presence of this muscle shelf results in a delayed opening of the right coronary leaflet relative to that of the left and the non-coronary leaflets (Leonardus, 2007).

As verified by statistical analysis (Appendix C), there was no significant difference between the valve sizes in the different groups of repaired valves; therefore, valve size was not a factor influencing the findings about hemodynamic performance.

The replacement materials included in the experiments were chosen based on their clinical availability and relevance. However, it was clear from the beginning that the HEMASHIELD patch was an unlikely candidate. Although this material is widely used in vascular reconstruction and was included for completeness, it is fairly stiff and not convenient to work within a tight environment such as inside the aortic valve. Some of the materials included represent the latest attempts by private companies to produce suitable replacement materials.

The ViVitro left-heart simulator used in this study is arguably the most physiological one available on the market. As such, it benefits from a track-record of several decades and hundreds of research customers worldwide in the academic, private and government sectors. Therefore, we can be confident that the in vitro conditions in which the valves were tested are not only reproducible, but that they are representative of physiological in vivo conditions.

The hemodynamic performance of the valves was measured by the following five parameters: valve opening velocity (VO), valve slow closing velocity (VSC), valve closing velocity (VC), maximum geometric orifice area (GOA), and left ventricular work (LVW). The first three parameters have already been studied using three-dimensional echocardiography in patients with normal and stenotic valves (Handke et al., 2003). In normal valves, they found VO = 42 ± 23 cm^2/s, VSC = 8.0 ± 5.2 cm^2/s and VC = 50 ± 23 cm^2/s. Inspection of Tables 3 and Appendix B reveals that our measurements in both native and repaired valves are in very good agreement with the values from Handle et al., except for VO, where our measurements are approximately three to four times larger than expected. This discrepancy was traced to the difficulty, in our data processing, to accurately determine the time at which the valve started to open. Slow closing velocity results in this study did not

show any statistically significant difference between any experimental groups. Therefore, VSC was not considered further. On the other hand, the values for VO and VC in Table 8 from the finite element models are also in good agreement with those from Handke et al., confirming the validity of the models regarding these aspects.

Measuring GOA made logical sense because a valve needs to open fully to function properly. It is also known that GOA is markedly low in stenotic valves (e.g. down to 0.5-1.0 cm^2) (Gaillard et al., 2010). With the vast majority of GOA values above 4 cm^2 (Tables 3 and 8; Appendix B, Table B-1), except for a couple of failed tests, the valves in our experiments and computational models exhibited unrestricted opening, which is a desirable feature.

The left-ventricular work is also a useful measure in the case of stenotic valves, as more work is needed from the heart to push blood through a valve that is hardly open. Since the valves considered in this study were normal or close to normal in spite of their replaced leaflet, LVW did not prove to be a good marker to try and determine the influence of different replacement materials on valve performance (Tables 3 and 4; Appendix B, Table B-1).

Finite element modeling of the aortic valve has become increasingly accurate over the years, and recent publications show excellent agreement between experimental in vitro data and computational findings (Labrosse et al., 2010). The present study relies on the expertise accumulated regarding the valve geometry (Labrosse et al., 2006, 2011), the material characterization of aortic tissues (Labrosse et al., 2009, 2013), and computational aspects such as mesh density requirements, scaled computational time and automated processing of result files for GOA (Labrosse et al., 2010, 2011). In particular, it is worth noting that the stress values are not significantly affected by mesh refinement (e.g. adding one element across the aortic and leaflets thickness did not globally affect the strains or stresses) (Labrosse

et al., 2010). Simulation time was 1/10 of the real time as previous analyses with real time or scaled time yielded results within 2% of each other, due to comparatively small inertial loads (Labrosse et al., 2010). In addition, although the unpressurized configuration of the valve leaflets is such that they would interfere with each other (Figure 41 at Time 0), the initial pressurization of the model to 80 mmHg separates the leaflets before the cardiac cycle starts (Figure 41 at Time 1), making the computational model consistent with normal physiology.

As already mentioned above, the values for VO and VC in Table 8 agree well with in vivo measurements by Handke et al. Given that the geometry and the dynamics of the valve are well reproduced in the computational models, evaluation of stress levels hinges on the accuracy of the material models used. As seen in Figure 35, the present models are able to capture the complex anisotropic hyperelastic behavior of the native and replacement materials. This means that at minimum, significant comparisons regarding stress levels can be made between the models to determine which materials provide the best performance.

5.1 Experimental and computational results

The autologous porcine pericardium (APP) used was derived from fresh porcine pericardium and exhibited poor handling qualities due to its fragile structure. Post-repair VO ($P = 0.03$) and VC ($P = 0.02$) were significantly reduced as compared to unrepaired valves; however, the GOA and LVW were unchanged.

When the HEMASHIELD patch was used to replace the non-coronary leaflet, VC ($P = 0.01$) and GOA ($P < 0.05$) were significantly reduced while other parameters including LVW, VSC, and VO were similar.

For aortic valves repaired with CorMatrix, all valvular hemodynamic parameters including VO (P = 0.0001), VSC (P = 0.01), VC (P = 0.0001), and GOA (P = 0.0001) were significantly reduced when compared to baseline assessment. There was a slight increase in LVW post CorMatrix repair but it did not reach statistical significance (P = 0.4).

After repair with a bovine pericardial patch (BPP), hemodynamic function was found to be similar to baseline across all parameters (VO, VSC, VC, GOA, and LVW).

The valvular hemodynamic measurements based on *ex vivo* left heart simulation models suggest that APP and BPP would be the best suited replacement material candidates for valve repair; however, these conclusions do not factor in information about the mechanical stress experienced by the individual leaflets (non-coronary leaflet, left and right non-repaired leaflets). Thus, experiments were carried out on these materials and a FE model was generated to evaluate all four replacement materials used along with another bovine pericardial patch provided in kind by St. Jude Medical (SJM).

In the FE models, while the VO, VC, and GOA values did not differ by more than 9 % between all materials and un-repaired valves, the Von Mises stresses varied significantly between replacement material properties in both the non-coronary leaflet (repaired leaflet) and the left/right non-repaired leaflets. The SJM bovine pericardial patch resulted in the least increase in non-coronary leaflet (+4%; 1,809 kPa) and left/right non-repaired leaflet stresses (+24%; 2,159). Following closely, the APP demonstrated the next least increase in non-coronary leaflet (5%; 1,841) and left/right non-repaired leaflet stresses (+26%; 2,206). HEMASHIELD, CorMatrix, and BPP demonstrated increased stresses ranging from 11 – 32% when compared to the control model. Large stresses are expected to promote tears or local calcification by increasing cell death in tissues; therefore, they are not desirable. Thus,

based on our FE results, SJM and APP represent the best suited materials for repaired valve. Although the *ex vivo* data suggested that BPP would be a good material as well, increased leaflet stresses determined by FE analysis lowered its ranking as a suitable material.

In all repaired valves, the stresses in the replaced leaflets were below the materials' expected strengths, and therefore were not likely to cause immediate tearing. However, higher stresses in the repaired leaflet mean that the suture line may be at higher risk of rupturing or initiating tears in the leaflets materials due to localized stress concentration effects.

5.2 Clinical relevance

Clinical applications of autologous human pericardial tissue have been used for repaired valve, aortic root enlargement, and LV aneurysm repair (Nosal et al., 2012; Pinchuk et al., 2008). Since autologous porcine pericardium (APP) has characteristics similar to human pericardial tissue, APP was used in this study as a surrogate to human pericardium (Price & El Khoury, 2012; Badiu, et al., 2011). Thus, APP would be a reasonable choice of material to use since its valvular hemodynamic characteristics are similar to those of the native valve.

Hemodynamic measurements results suggest that despite no increase in LVW, the noncompliant nature of the HEMASHIELD material led to slower VC and smaller GOA. While HEMASHIELD has been used for aortic root enlargement and LV aneurysm repair, it has not been used for aortic valve repair in a clinical setting (Myers et al., 2010).

CorMatrix represents the least ideal product for aortic valve repair. CorMatrix is an approved sheet for the use in cardiac surgical septal repair, and pericardial closure, but little

information is available in the literature about its clinical application for Aortic valve repair (Quarti et al., 2012; Scholl et al., 2010).

The results of this study suggest that BPP may be another reasonable choice for material selection in aortic valve repair, especially as it is easy to work with. Some studies indeed demonstrate good short-term outcomes following leaflet restoration with bovine pericardial patch. Also, fresh and photo-fixed autologous pericardium trended toward better durability than glutaraldehyde fixed bovine pericardium but predictors of re-operation did not include the material used.

Von Mises stress represents a combination of all stresses acting in a particular location. This variable has been measured in previous studies in determining specific areas, like the aortic commissures, with highest stress under static and dynamic loads (Hoffman et al., 1992; Labrosse et al., 2010). By understanding the values and patterns of valvular stresses, surgeons could utilize better, more stress-compatible materials in the reparative process thereby reducing the incidence of aortic valve repair related failure.

5.3 Limitations of current study and recommendations for future work

Limitations behind this study include the lack of an *in vivo* model to measure post-repair hemodynamics and utilization of a finite element model to derive stress patterns. While an *in vivo* model would provide more realistic settings, it would be very difficult to perform precise and accurate measurements like those executed in this study.

The finite element solvers have limitations in terms of numerical stability. For instance, with Guccione's model in LS-Dyna, the first material constant (c_1) should not be less than 1 kPa for numerical stability. In addition, small elements lead to impractically long

computation times. As the actual measured thickness of some materials (e.g. APP) was very small, and it had to be artificially increased. In turn, the material properties had to be corrected to preserve an equivalent mechanical behavior (Table 6).

For future work, more analyses may be run with other valve configurations and replacement materials for evaluation of their different features. For instance, using patient-specific data derived from 3-D TEE, actual valve geometries could be modeled instead of idealized ones, and repair on more than one leaflet could be investigated. However, patient-specific real-time simulations are still beyond reach since the computations done for present study took between 4 and 9 hour for one cardiac cycle (depending mostly on the contact geometry between leaflets). Instead, pre-operative data may be used to set up simulations and identify the best replacement material graft for a given situation.

Simulating sutures may also bring new findings. For example, after replacing a leaflet, high stresses carried by the replacement leaflet may lead to tears at the commissural attachments or at the suture line in the belly. Sutures to repair the leaflet could be included in the model with additional elements (Labrosse et al., 2011). The type (strength and diameter) and placement of the sutures would likely change the stress distribution in the region of the suture. Such investigation may help to provide guidelines for what and how sutures should be placed to minimize stress concentrations.

6 Conclusions

In conclusion, the methodology presented here provides valuable tools and techniques to study the effects, in terms of hemodynamic performance and mechanical stress levels, of different clinically relevant replacement materials that may be used in aortic valve repair.

This study demonstrates that, although the *ex vivo* left-heart simulator models suggested that the autologous and bovine pericardial patches would be best suited for aortic valve repair, finite element modeling determined increased stresses in the bovine pericardial, HEMASHIELD™, and CorMatrix™ patches which may be associated with late repair failure. Finally, the autologous pericardial and St Jude Medical patches had the closest profiles to normal aortic valves in both modalities; therefore, use of either replacement material may be best suited.

References

AbuRahma A, Robinson PA , Hannay RS, Hudson J, Cutlip L, 2001. Prospective controlled study of carotid endarterectomy with hemashield patch: is it thrombogenic? *Vascular surgery,* 35(3): 167-74.

Agabegi S S, 2008. *Step-Up to Medicine.* Hagerstown, MD, United States: Lippincott Williams & Wilkins.

Aksoy O, O'Brien B L & Menon V, 2013. Options for managing severe aortic stenosis: A case-based review. *Cleveland clinic journal of medicine ,* 80: 243-252.

Al Fagih M, al Kasab S & Ashmeg A, 1988. Aortic valve repair using bovine pericardium for cusp extension. *Thorac Cardiovasc Surg,* 96: 760-4.

Al-Halees Z, Gometza B & Duran C, 1998. Aortic valve repair with bovine pericardium. *The Annals of thoracic surgery,* 65(2): 601-2.

Anderson R H, 2000. ANATOMY: Clinical anatomy of the aortic root. *Heart,* Volume 84: 670-673.

Arcidiacono G, Corvi A & Severi T, 2005. Functional analysis of bioprosthetic heart valves. *Journal of Biomechanics,*38: 1483–1490.

Azadani A N, Chitsaz S & Mat P B, 2012. Comparison of Mechanical Properties of Human Ascending Aorta and Aortic Sinuses. *Ann Thorac Surg,* 93: 87–94.

Badiu CC, Bleiziffer S, Eichinger WB, Zaimova I, Hutter A, Mazzitelli D, 2011. Are bicuspid aortic valves a limitation for aortic valve repair? *European journal of cardio-thoracic surgery,* 40(5): 1097-104.

Billiar K & Sacks M, 2000. Biaxial Mechanical Properties of the Natural and Glutaraldehyde Treated Aortic Valve Cusp. *Journal of Biomechanical Engineering,*122: 23-30.

Black M M, Howard IC, Huang X & Pat E A, 1991. A Three-dimensional analysis of a bioprosthetic heart valve. *Biomechanics ,* 24(9): 793-801.

Bloomfield P, 2002. Choice of heart valve prosthesis. *Heart,* 87: 583–589.

Boodhwani M, De Kerchove LDK & David G, 2009. Repair of aortic valve cusp prolapse. *European Association for Cardio-thoracic Surgery,* 10: 1-6.

Boodhwani M, De Kerchove LDK & Gebrine E, 2009. Aortic root replacement using the reimplantation technique:tips and tricks. *Interactive CardioVascular and Thoracic Surgery,*8: 584–586.

Boodhwani M, De Kerchove L, Glineur D, Poncelet A, Rubay J, 2009. Repair-oriented classification of aortic insufficiency: Impact on surgical techniques and clinical outcomes. *Thoracic and Cardiovascular Surgery,* 286-293.

Boodhwani M, De Kerchove L, Glineur D, Rubay J, Vanoverschelde JL, Noirhomme P, 2010. Repair of regurgitant bicuspid aortic valves: a systematic approach. *J Thorac Cardiovasc Surg,* 140(2): 276-84.

Čanádyová J, Mokráček A & Bush R, 2011. Aortic Valve Sparing Operation. In: *Aneurysmal Disease of the Thoracic and Abdominal Aorta* . Rijeka: InTech, 101-120.

Carr J & Savage E, 2004. Aortic valve repair for aortic insufficiency in adults: a contemporary review and comparison with replacement techniques. *European journal of cardio-thoracic surgery,* 25(1): 6-15.

Clark, Swanson WM & Richard E, 1974. Dimensions and Geometric Relationships of the Human Aortic Value as a Function of Pressure. *American Heart Association,*35: 871-882.

Conti C A, Votta E & De A, 2010. Dynamic finite element analysis of the aortic root from MRI-derived parameters. *Medical Engineering & Physics,* Volume 32: 212–221.

Conti FA, Morganti S & Totarod P, 2011. A computational tool to support pre-operative planning of stentless aortic valve implant. *Medical Engineering & Physics,*33: 1183– 1192.

Cox M AJ, Driessen NJB, Bouten CVC & Baaijens FPT, 2006. Mechanical characterization of anisotropic planar biological soft tissues using large indentation: a computational feasibility study. *Journal of Biomechanical Engineering,* 128: 428-436.

De Kerchove L, Boodhwani M & Glineur D, 2009. Cusp Prolapse Repair in Trileaflet Aortic Valves: Free Margin Plication and Free Margin Resuspension Techniques. *Ann Thorac Surg,* Volume 88: 455-461.

Doss M, Sirat S, Risteski P, Martens S, Moritz A, 2008. Pericardial patch augmentation for repair of incompetent bicuspid aortic valves at midterm. *Eur J Cardio-thorac Surg,* 35(5): 881-4.

Fattouch K, Murana G, Castrovinci S, Nasso G, Moss, 2012. Outcomes of aortic valve repair according to valve morphology and surgical techniques. *Interactive cardiovascular and thoracic surgery.,*15(4): 644-650.

Fung YC, Fronek K & Patitucci P, 1979. Pseudoelasticity of arteries and the choice of its mathematical expression. *American Journal of Physiology - Heart and Circulatory Physiology,* 237: 620-631.

Fung Y-C & Han H-C, 1995. Longitudinal strain of canine and porcine aorta. *Biomechanics,* 28(5): 637-641.

Gaillard E, Garcia D, Kadem L, Pibarot P, Durand L-G, 2010. In Vitro Investigation of the Impact of Aortic Valve Stenosis Severity on Left Coronary Artery Flow. *Journal of Biomechanical Engineering,* 132: 044502-4.

Grande-Allen KJ, Cochran R P & RPG, 2001. Mechanisms of aortic valve incompetence: Finite-element modeling of Marfan syndrome. *J Thorac Cardiovasc Surg,* 122: 946-954.

Grande K, Cochran RP & Renhall PG, 1998. A Stress Variations in the Human Aortic Root and Valve: The Role of Anatomic Asymmetry. *Annals of Biomedical Engineering,* 26: 534–545.

Guccione J, McCulloh A & Waldman L, 1991. Passive material properties of intact ventricular myocardium determined from a cylindrical model. *Biomech Eng,* 113: 42–55.

Gundiah N, Matthews PB & Karimi R, 2008. Significant Material Property Differences Between the Porcine Ascending Aorta and Aortic Sinuses. *Heart Valve Disease*, 17: 606-613.

Gundiah N, Matthews PB, Karimi R & Aza A, 2008. Significant Material Property Differences Between the Porcine Ascending Aorta and Aortic Sinuses. *The Journal of Heart Valve Disease,* 17: 606-613.

Hammer PE, Chen P & Del Nido RP, 2012. Computational model of aortic valve surgical repair using grafted pericardium. *Journal ofBiomechanics,* 45: 1199–1204.

Handke M, Heinrichs G, Beyersdorf F, Olschewski M, Bode C, Geibel A, 2003. In vivo analysis of aortic valve dynamics by transesophageal 3-dimensional echocardiography with high temporal resolution. *The Journal of Thoracic and Cardiovascular Surgery ,* 125(6): 1412-19.

Harringer W, Pethig K, Hagl C, Meyer GP, Haverich A, 1999. Ascending Aortic Replacement With Aortic Valve Reimplantation. *Circulation,* 100: 23-28.

Hearn K, Somerville J, Sutton R, Wright J, Ross D, 1973. Aortic valve replacement with unsupported fascia lata. *Thorax,* 28(5): 603-7.

Hoffman D, Gong G, Liao K, Macaluso F, Nikolic SD, Frater RW, 1992. Spontaneous host endothelial growth on bioprostheses. Influence of fixation.. Circulation, 86(5): 75-9.

Hopkins RA , Bert AA, Buchholz B, Guarino K, 2004. Surgical patch closure of atrial septal defects. *Ann Thorac Surg,* 77(6): 2144-9.

Ho S Y, 2009. Structure and anatomy of the aortic root. *European Journal of Echocardiography,*10: i3–i10.

Huang X, Black MM, Howard IC & Paite EA, 1989. A two-dimensional finite element analysis of abioprosthetic heart valve. *Journal of biomechanics.*, 23(8): 753-762.

Humphrey JD, 2002. Cardiovascular solid mechanics:Cells, tissues, and organs. Dans: New York: Springer verlag.

Ioan Ionasec R, Voigt I & Georges B, 2010. Patient-Specific Modeling and Quantification of the Aortic and Mitral Valves From 4-D Cardiac CT and TEE. *IEEE transactions on medical imaging,* 29(9): 1636-1651.

Koch TM, Reddya BD, Zilla P & Franz T, 2010. Aortic valve leaflet mechanical properties facilitate diastolic valve function. *Computer Methods in Biomechanics and Biomedical Engineering,* 13(2): 225–234.

Labrosse MR, Beller CJ, Mesana T & Veinot JP, 2009. Mechanical behavior of human aortas: Experiments, material constants and3-D finite element modeling including residual stress. *Journal of Biomechanics,* 42: 996–1004.

Labrosse MR, Beller CJ, Robicsek F & Thubrikar MJ, 2006. Geometric modeling of functional trileaflet aortic valves:Development and clinical applications. *Journal of Biomechanics,* 39: 2665–2672.

Labrosse MR, Boodhwani M & Sohmer B, 2011. Modeling leaflet correction techniques in aortic valve repair:A finite element study. *Journal of Biomechanics,* 44: 2292–2298.

Labrosse MR, Gerson ER, Veinot JP & Beller CJ, 2013. Mechanicalcharacterizationofhumanaortasfrom pressurization testing and a paradigm shift for circumferentia lresidual stress. *Journal of the mechanical behavior of biomedical materials,*17: 44-55.

Labrosse MR, Lobo K & Beller C, 2010. Structural analysis of the natural aortic valve in dynamics:From unpressurized to physiologically loaded. *Journal of Biomechanics,* 43: 1916–1922.

Langer F, Aicher D, Kissinger A, Wendler O, Lausberg H, Fries R et al., 2004. Aortic valve repair using a differentiated surgical strategy. *Circulation,* 110: 67-73.

Lansac L, Di Centa I & Bonnet N, 2006. Aortic prosthetic ring annuloplasty: a useful adjunct to a standardized aortic valve-sparing procedure. *European Journal of Cardio-thoracic Surgery,* 29: 537—544.

Lausberg H, Aicher D, Langer F & Schafers H J, 2006. Aortic valve repair with autologous pericardial patch. *Eur J Cardio-thorac Surg.,* 30(2): 244-9.

le Polain de Waroux J-B, Pouleur A-C, Robert A, Pasquet A, Gerber BL, Noirhomme P, El Khoury G et al., 2009. Mechanisms of Recurrent Aortic Regurgitation After Aortic Valve Repair. *After Aortic Valve Repair,* 2(8): 931-939.

Leonardus F J, 2007. *A novel approach in cross-linking of bioprosthetic heart valves.* s.l.:Everaerts.

Li J, Luo X & Kuang Z, 2001. A nonlinear anisotropic model for porcine aortic heart valves. *Journal of Biomechanics,* 34: 1279–1289.

Marieb EN & Hoehn K, 2013. *Human Anatomy and physiology.* 9 éd. s.l.:Pearson.

Maselli D & Ruggero De Paulis R, 2007. Sinotubular Junction Size Affects Aortic Root Geometry and Aortic Valve Function in the Aortic Valve Reimplantation Procedure: An In Vitro Study Using the Valsalva Graft. *Ann Thorac Surg,* 1214–8.

Matalanis G, Y Shi, W & A R Hayw P, 2010. Correction of leaflet prolapse extends the spectrum of patients suitable for valve-sparing aortic root replacement. *European Journal of Cardio-thoracic Surgery,* 37: 1311—1316.

Miller DC, 2007. Valve-Sparing Aortic Root Replacement: Current State of the Art and Where Are We Headed? *Ann Thorac Surg,* 83: 736-739.

Myers, PO; Tissot C, Christenson JT, Cikirikcioglu M, Aggoun Y, Kalangos A, 2010. Aortic valve repair by cusp extension for rheumatic aortic insufficiency in children: Long-term results and impact of extension material. *Thorac Cardiovasc Surg,* 140(4): 836-44.

Nosal M, Poruban R, Valentik P, Sagat M, Nagi AS, Kantorova A, 2012. Initial experience with polytetrafluoroethylene leaflet extensions for aortic valve repair. *European journal of cardio-thoracic surgery : official journal of the European Association for Cardi,* 41(6): 1255-7.

Pai R K & Fort S, 2011. Aortic Insufficiency.

Peppas NA, Zach Hilt J & Bro J, 2007. *Nanotechnology in Therapeutics: Current Technology and Applications.* Norfolk: Horizon Scientific Press.

Pinchuk L, Wilson GL, Barry JJ, Schoephoerster RT, Parel JM, Kennedy JP, 2008. Medical applications of poly(styrene-block-isobutylene-block-styrene) ("SIBS"). *Biomaterials,* 29(4): 448-60.

Price J & El Khoury G, 2012. Aortic valve insufficiency leaflet reconstruction techniques. *Seminars in thoracic and cardiovascular surgery Pediatric cardiac surgery annual.,* 15(1): 3-8.

Puig LB, Verginelli G, Belotti G, Kawabe L, Frack CC, Pileggi F et al.,1972. Homologous dura mater cardiac valve. Preliminary study of 30 cases. *J Thorac Cardiovasc Surg,* 64(1): 154-60.

Quarti M, Nardone S, Colaneri M, Santoro G, Pozzi M, 2012. Preliminary experience in the use of an extracellular matrix to repair congenital heart disease. *Interactive cardiovascular and thoracic surgery,* 13(6): 569-72.

Ranga A, Bouchot O & Mongrain R, 2006. Computational simulations of the aortic valve validated by imaging data:evaluation of valve-sparing techniques. *Interact CardioVasc Thorac Surg,* 5: 373-378.

Rankin JS, Conger JL, Tuzun E, Winkler JA, Harms KM, Beavan LA, et al., 2012. In vivo testing of an intra-annular aortic valve annuloplasty ring in a chronic calf model. *journal of the European Association for Cardio-thoracic Surgery,* 42: 149-54.

Robarts P, 2007. *A novel approach in cross-linking of bioprosthetic heart valves.* Enschede, The Netherlands: Netherlands Heart Foundation.

Salomon D, 2006. *Curves and Surfaces for Computer Graphics.* New York: Springer Verlag.

Scholl FG, Boucek MM, Chan K-C, Valdes-Cruz L, Perryman R, 2010. Preliminary Experience With Cardiac Reconstruction Using Decellularized Porcine Extracellular Matrix Scaffold. *World Journal for Pediatric and Congenital Heart Surgery,* 1(1): 132-6.

Silver M & William, C. R., 1965. Detailed Anatomy of the Normally Functioning Aortic Valve in Hearts of Normal and Increased Weight. *Am J Cardiol,* 55: 454-461.

Soncini M, Votta E & Zinicchino S, 2009. Aortic root performance after valve sparing procedure:A comparative finite element analysis. *Medical Engineering & Physics,* 31: 234–243.

Stella J, 2007. on the biaxial mechanical properties of the layers of the aortic valve Leaflets. *jornal of biomechanical Engineering,* 129(5): 757-766.

Takamizawa K & Hayashi K, 1987. Strain energy density function and uniform strain hypothesis for arterial mechanics. *Journal of Biomechanics,* 20(1): 7–17.

Takkenberg, Yacoub M & JJM, 2005. Will heart valve tissue engineering change the world? *Nature clinical practice cardiovascular medicine,* 2(2): 61-62.

Tamás É & Nylander E, 2007. Echocardiographic Description of the Anatomic Relations within the Normal Aortic Root. *The Journal of Heart Valve Disease,* 16; 240-246.

Thubrikar M, 1990. *The aorticvalve.* Boca Raton, Florida: CRC Press.

Thubrikar MJ, Gong GG, Konstantinov IE, Se lim GA, Fowler BL, Robicsek F, 2000. Infuence o f sizing and subcoronary implantation technique on the function of porcine aortichomo grafts. *Journal of Medical Engineering & Technology,* 24:173–180.

Thubrikar MJ & Robicsek F, 2001. A New Aortic Root Prosthesis With Compliant Sinuses for Valve-Sparing Operations. *Ann Thorac Surg,* 1: 318-322.

Underwood MJ, EL Khoury, G. & Deronck, D., 2000. The aortic root: structure, function, and surgical reconstruction. *Heart,* 83: 376–380.

Vermeulen F, Schepens M, de Valois J, Wijers L, Kelder J, 2001. The Hemashield Woven prosthesis in the thoracic aorta: a prospective computer tomography follow-up study. *Cardiovasc Surg,* 9(6): 580-5.

Vesely I, 2005. Heart Valve Tissue Engineering. *Circulation Research,* 97: 743-755.

Yacoub MH, Gehle P & Chan V, 1998. Late results of a valve-preserving operation in patients with aneurysms ofthe ascending aorta and root. *The Journal of Thoracic and Cardiovascular Surgery,* 115(5):1080-90.

Yacoub M & Takkenberg J, 2005. Will heart valve tissue engineering change the world? *Nature clinical practice cardiovascular medicine,* 2(2): 61-62.

Appendix A – MatLab code for GOA measurements

```
function GOA_versus_time_measurements()
    clc;
    clear;
    camera_frame_rate = 800;        % camera setting in fps
    cannula_inner_diameter = 2.05;  % in centimeters, as measured
    interval = 10;                  % 1 in "interval" original frames are
used for analysis

    originalFolder = pwd;
    [FileName,sourPathName] = uigetfile({'*.avi'},'Browse for input data
file (.avi format), double-click on it, and wait...');
    c = textscan(FileName,'%[^.]');
    SaveName = horzcat(char(c{1}),'.txt');

    MovieObj = VideoReader(FileName);

    % Read in all video frames.
    vidFrames = read(MovieObj);
    % Get the number of frames.
    numFrames = get(MovieObj, 'NumberOfFrames');

    [~,~,~,nFrames] = size(vidFrames);
    first = 1;

    % Converting frames to grayscale images for processing
    k = 1;
    [row,col,~,~] = size(vidFrames(:,:,:,1));
    images = zeros(row,col,1,round(nFrames/interval));
    for i = 1:interval:nFrames-1
        images(:,:,1,k) = .2989*vidFrames(:,:,1,i + first) +
.5870*vidFrames(:,:,2,i + first) + .1140*vidFrames(:,:,3,i + first);
        k = k + 1;
    end

    scrsz = get(0,'ScreenSize');
    choice = 2;
    ncols = 6;
    warning off all;
    while choice == 2
        figure('Name','Follow steps to calibrate images and measure GOA -
Double-click to confirm','WindowStyle','modal','NumberTitle','off');
        montage(images,'Size',[NaN
ncols],'DisplayRange',[],'Indice',1:1:round(nFrames/interval));
        h =
impoint(gca,0.5*col*ncols,round(0.5*nFrames/interval/ncols)*row);
        setString(h,'Drag to first picture with maximally open valve');
        pos = wait(h);
        colf = ceil(pos(1,1)/col);
        rowf = ceil(pos(1,2)/row);
        kf = (rowf-1)*ncols + colf;
        h =
impoint(gca,0.5*col*ncols,round(0.5*nFrames/interval/ncols)*row);
        setString(h,'Drag to a picture with bottom cannula');
        pos = wait(h);
        colb = ceil(pos(1,1)/col);
```

```
        rowb = ceil(pos(1,2)/row);
        kbot = (rowb-1)*ncols + colb;
        h =
impoint(gca,0.5*col*ncols,round(0.5*nFrames/interval/ncols)*row);
        setString(h,'Drag to last picture with almost maximally open
valve');
        pos = wait(h);
        coll = ceil(pos(1,1)/col);
        rowl = ceil(pos(1,2)/row);
        kl = (rowl-1)*ncols + coll;
        close(gcf);

        figure('Name','Move/Resize cannula perimeter - Double-click to
confirm','NumberTitle','off','OuterPosition',[scrsz(1) scrsz(2) scrsz(3)
scrsz(4)]);

imshow(squeeze(images(:,:,1,kbot)),'DisplayRange',[],'InitialMagnification'
,'fit');
        set(gca,'PlotBoxAspectRatio',[1 1 1]);
        h = imellipse(gca, [col/2 row/2 100 100]);
        setFixedAspectRatioMode(h,'True');
        setColor(h,'r');
        posi = wait(h);
        diam = max(posi(:,1)) - min(posi(:,1));
        choice = menu('Options','Continue','Redo');
        close(gcf);
    end

    choice = 1;
    kmax = kf + (round(nFrames/interval) - kl) + 1;
    GOA = zeros(kmax,1);
    time = zeros(kmax,1);
    k = 1;
    while choice == 1 && k <= kf
        figure('Name','Trace GOA
contour','NumberTitle','off','OuterPosition',[scrsz(1) scrsz(2) scrsz(3)
scrsz(4)]);
        img = squeeze(images(:,:,1,k));
        h_im = imshow(img,'DisplayRange',[],'InitialMagnification','fit');
        roi = imfreehand;
        BW = createMask(roi,h_im);
        pixarea = bwarea(BW);
        GOA(k,1) =
pixarea*(0.25*pi*cannula_inner_diameter^2/(0.25*pi*diam^2));
        time(k,1) = (k-1)*1/(camera_frame_rate/interval);
        choice = menu('Options','Continue','Redo tracing');
        close(gcf);
        if choice == 1
            k = k + 1;
        elseif choice == 2
            choice = 1;
        end
    end

    k = 1;
    while choice == 1 && k <= round(nFrames/interval) - kl + 1
```

```
        figure('Name','GOA
measurement','NumberTitle','off','OuterPosition',[scrsz(1) scrsz(2)
scrsz(3) scrsz(4)]);
        img = squeeze(images(:,:,1,k-1+kl));
        h_im = imshow(img,'DisplayRange',[],'InitialMagnification','fit');
        roi = imfreehand;
        BW = createMask(roi,h_im);
        pixarea = bwarea(BW);
        GOA(k+kf,1) =
pixarea*(0.25*pi*cannula_inner_diameter^2/(0.25*pi*diam^2));
        time(k+kf,1) = (k-1+kl)*1/(camera_frame_rate/interval);
        choice = menu('Options','Continue','Redo tracing');
        close(gcf);
        if choice == 1
            k = k + 1;
        elseif choice == 2
            choice = 1;
        end
    end

    % Save to file
    fid = fopen(SaveName,'wt');
    for i = 1:kmax
        fprintf(fid, '%6.3f %10.2f\n',time(i,1),GOA(i,1));
    end
    fprintf(fid, '%6.0f %6.1f %6.0f\n',(GOA(kf,1)-GOA(2,1))/(time(kf,1)-
time(2,1)),(GOA(kf,1)-GOA(kf+1,1))/(time(kf+1,1)-time(kf,1)),(GOA(kf+1,1)-
GOA(kmax,1))/(time(kmax,1)-time(kf+1,1)));
    fclose(fid);

    % Graph
    figure('Name','GOA versus
time','NumberTitle','off','OuterPosition',[scrsz(1) scrsz(2) scrsz(3)
scrsz(4)]);
    plot(time(:,1),GOA(:,1),'bo-');
    xlabel('Time (s)');
    ylabel('Geometric Orifice Area (sq.cm)');
end
```

Appendix B – Measurements of hemodynamic performance

Table B-1: Hemodynamic parameters as measured in valves.

STJ		Before repair						After repair				
Diameter	Case	CO	Velocities			Max GOA	LV work	Velocities			Max GOA	LV work
(mm)		(L/min)	(sq.cm/s)			(sq.cm)	(mJ)	(sq.cm/s)			(sq.cm)	(mJ)
22	H1	2.5	144	5.5	71	5.42	614	101	5.1	48	3.83	743
		5.0	136	-2.6	63	5.58	863	100	3.8	65	3.93	1102
		6.5	132	0.1	83	6.74	NA	140	0.7	75	3.9	1417
22	H2	2.5	103	0.1	47	6.42	692	40	9.8	32	6.78	841
		5.0	171	-0.2	64	6.43	1000	42	8.1	35	6.3	1223
		6.5	167	-2.4	59	6.69	1248	45	5.3	46	6.69	1435
21	H3	2.5	113	4.3	66	5.67	666	97	2.4	36	4.87	763
		5.0	94	3.3	61	5.91	1129	143	4.4	51	5.36	1106
		6.5	127	0.3	63	4.77	1301	115	2.4	39	4.32	1370
24	H4	2.5	104	0.4	61	3.91	737	39	4.6	22	3.39	743
		5.0	108	0.6	52	4.04	1051	105	-3.4	34	3.41	1249
		6.5	109	1.8	60	4.1	1301	169	2.4	33	4.75	2076
24	H5	2.5	116	8.3	45	5.81	674	139	8	60	5.31	742
		5.0	161	9.5	60	6.06	1121	212	10.7	46	5.73	1209
		6.5	164	8.8	78	6.18	1339	209	8.5	61	5.44	1430
22	H6	2.5	155	7.5	70	5.8	686	120	2.4	14	4.52	658
		5.0	175	13.4	92	6.56	1032	164	4.1	54	4.24	1009
		6.5	218	2.3	104	5.69	1274	101	5.6	52	5.06	1232
26	H7	2.5	95	8.1	47	5.98	666	150	1.7	86	5.7	662
		5.0	195	5.8	33	7.3	1004	211	1.7	66	8.01	992
		6.5	175	5	76	6.6	1217	195	6.7	100	7.52	1233
22	P1	2.5	140	5.5	69	5.28	636	267	8.5	84	7.13	947
		5.0	NA	NA	NA	NA	1070	118	5.2	44	4.44	932
		6.5	213	7.9	79	5.74	1242	109	-0.7	49	4.25	1134
22	P2	2.5	149	1.4	43	5.63	657	60	8.4	36	6.05	632
		5.0	NA	NA	NA	NA	1002	67	5.4	47	5.89	988
		6.5	147	0	65	5.83	1320	61	5.6	38	5.35	1229
22	P3	2.5	108	8	54	5.39	703	NA	NA	NA	NA	680
		5.0	140	0.5	69	5.26	981	191	3.6	74	7.18	936
		6.5	103	10.4	51	5.19	1222	195	6.3	120	7.33	1170
28	P4	2.5	157	6.3	94	5.91	649	138	7.4	45	5.2	997
		5.0	181	8.6	66	7.06	994	239	0.9	55	3.62	1330
		6.5	220	6.2	88	5.65	1249	NA	NA	NA	4.06	1627
24	P5	2.5	214	5.9	76	5.81	658	98	1.3	53	4.91	734
		5.0	214	1.3	77	6.02	1004	163	8.2	52	6.11	1033

		6.5	247	4.5	69	6.87	1238	158	6.9	61	5.93	1292
22	P6	2.5	107	6.8	48	5.37	691	NA	NA	NA	1.92	744
		5.0	138	7	42	5.29	1042	45	1.6	37	2.23	1151
		6.5	189	5.2	53	5.04	1241	43	2.6	44	2.23	1356
22	P7	2.5	145	18.8	53	7.27	712	104	5.3	5.3	5.18	657
		5.0	191	11.2	68	7.18	990	104	4.3	45	5.7	1016
		6.5	194	6.5	70	7.3	1249	147	5.4	53	5.58	1286
24	B1	2.5	153	5.8	48	5.76	736	126	7.6	57	4.73	714
		5.0	142	3.9	46	5.32	1083	203	7.8	55	5.16	1023
		6.5	135	2.2	63	5.29	1242	190	7.4	62	5	1287
22	B2	2.5	78	1.7	46	4.9	684	108	4	40	4.09	700
		5.0	197	2.9	91	4.99	1045	121	4.1	53	4.54	1075
		6.5	212	4.7	62	5.31	1287	156	4.4	61	4.48	1253
29	B3	2.5	169	8.5	83	6.36	709	186	3.3	74	6.96	1029
		5.0	177	9.3	86	6.64	983	262	0.4	75	6.62	1391
		6.5	265	5.5	94	6.67	1190	201	7.3	87	7.52	1611
22	B4	2.5	144	11.2	64	5.39	703	111	1.4	46	4.16	730
		5.0	246	13.8	60	6.23	1053	176	3.6	65	4.56	986
		6.5	213	11.3	78	5.58	1280	156	3.3	80	4.49	1199
22	B5	2.5	173	19.6	54	6.5	661	195	4	88	4.93	694
		5.0	240	11.5	69	6.06	1033	158	3.4	113	6.08	1062
		6.5	255	13.5	89	6.49	1222	207	-0.2	142	5.3	1205
26	B6	2.5	177	7.3	74	4.62	686	127	11.2	77	6.37	717
		5.0	153	6.2	67	4.18	1018	178	10	71	6.7	1057
		6.5	180	7.2	58	4.54	1250	171	11.8	79	6.59	1256
24	C1	2.5	159	13.1	51	5.98	694	104	1.1	43	3.97	731
		5.0	229	5.3	86	6.11	1078	119	1.1	44	4.59	1109
		6.5	244	5.1	69	6.61	1275	166	2.4	48	4.55	1280
22	C2	2.5	143	9.1	82	5.36	690	70	3.2	45	4.39	714
		5.0	219	6.2	78	5.68	1033	207	0.4	60	5.28	1002
		6.5	212	5.2	95	5.47	1235	150	4.3	80	5.63	1222
24	C3	2.5	241	8	59	6.07	703	64	5	47	4.77	699
		5.0	211	5.7	68	5.82	1026	181	3.2	65	4.57	1087
		6.5	188	5.9	81	6.83	1342	143	4.9	63	5.38	1262
26	C4	2.5	155	9	79	5.82	682	81	7.8	43	5.27	727
		5.0	220	-1.4	97	6.08	998	111	6	65	5.56	1049
		6.5	232	-6.8	88	6.67	1172	133	6.3	60	5.25	1241
22	C5	2.5	198	19.5	73	7.44	633	62	9.6	38	5.42	707
		5.0	274	13.9	83	6.91	1051	77	4.4	52	5.74	1086
		6.5	278	19	81	7.21	1221	76	1.5	62	5.67	1298

Table B-2: Valve hemodynamic in un-repaired porcine valves at different cardiac outputs (CO).

Measure	Combined (N=75)	CO 2.5 L/min (N=25)	CO 5.0 L/min (N=25)	CO 6.5 L/min (N=25)	P value
VO (cm^2/s)	171 (140-213)	145 (116-159)	181 (142-219)	194 (164-220)	0.002
VSC (cm^2/s)	5.9 (2.9-8.8)	7.5 (5.5-9)	5.8 (1.3-9.5)	5.2 (2.2-7.2)	0.12
VC (cm^2/s)	68 (59-79)	61 (48-73)	68 (60-83)	76 (63-83)	0.05
GOA (cm^2)	5.82 (5.37-6.5)	5.8 (5.4-5 .99)	6.06 (5.32-6.56)	5.83 (5.31-6.67)	0.5
LVW (mJ)	1029 (703-1222)	686 (661-703)	1032 (1000-1051)	1249 (1229-1283)	0.001

Appendix C – Boxplot comparison of valve sizes

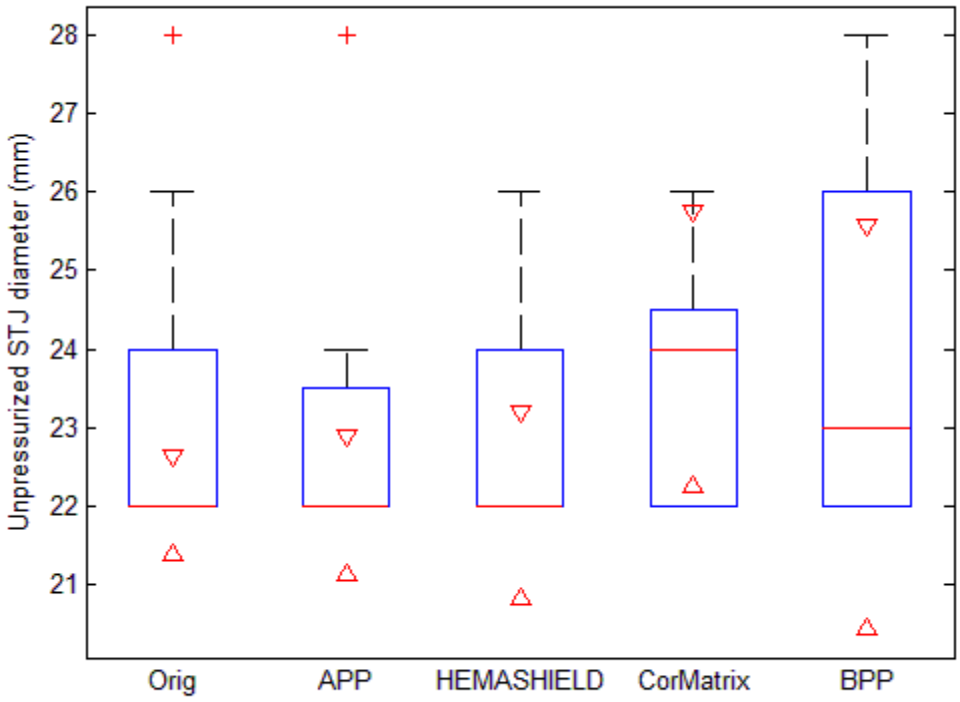

Appendix D – MatLab / Excel interface for statistical analysis of data

```
A=xlsread('Hadi_Ovais_Results.xlsx');

Diam=A(:,1);
for i=1:length(Diam)/3
    Diam(3*(i-1)+1:3*(i-1)+3)=Diam(3*(i-1)+1);
end
%Idx_1=find(Diam==22);
%Idx_2=find(Diam==24);
%Idx_3=find(Diam==26);
%Idx_4=find(Diam==28);

%Var_bef_aft=A(:,4:end)

Co=A(:,3);
Velo_Before_o=A(:,4);
Velo_Before_sc=A(:,5);
Velo_Before_c=A(:,6);
MGoa_Before=A(:,7);
Lv_Before=A(:,8);
Velo_After_o=A(:,9);
Velo_After_sc=A(:,10);
Velo_After_c=A(:,11);
MGoa_After=A(:,12);
Lv_After=A(:,13);

%Lv_After(Idx)=[];

Idx_1=find(Diam==22 & isnan(Velo_Before_o)==0);
Idx_2=find(Diam==24 & isnan(Velo_Before_o)==0);
Idx_3=find(Diam==26 & isnan(Velo_Before_o)==0);
Idx_4=find(Diam==28 & isnan(Velo_Before_o)==0);

Idx_5=find(Diam==22 & isnan(Velo_After_o)==0);
Idx_6=find(Diam==24 & isnan(Velo_After_o)==0);
Idx_7=find(Diam==26 & isnan(Velo_After_o)==0);
Idx_8=find(Diam==28 & isnan(Velo_After_o)==0);

MMM_Velo_Before_after_o_1=[mean(Velo_Before_o(Idx_1))
max(Velo_Before_o(Idx_1)) min(Velo_Before_o(Idx_1))
mean(Velo_After_o(Idx_5)) max(Velo_After_o(Idx_5))
min(Velo_After_o(Idx_5))]
MMM_Velo_Before_after_o_2=[mean(Velo_Before_o(Idx_2))
max(Velo_Before_o(Idx_2)) min(Velo_Before_o(Idx_2))
mean(Velo_After_o(Idx_6)) max(Velo_After_o(Idx_6))
min(Velo_After_o(Idx_6))]
MMM_Velo_Before_after_o_3=[mean(Velo_Before_o(Idx_3))
max(Velo_Before_o(Idx_3)) min(Velo_Before_o(Idx_3))
mean(Velo_After_o(Idx_7)) max(Velo_After_o(Idx_7))
min(Velo_After_o(Idx_7))]
MMM_Velo_Before_after_o_4=[mean(Velo_Before_o(Idx_4))
max(Velo_Before_o(Idx_4)) min(Velo_Before_o(Idx_4))
```

```
mean(Velo_After_o(Idx_8)) max(Velo_After_o(Idx_8))
min(Velo_After_o(Idx_8))]

Idx_1=find(Diam==22 & isnan(Velo_Before_c)==0);
Idx_2=find(Diam==24 & isnan(Velo_Before_c)==0);
Idx_3=find(Diam==26 & isnan(Velo_Before_c)==0);
Idx_4=find(Diam==28 & isnan(Velo_Before_c)==0);

Idx_5=find(Diam==22 & isnan(Velo_After_c)==0);
Idx_6=find(Diam==24 & isnan(Velo_After_c)==0);
Idx_7=find(Diam==26 & isnan(Velo_After_c)==0);
Idx_8=find(Diam==28 & isnan(Velo_After_c)==0);

MMM_Velo_Before_after_c_1=[mean(Velo_Before_c(Idx_1))
max(Velo_Before_c(Idx_1)) min(Velo_Before_c(Idx_1))
mean(Velo_After_c(Idx_5)) max(Velo_After_c(Idx_5))
min(Velo_After_c(Idx_5))]
MMM_Velo_Before_after_c_2=[mean(Velo_Before_c(Idx_2))
max(Velo_Before_c(Idx_2)) min(Velo_Before_c(Idx_2))
mean(Velo_After_c(Idx_6)) max(Velo_After_c(Idx_6))
min(Velo_After_c(Idx_6))]
MMM_Velo_Before_after_c_3=[mean(Velo_Before_c(Idx_3))
max(Velo_Before_c(Idx_3)) min(Velo_Before_c(Idx_3))
mean(Velo_After_c(Idx_7)) max(Velo_After_c(Idx_7))
min(Velo_After_c(Idx_7))]
MMM_Velo_Before_after_c_4=[mean(Velo_Before_c(Idx_4))
max(Velo_Before_c(Idx_4)) min(Velo_Before_c(Idx_4))
mean(Velo_After_c(Idx_8)) max(Velo_After_c(Idx_8))
min(Velo_After_c(Idx_8))]

Idx_1=find(Diam==22 & isnan(Velo_Before_sc)==0);
Idx_2=find(Diam==24 & isnan(Velo_Before_sc)==0);
Idx_3=find(Diam==26 & isnan(Velo_Before_sc)==0);
Idx_4=find(Diam==28 & isnan(Velo_Before_sc)==0);

Idx_5=find(Diam==22 & isnan(Velo_After_sc)==0);
Idx_6=find(Diam==24 & isnan(Velo_After_sc)==0);
Idx_7=find(Diam==26 & isnan(Velo_After_sc)==0);
Idx_8=find(Diam==28 & isnan(Velo_After_sc)==0);

MMM_Velo_Before_after_sc_1=[mean(Velo_Before_sc(Idx_1))
max(Velo_Before_sc(Idx_1)) min(Velo_Before_sc(Idx_1))
mean(Velo_After_sc(Idx_5)) max(Velo_After_sc(Idx_5))
min(Velo_After_sc(Idx_5))]
MMM_Velo_Before_after_sc_2=[mean(Velo_Before_sc(Idx_2))
max(Velo_Before_sc(Idx_2)) min(Velo_Before_sc(Idx_2))
mean(Velo_After_sc(Idx_6)) max(Velo_After_sc(Idx_6))
min(Velo_After_sc(Idx_6))]
MMM_Velo_Before_after_sc_3=[mean(Velo_Before_sc(Idx_3))
max(Velo_Before_sc(Idx_3)) min(Velo_Before_sc(Idx_3))
mean(Velo_After_sc(Idx_7)) max(Velo_After_sc(Idx_7))
min(Velo_After_sc(Idx_7))]
MMM_Velo_Before_after_sc_4=[mean(Velo_Before_sc(Idx_4))
max(Velo_Before_sc(Idx_4)) min(Velo_Before_sc(Idx_4))
mean(Velo_After_sc(Idx_8)) max(Velo_After_sc(Idx_8))
min(Velo_After_sc(Idx_8))]
```

```
Idx_1=find(Diam==22 & isnan(MGoa_Before)==0);
Idx_2=find(Diam==24 & isnan(MGoa_Before)==0);
Idx_3=find(Diam==26 & isnan(MGoa_Before)==0);
Idx_4=find(Diam==28 & isnan(MGoa_Before)==0);

Idx_5=find(Diam==22 & isnan(MGoa_After)==0);
Idx_6=find(Diam==24 & isnan(MGoa_After)==0);
Idx_7=find(Diam==26 & isnan(MGoa_After)==0);
Idx_8=find(Diam==28 & isnan(MGoa_After)==0);

MMM_MGoa_Before_after_1=[mean(MGoa_Before(Idx_1)) max(MGoa_Before(Idx_1))
min(MGoa_Before(Idx_1)) mean(MGoa_After(Idx_5)) max(MGoa_After(Idx_5))
min(MGoa_After(Idx_5))]
MMM_MGoa_Before_after_2=[mean(MGoa_Before(Idx_2)) max(MGoa_Before(Idx_2))
min(MGoa_Before(Idx_2)) mean(MGoa_After(Idx_6)) max(MGoa_After(Idx_6))
min(MGoa_After(Idx_6))]
MMM_MGoa_Before_after_3=[mean(MGoa_Before(Idx_3)) max(MGoa_Before(Idx_3))
min(MGoa_Before(Idx_3)) mean(MGoa_After(Idx_7)) max(MGoa_After(Idx_7))
min(MGoa_After(Idx_7))]
MMM_MGoa_Before_after_4=[mean(MGoa_Before(Idx_4)) max(MGoa_Before(Idx_4))
min(MGoa_Before(Idx_4)) mean(MGoa_After(Idx_8)) max(MGoa_After(Idx_8))
min(MGoa_After(Idx_8))]

Idx_1=find(Diam==22 & isnan(Lv_Before)==0);
Idx_2=find(Diam==24 & isnan(Lv_Before)==0);
Idx_3=find(Diam==26 & isnan(Lv_Before)==0);
Idx_4=find(Diam==28 & isnan(Lv_Before)==0);

Idx_5=find(Diam==22 & isnan(Lv_After)==0);
Idx_6=find(Diam==24 & isnan(Lv_After)==0);
Idx_7=find(Diam==26 & isnan(Lv_After)==0);
Idx_8=find(Diam==28 & isnan(Lv_After)==0);

MMM_Lv_Before_after_1=[mean(Lv_Before(Idx_1)) max(Lv_Before(Idx_1))
min(Lv_Before(Idx_1)) mean(Lv_After(Idx_5)) max(Lv_After(Idx_5))
min(Lv_After(Idx_5))]
MMM_Lv_Before_after_2=[mean(Lv_Before(Idx_2)) max(Lv_Before(Idx_2))
min(Lv_Before(Idx_2)) mean(Lv_After(Idx_6)) max(Lv_After(Idx_6))
min(Lv_After(Idx_6))]
MMM_Lv_Before_after_3=[mean(Lv_Before(Idx_3)) max(Lv_Before(Idx_3))
min(Lv_Before(Idx_3)) mean(Lv_After(Idx_7)) max(Lv_After(Idx_7))
min(Lv_After(Idx_7))]
MMM_Lv_Before_after_4=[mean(Lv_Before(Idx_4)) max(Lv_Before(Idx_4))
min(Lv_Before(Idx_4)) mean(Lv_After(Idx_8)) max(Lv_After(Idx_8))
min(Lv_After(Idx_8))]


Idx_1=find(Diam==22 & isnan(Velo_Before_o)==0);
Idx_2=find(Diam==24 & isnan(Velo_Before_o)==0);
Idx_3=find(Diam==26 & isnan(Velo_Before_o)==0);
Idx_4=find(Diam==28 & isnan(Velo_Before_o)==0);

Idx_5=find(Diam==22 & isnan(Velo_After_o)==0);
Idx_6=find(Diam==24 & isnan(Velo_After_o)==0);
Idx_7=find(Diam==26 & isnan(Velo_After_o)==0);
```

```
Idx_8=find(Diam==28 & isnan(Velo_After_o)==0);

P_Velo_o_1= ranksum(Velo_Before_o(Idx_1),Velo_After_o(Idx_5))
P_Velo_o_2= ranksum(Velo_Before_o(Idx_2),Velo_After_o(Idx_6))
P_Velo_o_3= ranksum(Velo_Before_o(Idx_3),Velo_After_o(Idx_7))
P_Velo_o_4= ranksum(Velo_Before_o(Idx_4),Velo_After_o(Idx_8))

Idx_1=find(Diam==22 & isnan(Velo_Before_sc)==0);
Idx_2=find(Diam==24 & isnan(Velo_Before_sc)==0);
Idx_3=find(Diam==26 & isnan(Velo_Before_sc)==0);
Idx_4=find(Diam==28 & isnan(Velo_Before_sc)==0);

Idx_5=find(Diam==22 & isnan(Velo_After_sc)==0);
Idx_6=find(Diam==24 & isnan(Velo_After_sc)==0);
Idx_7=find(Diam==26 & isnan(Velo_After_sc)==0);
Idx_8=find(Diam==28 & isnan(Velo_After_sc)==0);

P_Velo_sc_1= ranksum(Velo_Before_sc(Idx_1),Velo_After_sc(Idx_5))
P_Velo_sc_2= ranksum(Velo_Before_sc(Idx_2),Velo_After_sc(Idx_6))
P_Velo_sc_3= ranksum(Velo_Before_sc(Idx_3),Velo_After_sc(Idx_7))
P_Velo_sc_4= ranksum(Velo_Before_sc(Idx_4),Velo_After_sc(Idx_8))

Idx_1=find(Diam==22 & isnan(Velo_Before_c)==0);
Idx_2=find(Diam==24 & isnan(Velo_Before_c)==0);
Idx_3=find(Diam==26 & isnan(Velo_Before_c)==0);
Idx_4=find(Diam==28 & isnan(Velo_Before_c)==0);

Idx_5=find(Diam==22 & isnan(Velo_After_c)==0);
Idx_6=find(Diam==24 & isnan(Velo_After_c)==0);
Idx_7=find(Diam==26 & isnan(Velo_After_c)==0);
Idx_8=find(Diam==28 & isnan(Velo_After_c)==0);

P_Velo_c_1= ranksum(Velo_Before_c(Idx_1),Velo_After_c(Idx_5))
P_Velo_c_2= ranksum(Velo_Before_c(Idx_2),Velo_After_c(Idx_6))
P_Velo_c_3= ranksum(Velo_Before_c(Idx_3),Velo_After_c(Idx_7))
P_Velo_c_4= ranksum(Velo_Before_c(Idx_4),Velo_After_c(Idx_8))

Idx_1=find(Diam==22 & isnan(MGoa_Before)==0);
Idx_2=find(Diam==24 & isnan(MGoa_Before)==0);
Idx_3=find(Diam==26 & isnan(MGoa_Before)==0);
Idx_4=find(Diam==28 & isnan(MGoa_Before)==0);

Idx_5=find(Diam==22 & isnan(MGoa_After)==0);
Idx_6=find(Diam==24 & isnan(MGoa_After)==0);
Idx_7=find(Diam==26 & isnan(MGoa_After)==0);
Idx_8=find(Diam==28 & isnan(MGoa_After)==0);

P_MGoa_1=ranksum(MGoa_Before(Idx_1),MGoa_After(Idx_5))
P_MGoa_2=ranksum(MGoa_Before(Idx_2),MGoa_After(Idx_6))
P_MGoa_3=ranksum(MGoa_Before(Idx_3),MGoa_After(Idx_7))
P_MGoa_4=ranksum(MGoa_Before(Idx_4),MGoa_After(Idx_8))

Idx_1=find(Diam==22 & isnan(Lv_Before)==0);
Idx_2=find(Diam==24 & isnan(Lv_Before)==0);
Idx_3=find(Diam==26 & isnan(Lv_Before)==0);
```

```
Idx_4=find(Diam==28 & isnan(Lv_Before)==0);

Idx_5=find(Diam==22 & isnan(Lv_After)==0);
Idx_6=find(Diam==24 & isnan(Lv_After)==0);
Idx_7=find(Diam==26 & isnan(Lv_After)==0);
Idx_8=find(Diam==28 & isnan(Lv_After)==0);

P_Lv_1=ranksum(Lv_Before(Idx_1),Lv_After(Idx_5))
P_Lv_2=ranksum(Lv_Before(Idx_2),Lv_After(Idx_6))
P_Lv_3=ranksum(Lv_Before(Idx_3),Lv_After(Idx_7))
P_Lv_4=ranksum(Lv_Before(Idx_4),Lv_After(Idx_8))
```